

Phase Behavior Analysis of a Gas Condensate Reservoir



By

**Nadia Mahjabin
17MET012P**

A thesis submitted in partial fulfilment of the requirements for the degree of
MASTER of SCIENCE in Energy Technology

Institute of Energy Technology

CHITTAGONG UNIVERSITY OF ENGINEERING AND TECHNOLOGY

March 2024

APPROVAL

The thesis titled "PHASE BEHAVIOR ANALYSIS OF A GAS CONDENSATE RESERVOIR" submitted by Nadia Mahjabin, ID No: 17MET012P and Session: 2017-2018 has been accepted as satisfactory in partial fulfillment of the requirements for the degree of Master of Science (M.Sc.) in Energy Technology on 11th March, 2024.

BOARD OF EXAMINERS



.....
Dr. Sajal Chandra Banik
Professor, Dept. of ME, CUET

Chairman
(Supervisor)



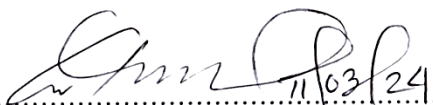
.....
Director
Institute of Energy Technology, CUET

Member
(Ex-Officio)



.....
Md. Adnan Faisal Siddique
Research Lecturer, IET, CUET

Member
(Internal)



.....
Dr. Muhammad Farhad Howladar
Professor, Dept. of PME, SUST

Member
(External)

Declaration

I hereby declare that the work contained in this thesis has not been previously submitted to meet requirements for an award at this or any other higher education institution. To the best of my knowledge and belief, the thesis contains no material previously published or written by another person except where due reference is cited. Furthermore, the Thesis compiles with PLAGIARISM and ACADEMIC INTEGRITY regulation of CUET.

Nadia Mahjabin

17MET012P

Institute of Energy Technology

Chittagong University of Engineering & Technology (CUET)

Copyright © Nadia Mahjabin, 2024

This work may not be copied without permission of the author or Chittagong University of Engineering & Technology

List of Publications

Conference

- Publication 1: *Nadia Mahjabin**, *Kakon Sultana*, *Dr. Md. Tazul Islam*, *Md. Mostafijul Karim*, “Condensate Characterization: An Approach to Evaluate the Performance of Condensate as a Feedstock in Oil Refinery”, *International Conference on Mechanical, Industrial and Energy Engineering, Khulna, Bangladesh, 22-24 December, 2022*, pg-4, ICMIEE22-003

Approval by the Supervisor

This is to certify that Nadia Mahjabin (ID:17MET012P) has carried out this work under my supervision, and that she has fulfilled relevant Academic Ordinance of the Chittagong University of Engineering and Technology, so that she is qualified to submit the following thesis in application for the degree of MASTER of SCIENCE in Energy Technology. Furthermore, the Thesis compiles with PLAGIARISM and ACADEMIC INTEGRITY regulation of CUET.

Dr. Sajal Chandra Banik

Professor

Department of Mechanical Engineering

Chittagong University of Engineering & Technology

Acknowledgment

I would like to begin by expressing my gratitude towards the Almighty for giving me the wisdom and skills necessary to complete the task. I would like to sincerely thank my supervisor, Professor Dr. Sajal Chandra Banik, Department of Mechanical Engineering, CUET, for all his help and support.

I am also indebted to Mostafijul Karim, Assistant Professor, Department of Petroleum and Mining Engineering, CUET, for the information and guidelines he has provided during the tenure of the study. I am also grateful to my fellow mates and to my friends. I express my gratitude to Super Refinery Pvt. (Ltd.) officials for providing me with the chance to work in their laboratory.

Last, but not least, I am indebted to my family for providing me the courage and support to carry out the work.

Abstract

Retrograde condensation is the term used to describe certain unusual features that result from condensate production in gas reservoirs. Unlike traditional gas reservoirs, this kind of reservoir experiences phase behaviour changes that affect the flow characteristics. This study's primary goal is to examine the nature of a specific gas condensate reservoir and create a model to track changes in fluid flow under specified circumstances. In this case, the Kailashtila gas field of Bangladesh has been taken into consideration. Both laboratory tests and simulations are performed to analyse the fluid composition, phase behaviour. Results are then summarized using simulation software (PVTSIM) to develop the phase diagram and other property curves of the fluid. The simulated and lab results implicate the reservoir to be a lean gas reservoir which is retrograde in nature. In the second part, a mathematical model is developed to represent the changes in flow pattern due to condensate banking near well-bore region.

The condensate banking surrounding the wellbore has a significant impact on the deliverability of gas wells producing below the dew-point pressure. The pressure transient test analysis is further complicated by condensate banking because of the multiphase flow and mixture composition shift. Analytical approach has been employed to find a solution of the model and then the sensitivity analysis of the model has been performed by incorporating real field test data. According to the model, the reservoir is the total of three flow zones. The three flow areas are as follows: outer region 3 contains just gas; middle region 2 contains both gas and condensate but only gas is mobile; and inner region 1, which contains both gas and condensate flowing simultaneously. The pressure squared approach has been selected to determine the flow rate considering real field production and pressure transient test data under specified condition. The response obtained from the analysis matches with the trend of typical flow curve but showed deviation in the calculated and observed results.

The condensate utilized as a feedstock in oil refineries is the subject of the study's third section. To produce assay data both laboratory tests and computer-aided analysis has been performed. The goal of this work is to develop a method to a comprehensive and organized characterization of gas condensate as a refining feedstock. The study also focuses on a critical examination of the assay data from samples of gas condensate that were taken from Kailashtila (KTL) gas fields. The study initially carried out laboratory tests to establish the boiling point. Empirical correlations are used to determine the necessary physical parameters for calculations involving the refining process. Utilizing Peng Robinson's thermodynamic model, a simulation software (DWSIM) helps in creating pseudo-components and their associated attributes using the generated true boiling point data. Thus, the study investigated the fluid's overall phase behaviour in both subsurface and surface conditions. The study's findings showed that by adjusting the number of trays or equilibrium stages in the distillation column, one can modify the amount and quality of product obtained as well as lower the energy consumption of a specific distillation process.

Although condensates are usually defined through compositional analysis, this study took a slightly different approach than it would with crude oil. Oil refineries that are thinking about using condensate as an alternate of crude oil, may find the study helpful in constructing and simulating the refining process, assessing feedstocks, and determining economic worth.

বিমূর্ত

রেট্রোগ্রেড কনডেনসেশন শব্দটি কোনো গ্যাস রিজার্ভারে কনডেনসেশনের ফলে যে অস্বাভাবিক বৈশিষ্ট্য পরিলক্ষিত হয় তা বোঝানোর জন্য ব্যবহৃত হয়। প্রথাগত গ্যাস রিজার্ভার থেকে ভিন্ন, এই ধরনের রিজার্ভারে ফেজ আচরণের পরিবর্তন হয় যা ফ্লুইড এর প্রবাহকে প্রভাবিত করে। এই গবেষণার প্রাথমিক লক্ষ্য ছিল একটি নির্দিষ্ট গ্যাস কনডেনসেট রিজার্ভারের প্রকৃতি পরীক্ষা করা এবং নির্দিষ্ট পরিস্থিতিতে তরল প্রবাহের পরিবর্তনগুলি অনুসন্ধানের জন্য একটি মডেল তৈরি করা। এক্ষেত্রে বাংলাদেশের কৈলাশটিলা গ্যাসক্ষেত্রকে বিবেচনায় নেওয়া হয়েছে। গ্যাস স্যাম্পলের গঠন বিন্যাস এবং ফেজ আচরণ বিশ্লেষণ করার জন্য পরীক্ষাগার পরীক্ষা এবং সিমুলেশন উভয়ই সম্বলিত হয়েছে। প্রাপ্ত ফলাফল বিশ্লেষণ করে PVTSIM সফটওয়্যার এর মাধ্যমে রিজার্ভারটির ফেজ ডায়াগ্রাম এবং তরলের অন্যান্য বৈশিষ্ট্যমূলক বক্ররেখা প্রস্তুত করা হয়েছে। সিমুলেটেড এবং পরীক্ষাগার থেকে প্রাপ্ত ফলাফল বিশ্লেষণ করে এই সিদ্ধান্ত নেয়া যায় যে, রিজার্ভারটি একটি লিন গ্যাস রিজার্ভার এবং এটি রেট্রোগ্রেড স্বভাব প্রদর্শন করে। দ্বিতীয় অংশে, একটি গাণিতিক মডেল তৈরি করার চেষ্টা করা হয়েছে যা ওয়েল-বোর অঞ্চলের কাছে কনডেনসেট ব্যাকিংয়ের কারণে প্রবাহের ধরণে পরিবর্তনগুলিকে উপস্থাপন করতে পারে।

কূপের আশেপাশের ঘনীভূত কনডেনসেটের ডিউ পয়েন্ট প্রেশারের নিচে উত্পাদিত গ্যাস, কূপের সরবরাহযোগ্যতার উপর উল্লেখযোগ্য প্রভাব ফেলে। কনডেনসেট ব্যাকিং এর প্রভাবে মাল্টিফেজ প্রবাহ এবং মিশ্রণের কম্পজিশন পরিবর্তিত হয় যা চাপের ক্ষণস্থায়ী পরীক্ষাকে জটিল করে তোলে। মডেলের একটি সমাধান খোঁজার জন্য বিশ্লেষণাত্মক পদ্ধতির ব্যবহার করা হয়েছে এবং তারপরে বাস্তবক্ষেত্র পরীক্ষার ডেটা অন্তর্ভুক্ত করে মডেলটির সংবেদনশীলতা বিশ্লেষণ করা হয়েছে। মডেল অনুসারে, রিজার্ভারটি মোট তিনটি প্রবাহ অঞ্চলে বিভক্ত। তিনটি প্রবাহ ক্ষেত্র নিম্নরূপ: বাইরের অঞ্চল ৩ এ শুধু গ্যাস রয়েছে; মধ্য অঞ্চল ২ এ গ্যাস এবং কনডেনসেট উভয়ই রয়েছে তবে শুধুমাত্র গ্যাসই প্রবাহিত; এবং অভ্যন্তরীণ অঞ্চল ১, যাতে একই সাথে প্রবাহিত গ্যাস এবং ঘনীভূত তরল উভয়ই রয়েছে। প্রকৃত ক্ষেত্রের উৎপাদন এবং চাপের ক্ষণস্থায়ী পরীক্ষার তথ্য বিবেচনা করে নির্দিষ্ট পরামিতিগুলির অধীনে প্রবাহের হার নির্ধারণ করতে চাপ বর্গ পদ্ধতি নির্বাচন করা হয়েছে। প্রাপ্ত ফলাফল বিশ্লেষণ করে দেখা যায় যে, প্রাপ্ত প্রতিক্রিয়া সাধারণ প্রবাহ বক্ররেখার প্রবণতার সাথে মেলে তবে গণনা করা এবং পর্যবেক্ষণ করা ফলাফলে কিছুটা বিচ্যুতি রয়েছে।

তেল শোধনাগারগুলিতে ফিডস্টক হিসাবে ব্যবহৃত কনডেনসেটটি গবেষণার তৃতীয় বিভাগের বিষয় ছিল। পরীক্ষাগার পরীক্ষা এবং কম্পিউটার-সহায়ক বিশ্লেষণ উভয়ের উপর ভিত্তি করে পরীক্ষা ডেটা তৈরি করা হয়, যার লক্ষ্য ছিল একটি পরিশোধন ফিডস্টক হিসাবে গ্যাস কনডেনসেটের একটি ব্যাপক এবং সংগঠিত বৈশিষ্ট্যের একটি পদ্ধতি বিকাশ করা। গবেষণাটি কৈলাশটিলা (KTL) গ্যাস ক্ষেত্র থেকে নেওয়া গ্যাস কনডেনসেটের নমুনাগুলি থেকে প্রাপ্ত অ্যাসে ডেটার একটি জটিল বিশ্লেষণের উপরও দৃষ্টি নিবদ্ধ করে। গবেষণাটি প্রাথমিকভাবে স্ফুটনাক্ষ বিন্দু নির্ধারণের জন্য পরীক্ষাগার পরীক্ষা করে। পরিমার্জন

প্রক্রিয়া জনিত গণনার জন্য প্রয়োজনীয় ফিজিক্যাল প্যারামিটার নির্ধারণ করতে গবেষণা মূলক সূত্র ব্যবহার করা হয়। DWSIM সফটওয়্যারে Peng Robinson থার্মোডাইনামিক মডেল ব্যবহার করে এবং TBP ডেটা ব্যবহার করে সিউডো-কম্পোনেন্ট এবং তাদের সম্পর্কিত বৈশিষ্ট্যগুলি প্রস্তুতকরা হয়েছে। এইভাবে, গবেষণায় তরলটির সামগ্রিক পর্যায়ে আচরণটি উপ-পৃষ্ঠ এবং পৃষ্ঠ উভয় অবস্থাতেই তদন্ত করার চেষ্টা করা হয়েছে। গবেষণার ফলাফলগুলি দেখিয়েছে যে পাতন কলামে ট্রে বা ভারসাম্যের স্তরগুলির সংখ্যা সামঞ্জস্য করে, কেউ প্রাপ্ত পণ্যের পরিমাণ এবং গুণমান পরিবর্তন করতে পারে এবং সেই সাথে একটি নির্দিষ্ট পাতন প্রক্রিয়ার শক্তি খরচ কমাতে পারে।

যদিও কনডেনসেটকে সাধারণত কম্পোজিশনাল বিশ্লেষণের মাধ্যমে সংজ্ঞায়িত করা হয়, তবে এই গবেষণাটি অপরিশোধিত তেলের সংজ্ঞায়ণ প্রক্রিয়ার তুলনায় কিছুটা ভিন্ন পদ্ধতি গ্রহণ করেছে। তেল শোধনাগারগুলি যেগুলি অপরিশোধিত তেলের বিকল্প হিসাবে কনডেনসেট ব্যবহার করার কথা ভাবছে, তারা পরিশোধন প্রক্রিয়া নির্মাণ এবং অনুকরণে, ফিডস্টকের মূল্যায়ন এবং অর্থনৈতিক মূল্য নির্ধারণে গবেষণাটিকে সহায়ক বলে মনে করতে পারে।

Table of Contents

Abstract.....	v
বিমূর্ত.....	vii
Table of Contents	ix
List of Figures	xiii
List of Tables	xvi
Nomenclature	xx
Chapter 1: INTRODUCTION.....	1
1.1 Background.....	1
1.2 Context	2
1.3 Purposes	2
1.4 Significance, Scope and Definitions	3
1.4.1 Significance of the Study	3
1.4.2 Scope and Limitations of the Study	4
1.5 Thesis Outline.....	5
Chapter 2: LITERATURE REVIEW	7
2.1 Natural Gas Condensate and Condensate Banking.....	7
2.2 Phase Behavior	8
2.3 Equation of States	9
2.4 Multiphase flow	14
2.5 Field Description.....	16
2.6 PVT Tests.....	22
2.6.1 Constant Composition Expansion (CCE) / Constant Mass Expansion (CME) Test.....	22

2.6.2	DL (Differential Liberation) Test	23
2.6.3	CVD (Constant Volume Depletion) Test.....	24
2.6.4	Separator Test.....	24
2.7	Condensate Characterization	25
2.7.1	Defining Pseudo-Components.....	26
2.7.1.1	Generating Pseudo-components:.....	26
2.8	Summary and Implications	27
Chapter 3 : RESEARCH METHODOLOGY		29
3.1	Methodology and Research Design	29
3.1.1	Methodology	29
3.1.2	Flow Chart:	32
3.1.2.1	Quantitative	33
3.2	Samples.....	36
3.3	Instruments.....	36
3.3.1	SCION 456 GC	36
3.3.2	ASTM D86 Test Method	37
3.4	Procedure and Timeline.....	38
3.5	Analysis.....	39
3.6	Ethics and Limitations.....	39
Chapter 4 : PHASE BEHAVIOR ANALYSIS OF KAILASHTILA GAS FIELD		41
4.1	Rock and Fluid Properties of KTL field	41
4.1.1	Upper Gas Sand (UGS) Fluid Composition and Properties	46
4.1.2	Middle Gas sand Fluid (MGS) Composition and Properties	47
4.1.3	Lower Gas sand Fluid (LGS) Composition and Properties	47
4.2	Simulation Results	53
4.2.1	Saturation Test	53
4.2.2	Separator Test.....	55

4.2.3 Constant Mass Expansion (CME) Test	57
4.2.4 CVD Test.....	62
Chapter 5 : MULTI-PHASE FLOW MODELLING.....	71
5.1 Reservoir Model for Multi-phase Flow in Near Well-bore region.....	71
5.1.1 Partial Differential Model for Region 1, i.e. for near well bore region....	72
5.2 Analytical Solution	75
5.3 Sensitivity Analysis	77
5.3.1 Well 1.....	77
5.3.2 Well 2.....	80
5.3.3 Well 3.....	82
Chapter 6 : Characterization and Performance Evaluation of KTL Condensate	88
6.1 Condensate Sampling.....	88
6.1.1 Property Estimation	90
6.2 Condensate Characterization	100
6.2.1 Atmospheric Distillation	107
Chapter 7 : ANALYSIS.....	121
7.1 Phase Behaviour of Kailashtila Gas Field.....	121
7.2 Model Analysis	125
7.3 Performance Evaluation of Condensate And Distillation Process.....	127
Chapter 8 : CONCLUSIONS.....	131
8.1 General	131
8.2 Key Findings.....	131
8.3 Limitation of the Study	132
8.4 Implication.....	133
8.5 Recommendation for Further Study	133

Bibliography	135
Appendix	141

List of Figures

Fig. 2.1: Phase diagram of a typical retrograde gas condensate reservoir at isothermal condition [3]	8
Fig. 2.2: Map of the Bengal Basin and adjoining areas and major geographic features [36].	17
Fig. 2.3 : Depth structure map of UGS [42]	19
Fig. 2.4: Depth structure map of MGS [42]	20
Fig. 2.5: Depth structure map of LGS [42]	21
Fig. 2.6: Constant Composition Expansion / Constant Mass Expansion Test [44]	23
Fig. 2.7: Differential liberation test [44]	23
Fig. 2.8: Constant volume depletion [44]	24
Fig.2.9: Separator test [44]	25
Fig. 3.1: Flow sheet of the research methodology	32
Fig. 4.1: Gas saturation and capillary pressure curve	44
Fig.4.2: Gas water relative permeability curve	45
Fig.4.3: Phase diagram for UGS	45
Fig.4.4: Phase diagram for LGS	46
Fig. 4.5: Z factor chart for upper gas sand	49
Fig. 4.6: Z factor chart for lower gas sand	49
Fig. 4.7: Gas viscosity curve for upper gas sand	50
Fig. 4.8: Gas viscosity curve for lower gas sand	50

Fig. 4.9: Formation volume factor curve for upper gas sand.....	51
Fig. 4.10: Formation volume factor curve for lower gas sand	51
Fig. 4.11: Retrograde liquid curve for upper gas sand	52
Fig. 4.12: Retrograde liquid curve for lower gas sand.....	52
Fig. 4.13: Density Vs Pressure for UGS.....	60
Fig. 4.14: Density Vs Pressure for LGS.....	60
Fig. 4.15: Z factor Chart for UGS.....	61
Fig. 4.16: Z factor Chart for LGS	61
Fig. 4.17: Relative volume (%) curve for UGS.....	62
Fig. 4.18: Relative volume (%) curve for LGS	62
Fig. 4.19: Percent production curve for UGS	67
Fig. 4.20: Percent production curve for LGS	67
Fig. 4.21: Gas viscosity curve for UGS	68
Fig. 4.22: Gas viscosity curve for LGS.....	68
Fig. 4.23: Z factor chart for UGS.....	69
Fig. 4.24: Z factor chart for LGS	69
Fig. 4.25: Two phase Z factor curve for UGS	70
Fig. 4.26: Two-phase Z factor curve for UGS.....	70
Fig. 5.1: Flow regions for a radial well producing from a gas condensate reservoir	71
Fig. 5.2: Radial multi-phase flow near well bore.....	72
Fig. 5.3: Flow rate at different location in reservoir for Well 1, 2 and 3	85
Fig. 5.4: Inflow performance curve for Well 1,2 and 3	85

Fig. 5.5: Reservoir pressure as a function of flow rate and radius for Well 1	86
Fig. 5.6: Reservoir pressure as a function of flow rate and radius for Well 2	86
Fig. 5.7: Reservoir pressure as a function of flow rate and radius for Well 3	87
Fig. 6.1: Phase diagram of recombined fluid	92
Fig. 6.2: Phase diagram of gas and condensate in separator condition	92
Fig. 6.3: Hoffman plot recombined fluid at separator condition	99
Fig. 6.4: Density vs. logarithmic carbon number for recombined fluid	99
Fig. 6.5 Mass balance closure plot for recombined fluid at separator condition	100
Fig. 6.6: Typical TBP curve of a petroleum mixture [49]	101
Fig. 6.7: ASTM and TBP curve for KTL condensate	103
Fig. 6.8: TBP and Molecular weight curve for KTL condensate	104
Fig. 6.9: Daubert's TBP extrapolation curve	104
Fig. 6.10: Representation of TBP curve for pseudo components	105
Fig. 6.11: Atmospheric distillation for KTL condensate	107
Fig. 6.12: Component flow inside distillation column	110
Fig. 6.13: Interstage flow inside distillation column	110
Fig. 6.14: Temperature profile inside distillation column	111
Fig. 6.15: Shortcut distillation for KTL condensate pseudo cuts (separator)	115

List of Tables

Table 2.1: Contribution of EOS for PVT modelling	13
Table 2.2: Coexistence of flow regions [4]	16
Table 2.3: Cut point ranges for refining calculations	27
Table 3.1: Estimated Rock, fluid and distillation properties	33
Table 3.2: Input and output parameters of pvtsim	34
Table 3.3: Flow/Pressure and Temperature condition [50]	37
Table 3.4: Time frame for work	38
Table 4.1: Kailashtila gas field properties for upper, middle, and lower sand field	42
Table 4.2: Upper and lower sand fluid composition	43
Table 4.3: The relative permeability and capillary pressure function	44
Table 4.4: Constant Composition Expansion for upper gas sand fluid	47
Table 4.5: Constant Composition Expansion for lower gas sand fluid	48
Table 4.6: Saturation temperature- and pressure for upper and lower sand ..	53
Table 4.7: Phase properties and composition in mole% for upper sand fluid	54
Table 4.8: Phase properties and composition in mole% for lower sand	55
Table 4.9: Separator test results for UGS	55
Table 4.10: Compositional mole% for liberated gas and residual oil for UGS fluid	56
Table 4.11: Separator test results for LGS	56

Table 4.12: Compositional mole% for liberated gas and residual oil for LGS fluid.....	57
Table 4.13: CME test for UGS fluid at reservoir temperature	58
Table 4.14: Phase properties at saturation pressure and reservoir temperature	58
Table 4.15: CME test for LGS fluid at reservoir temperature	59
Table 4.16 Phase properties at saturation pressure and reservoir temperature	59
Table 4.17: CVD test at reservoir temperature for UGS	63
Table 4.18: Produced well stream fluid composition mole%	63
Table 4.19: CVD test at reservoir temperature for LGS.....	64
Table 4.20: Produced well stream fluid composition mole%	65
Table 4.21: Residual oil % at CVD Test for UGS and LGS	66
Table 5.1: Well data For KTL Well 1, 2 and 3.....	77
Table 5.2: Kailashtila Well no. 1 lower gas sand deliverability	78
Table 5.3: Deliverability test results in terms of pressure squared.....	78
Table 5.4: Calculated value of $qM_{,,}$, relative error, P_{wf} and P_R	79
Table 5.5: Flow rate at different point in reservoir (steady state condition) ..	80
Table 5.6: Kailashtila well no.2 upper gas sand deliverability	80
Table 5.7: Deliverability test results in terms of pressure squared.....	81
Table 5.8: Calculated value of $qM_{,,}$, relative error, P_{wf} and P_R	81
Table 5.9: Flow rate at different point in reservoir (steady state condition) .	82
Table 5.10: Kailashtila well no. 3 Middle Gas Sand Deliverability	83
Table 5.11: Deliverability test results in terms of pressure squared.....	83

Table 5.12: Calculated value of $qM_{,,}$, relative error, P_{wf} and P_R	84
Table 5.13: Flow rate at reservoir pressure.....	84
Table 6.1: Compositional analysis of gas, condensate, and recombined fluid	89
Table 6.2: Critical properties and Normal Boiling Point (NBP) of recombined fluid.....	90
Table 6.3: Heat of formation, molecular weight parameters for recombined fluid.....	91
Table 6.4: Critical pressure and temperature of ktl recombined fluid	93
Table 6.5: Phase properties and composition mole% at critical conditions ...	94
Table 6.6: CVD experiment for recombined fluid	95
Table 6.7: Produced well stream and residual oil mole % from CVD experiment	96
Table 6.8: Separator test for recombined fluid.....	97
Table 6.9: Liberated gas mole % for recombined fluid.....	98
Table 6.10: Distillation data for KTL condensate	102
Table 6.11: Physical properties of pseudo cuts	106
Table 6.12: Property table for distillation column.....	109
Table 6.13: Feed property Data from Distillation column	112
Table 6.14: Distillate property data from distillation column	113
Table 6.15: Bottom product property and molar fraction	114
Table 6.16: Component molar fraction for pseudo component (Mixture).....	115
Table 6.17: Shortcut distillation column properties	116
Table 6.18: Critical properties and NBP for pseudo components.....	116

Table 6.19: Model specific property for pseudo components.....	117
Table 6.20: Pseudo component properties	117
Table 6.21: Property table for pseudo component (mixture).....	118
Table 6.22: Component molar fraction for pseudo component (vapor and overall liquid)	118
Table 6.23: Property table for pseudo component (mixture).....	119
Table 6.24: Composition molar fraction in distillate and bottom products ..	119
Table 7.1: Deviation for different rock and fluid properties.....	121
Table 7.2: Differences for relative volume (UGS).....	122
Table 7.3: Comparison for liquid vol%	122
Table 7.4: Z factor value from CCE/CME test.....	123
Table 7.5: Percent deviation for viscosity	123
Table 7.6: Differences for rel volume (LGS)	123
Table 7.7: Comparison of liquid vol% (LGS)	124
Table 7.8: Z factor value from CCE/CME test.....	124
Table 7.9: Percent deviation for viscosity(LGS)	124
Table 7.10: Calculated value for well1, 2 And 3	126
Table 7.11: Comparison between lab and simulated properties.....	128
Table 7.12: Quality check for KTL condensate	128
Table 7.13: Comparative chart for atmospheric and shortcut distillation	129

Nomenclature

Symbols Acronyms and Abbreviations

KTL	= Kailashtila
UGS	= Upper Gas Sand
MGS	= Middle Gas Sand
LGS	= Lower Gas Sand
CCE	= Constant Composition Expansion
CVD	= Constant Volume Depletion
A	= Area, acre
h	= Thickness, ft
K	= Permeability, mD
μ	= Viscosity, cP
ϕ	= Porosity
C_t	= Total Compressibility, 1/psi
U_T	= Mass Flow Rate, m/s
GOR	= Gas Oil Ratio, MMscf/bbl
LGR	= Liquid- Gas Ratio, bbl/MMscf
Rvol/Svol	= Reservoir Volume/Standard Volume
P_{dew}	= Dew Point Pressure, psia
P_{sat}	= Saturation Pressure, psia
EOs	= Equation of States
PR	= Peng Robinson
SRK	= Soave- Redlich- Kwong
q_M	= Mixed Volumetric Flow Rate, m ³ /s
IBP	= Initial Boiling Point, °C
EP	= End Point, °C
ERL	= Eastern Refinery Limited.

Chapter 1: INTRODUCTION

This chapter provides an overview of the study's history (1.1), context (1.2), and purpose (1.3), as well as its scope and implications (1.4). An overview of the thesis's remaining chapters is provided in section 1.5.

1.1 BACKGROUND

A gas condensate reservoir produces surface gas and a small quantity of oil, known as condensate or distillate. Though at reservoir condition, single phase exists in the reservoir, when pressure drops below the dew point pressure some gas bubble condensed out of the reservoir. This process is termed as retrograde condensation. In a gas condensate reservoir, a liquid bank of condensate is developed near the wellbore which disturbed the flow of fluid by reducing the well deliverability capacity; hence, the production is uninterrupted. The scenario is not same in a gas reservoir since it does not face such difficulties [1-3].

Since accurate fluid flow calculation in a retrograde reservoir considers phase changes, loss of condensate into smaller pore area, multi-phase-flow of the wet gas oil, redistribution of phases in and around the wellbore, re-vaporization of liquid into the condensate gas; proper assumption and modelling is crucial for estimating the reservoir characteristics [4].

1.1.1 Gas Condensate Reservoir in Bangladesh

Almost every gas field of Bangladesh produces dry gas only. Yet some fields produce a significant amount of condensate. The total initial reserve of condensate in Bangladesh' is 43.2 million barrels. Beanibazar, Jalalabad, and Kailashtila are the three most condensate rich gas fields in Bangladesh. These three condensate rich fields accumulate 63% of the total condensate reserve [5].

Over recent years several public and private companies got involved in the fractionation of condensate to yield petroleum fractions. Condensate is now an important issue from both a technical and economic perspective. Many private refineries have used the condensate as their feedstock. Condensate is processed in fractionation plant to produce LPG, motor spirit and kerosene. The products are then used in the local market [6,7].

1.2 CONTEXT

In a gas condensate reservoir, the production is hampered due to the banking of condensate near wellbore region. This occurs due to the reduction in gas relative permeability as compared to liquid or condensate. This condensate has a high saturation that acts to lower the gas permeability and thereby lower well deliverability. Normally three factors are considered to trigger this phenomenon; (i) relative permeabilities, (ii) PVT properties of reservoir fluid and (iii) the state of production of the well (whether the well is producing at constant rate and at constant BHP). Before 1990s the situation was not well understood.

First Muskat addressed this problem in the discussion of gas cycling, and then Fetkovich derived a rate- and time-dependent blockage skin effect to consider in standard gas rate equation [7]. Later, Kniazeff, Naville and Eilerts et al. [8,9] developed numerical and another model to focus on this phenomenon. Yet, the gas – condensate well deliverability has been a long-standing problem and no single model or equation can accurately represent this event.

1.3 PURPOSES

The main purpose of the study is to investigate the PVT behaviour of retrograde reservoir fluid during phase changes. Besides, it also focuses on assessing the practicality of using condensate as an alternate source of fuel in refinery. The aim, outcomes and drawbacks of the study are mentioned below.

The objectives of this study are to:

- (a) Analyze the PVT properties of a gas condensate reservoir and develop the phase diagram
- (b) Determine the critical and fluid properties of the reservoir
- (c) Analyze the retrograde behavior of that reservoir
- (d) Determine the composition, physical and critical properties of condensate

Outcomes of the Study:

- (a) Developing a multiphase flow model for gas condensate reservoir
- (b) Suggesting an analytical solution for the flow equation
- (c) Validate the solution with actual field data
- (d) Developing an approach to characterize and estimate the performance of condensate as a fuel.

The study's primary flaw was that the data it used were old. Utilizing latest production and field data will increase its dependability. The inability to evaluate the proposed model in an actual setting is another disadvantage. To reach a conclusion, the author has to rely on estimated results. Also, there were some missing data that required assumptions.

1.4 SIGNIFICANCE, SCOPE AND DEFINITIONS

The significances and scopes of the study are addressed in following sections.

1.4.1 Significance of the Study

In Bangladesh Beanibazar, Kailashtilla, Jalalabad, and Bibiyana gas fields yield the most condensate-enriched gas [5]. In fractionation factories, gas condensate has been fractionated to create various hydrocarbon solvents such as octane, kerosene, diesel, and gasoline. But the entire capacity of Bangladesh's condensate fractionation plants is currently less than the pace at which condensate is

produced overall [5,6]. So, the country has to import petroleum fuels to meet up demand. Since there is not a set procedure for analysing condensate's fuelling capacity, the goal of this study is to provide a methodical approach to close the gap. The author was further motivated to concentrate on this topic by the lack of a precise and detailed model to address the well deliverability of a gas condensate reservoir.

1.4.2 Scope and Limitations of the Study

A dry gas reservoir's fluid behaviour is not comparable to that of a gas condensate reservoir. Eilerts, Gondouin et al. [9] and Muskat, Fetkovich, Kniazeff, and Naville [10] have made important contributions to the solution of the condensate banking issue in a retrograde reservoir. While O'Dell and Miller [11] gave the first gas rate equation employing a pseudo-pressure function to characterize the effect of condensate blockage, Gondouin et al. [12] demonstrated the dependency of non-Darcy effect on gas back pressure calculation. Fussell [13] assesses how phase behaviour and relative permeability features affect production performance and provides EOS compositional simulations of radial gas condensate wells producing by pressure depletion below the dewpoint. For the most part, Jones and Raghavan [14] address the radial wells' transient pressure behaviour (drawdown and build-up). Øivind Fevang in 1995 [4] calculates well deliverability using a modified form of the classical Evinger-Muskat pseudo-pressure approach considering producing GOR accurately.

However, none of these studies address the simultaneous dependence of flow rate on rock, time, radius, and fluid characteristics. This study fills a vacuum in the literature by attempting to incorporate the factors in the flow model; that led to the creation of its scope.

The lack of current field data and the application of the suggested model in actual field settings are the study's shortcomings. The study focuses on the analytical solution considering the EOS functions; however, the inclusion of Laplace

transform theory and numerical technique can significantly improve the model's accuracy.

1.5 THESIS OUTLINE

The broad overview of the subject, parameters, objectives, and results of the work has been covered in **Chapter 1**.

Chapter 2 provides an overview of gas condensate reservoirs, the condensate banking issue near wellbore regions, multiphase flow modelling, reservoir and condensate characterization parameters, and field description.

The methods and procedure for gathering data of the study are covered in **Chapter 3**.

The PVT analysis of the Kailashtila gas field fluid is presented in **Chapter 4**. The phase behaviour of the field is determined by the lab experiments and the derived simulation findings.

A mathematical model for the gas-condensate reservoir in the vicinity of the wellbore is presented in **Chapter 5**. The model's sensitivity has been examined using actual field production and pressure transient data, and an analytical solution has been proposed.

Chapter 6 presents the condensate's characterization and performance assessment as a feedstock for refining. It has been hypothesized that distillation can increase product amount while consuming less energy.

The study's results are covered in detail in **Chapter 7** and the work's limitations, suggestions, and findings are listed in **Chapter 8**.

Chapter 2 : LITERATURE REVIEW

The details on gas-condensate reservoir, condensate banking problem, multi-phase flow modelling, description on Kailashtila gas filed etc are covered in this chapter. The discussion tries to form the conceptual framework of the study and bridging the gap of the discussed topics.

2.1 NATURAL GAS CONDENSATE AND CONDENSATE BANKING

Natural-gas condensate is normally produced from many natural gas fields in the world. When the pressure in the reservoir drops below the dew point pressure, the liquid condenses out from the gas [15]. The natural gas condensate is sometimes referred to as natural gasoline as it contains the hydrocarbons that have temperature within the gasoline boiling range.

The first droplet of condensate will develop near the wellbore where the reservoir pressure reaches its lowest. The volume where condensate oil is generated will progressively develop and expand radially into the reservoir as more gas is produced, which will cause the reservoir pressure to continue dropping. The liquid thus formed prevents the gas from flowing freely in certain cases.

Condensate oil reaches its critical saturation point it will start to flow and become continuous in the pore space. As a result, the draw down pressure will rise significantly, resulting in a drop in bottom hole pressure (in the event of constant surface gas production), and reservoir production will be characterized by two-phase flow [16,17].

The conversion from single to multi-phase in the area leads to two main problems: lost production due to the decrease in gas permeability and an early well production shutdown because of decreased well deliverability.

Additionally, the liquid banking creates a non-Darcy effect which in turn reduce the bottomhole flowing pressure [18-20].

2.2 PHASE BEHAVIOR

Phase behaviour explains the existence of one or more phases at a given condition of pressure, temperature, and volume. The Pressure- Temperature diagram is known as phase behaviour or PVT diagram. The phase diagram is typically used to reflect this behaviour for a particular fluid system. The reservoir condition and the phase envelope of the fluid system affect the flow behaviour of a gas condensate reservoir.

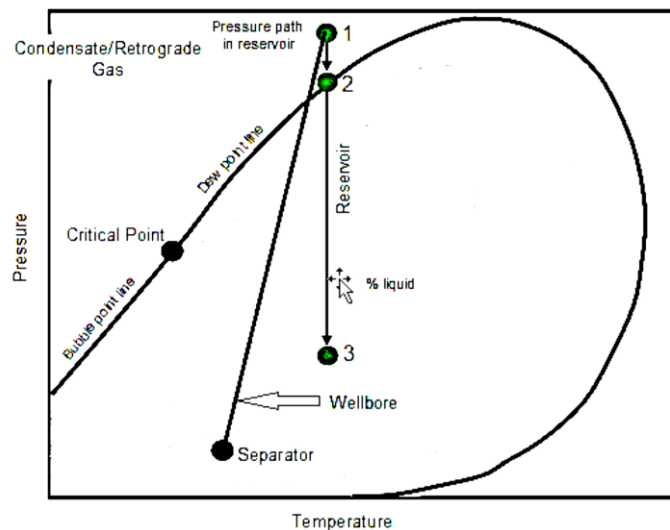


Fig. 2.1: Phase diagram of a typical retrograde gas condensate reservoir at isothermal condition [3]

From Figure 2.1, it has been seen that the retrograde gas has a critical temperature less than reservoir temperature. At point 1 in fig. 2.1, the retrograde gas is totally gas, i.e., at reservoir condition. The gas exhibits a decrease in pressure at point 2. Liquid condenses from the gas at decreasing pressure. It forms a free liquid zone in the reservoir. The situation is normally existing in a case, where the reservoir temperature is typically higher than critical temperature and lower than the cricondentherm and the initial reservoir pressure is above the cricondenbar in the single-phase gaseous state [21].

Analysing the phase behaviour of petroleum systems has taken years of research. Many numerical and mathematical methods have been proposed to describe the phenomenon. One fruitful result of this study is equation of state (EOS), which, despite the complexity of the hydrocarbon fluids found in subsurface reservoirs, has shown unexpected performance in the phase-behaviour computations of these complex fluids. An EOS is an analytical expression that connects pressure, temperature, and volume. This formula describes the volumetric behaviour, the vapor/liquid equilibria (VLE), and the thermal properties of mixes and pure materials [22].

2.3 EQUATION OF STATES

Due to the simplicity and extrapolative abilities beyond the correlation ranges, The Cubic Equations of State (CEOSs) are considered as the most important tools in PVT calculations. The most successful CEOSs are the Peng-Robinson (PR) and Soave-Redlich-Kwong (SRK) equations. These EOSs have been modified repeatedly to improve their accuracy in wider ranges of temperature and pressure. Ramdharee et al. Suggests that the original SRK EOS is a better candidate than original and alternative forms of PR EOS [23].

The accurate information of the PVT properties of petroleum fluids bears significant importance for oil and gas companies. But the experimental PVT data measurement is time-consuming and involves a complex procedure. Sometimes the validation of reported data is doubtful. That is why PVT models have attracted the attention and CEOSs serve the best performance in determining the PVT properties of reservoir fluid accurately.

Definition of Equation State

An Equation of State (EOS) describes the condition of a matter over a defined range of physical conditions. The equation is normally semi-empirical that tries to set up a relation among pressure, temperature, and volume of a pure substance. To apply these equations for mixtures the information of an additional

variable, that is composition, and the selection of an accurate mixing rule is necessary. The EOS can be expressed in functional as shown in Equation 2.1,

$$f(P, V, T, a_K, n_K, K = 1) = 0 \quad \text{Equation 2.1}$$

Here P, V, and T represent pressure, volume, and temperature. A_k and n_p show the categories of the equations of state. n_p indicates the complexity of the EOS.

In petroleum industries, the most acceptable and applicable EOSs are the PR and SRK EOS. These EOSs can successfully predict the thermo-physical properties of substances and the volumetric data. They also assist in the vapor-liquid equilibrium calculations.

Equation of state is applicable under a wide region of temperature and pressure as well as for pure components to complex mixtures. So they can be applied for light gas and heavy liquids. Petroleum industries consider EOSs as an important tool for predicting fluid behavior due to their simplicity.

The EOSs, used in industries, took the basic Van der Waals equation as basis and moderated it to match in defined ranges of pressure and temperature. In 1949 Redlich and Kwong presented the most successful modification of the Van Der Waals equation. The RK equations are cubic, applicable to the mixture using mixing rules to parameters, used in the equation of state. By giving a better explanation of the attractive term they improved the Van der Waals equation. This EOS normally requires a little data to predict component or mixture behavior. But their uses only limited to gas since they cannot predict liquid-liquid and vapor-liquid equilibrium data [23].

The general form of RK equation:

$$P = \frac{R-T}{v-b} - \frac{a}{(\sqrt{T}v(v+b))} \quad \text{Equation 2.2}$$

Where,

$$a = 0.42748 (R^2 T_c^{2.5}) / P_c$$

$$b = 0.08664 * R T_c / P_c$$

The cohesion function, a , is temperature dependent and this dependency increases the accuracy of results in RK EOS. But this equation is found to be

essentially empirical that mainly depends on the degree of approximation. They ignore a detailed discussion and are prone to circumstantial.

Peng Robinson Equation

Peng Robinson in 1976 performed the most accepted and popular modification of SRK CEOS. They reduced the limitations of the SRK equation by adding a term $b(V-b)$ in the denominator. They suggested that this addition to the attractive term in the denominator would remove the limitations of SRK equations in predicting liquid phase density [24]. But problems remain since they could not provide any proper justifications for their action. Like SRK CEOS the PR EOS also appeared to be empirical. Nevertheless, the PR EOS is suitable both for vapor and liquid properties prediction near equilibrium. This equation is a better choice than the SRK equation in predicting liquid phase densities and is also applicable to the natural gas system.

The equations are given shown in Equation:

$$\begin{aligned}
 P &= \frac{RT}{V_M - b} - \frac{a\alpha}{v(v+b)+b(v-b)} & \text{Equation (2.3)} \\
 a &= 0.45724 (R^2 * T_C^2) / P_C \\
 \alpha &= [1 + S \left(1 - \frac{T}{T_C}\right)]^2 \\
 S &= 0.37464 + 1.54266\omega - 0.26992\omega^2 \\
 b &= 0.07780 * \frac{RT_C}{P_C}
 \end{aligned}$$

In 1978, Peng and Robinson suggested that for $\omega > 0.49$, the value of S will be (Stryjek & Vera, 1986) as shown in Equation 2.4

$$S = 0.3796 + 1.4850\omega - 0.1644\omega^2 + 0.01666\omega^3 \quad \text{Equation 2.4}$$

They also suggested an equation (Equation 2.5) to predict the heavy hydrocarbons vapor pressure over a wide temperature range.

$$P = \frac{\rho NRT}{(1-b\rho)} - \frac{a\rho^2}{1+2b\rho-b^2\rho^2} \quad \text{Equation 2.5}$$

Where a and b can be calculated from

$$\begin{aligned}
 a &= a_c \omega \\
 a_c &= 0.45724 (R^2 * T_C^2) / P_C
 \end{aligned}$$

$$\alpha = \left[1 + k \left(1 - \frac{T}{T_c}\right)\right]^2$$

$$b = 0.07780 * \frac{RT_c}{P_c}$$

$$k = 0.37464 + 1.54266\omega - 0.26992\omega^2$$

Due to the simplicity and accuracy in predicting pressure-temperature relationship and phase compositions of a binary and multicomponent system, petroleum industries use both the PR and SRK equations widely. These equations only need Critical properties and acentric factor as input data. But the success of these EOSs has been limited in estimating the phase equilibrium pressure because the measured value is lower than the predicted saturated liquid volume.

PR, SRK, and RK Comparisons

The RK EOS is applicable for predicting gas-phase properties and is also assists in fugacity, enthalpy, and entropy departure calculations. But this equation cannot predict liquid phase properties. For gas and condensate system PR EOS is a better choice than SRK EOS, while for predicting polar system SRK shows an excellent output [25,26].

A lot of studies have been done in evaluating the superiority of SRK, RK, and PR EOS among each other. Some studies suggested PR EOS shows priority in predicting properties like vapor pressure, Liquid Molar Volume (LMV), Vapor Molar Volume (VMV), enthalpies of vaporization for liquid and vapor phase in the subcritical region. Though recent studies conducted by Le Guennec et al. over a hundred component and by Nasifar and Bolland show that for the prediction of vapor pressure SRK is advantageous than PR EOS. In this respect, it may be also added that Pazuki et al in 2007 revealed that PR EOS can poorly applicable in extrapolating liquid molar volume of heavy hydrocarbon [27-35]. The work founds that in high-pressure regions the error encountered is above one hundred percent.

Recently, Patel and Teja [36] suggested a CEOS which has three parameters in nature. This parameter encompasses critical pressure, critical temperature, and a

two substance-dependent parameter. The EOS shows a close similarity with PR CEOS and found to be empirical. The PT EOS is also modified in recent days. Ghanbar et al. [27] suggest the SRK equation reveals better extrapolation results than PR EOS in critical and subcritical regions. Their work shows that the derivatives of α -function in the PR CEOS do not meet with the zero points at very high temperatures; also, the second derivative of the function gives a wavy shaped curve, which denied the thermodynamic consistency. These drawbacks of the PR equation led to the generation of other basic incompatibilities. Previous studies show the PR equation overestimates at the peak of Joule Thompson Inversion curve. Recent studies deduce that at high-pressure region SRK CEOS shows better results in predicting vapor pressure than PR CEOS, where the PR CEOS exhibits the best result at a low-temperature range that extends from boiling to the critical point [25,26,30].

Table 2.1:Contribution of EOS for PVT modelling

Year of work	Name of Researcher(s)	Contributions
1660	Robert Boyle & Edme Mariotte	<ul style="list-style-type: none"> At low pressure, they calculate the PVT behavior of air Establish the inverse pressure-volume relationship at a constant temperature. The relationship is called Boyle-Marriott law.
1787 to 1803	Jacques-Alexander Cesar Charles & Joseph Louis Gay-Lussac	<ul style="list-style-type: none"> Establish an equal thermal gas expansion law at constant pressure. Work separately.
1834	Emile Clapeyron	<ul style="list-style-type: none"> Combined the Boyle-Mariotte and Charles-Gay-Lussac law and establish an equation of state $PV = R_0T$, where R_0 stands as gas-dependent constant
1845	Victor Regnault	<ul style="list-style-type: none"> Using Avagadro's theory of occupation of volume by one-mole gas he transforms

		Clapeyron's perfect gas equation into the ideal or perfect gas equation, $PV = nRT$
1873	Johannes Diderik Van Der Waals	<ul style="list-style-type: none"> Suggest two parameters to Regnault's ideal gas equation. Correct P with $(P + \frac{a}{v^2})$ and V with $(V-b)$ in the generalized ideal gas equation. [Walls, 1873].
1901	Heike Kamerlingh Onnes	<ul style="list-style-type: none"> Establish "Virial Expansion" for "Virial Equation of State" [Kamerlingh, 1901].
1927 and 1928	James A. Beattie & Oscar C. Bridgeman	<ul style="list-style-type: none"> Proposed "Beattie-Bridgeman Equation of State" based on the "Ones Virial Equation of State" [James et al, 1927; James et al 1928].
1940	Manson Benedict & George B. Webb & Louis C. Rubin	<ul style="list-style-type: none"> Suggested, "Benedict-Webb-Rubin (BWR) Equation of State" based on "Ones Virial Equation of State" [Benedict, 1940].
1949	Otto Redlich & J. N. S. Kwong	Established "Redlich-Kwong Equation of State" based on "Ones Virial Equation of State" [Redlich et al, 1949].
1972	Giorgio Soave	Modified "Redlich-Kwong Equation of State" as "Soave-Redlich-Kwong (SRK) Equation of State" [Soave, 1972].
1975	Byung Ik Lee & Michael G. Kesler	Proposed "Lee-Kesler Equation of State" according to "Pitzer's Correlation" [Lee & Kesler, 1975].
1976	Ding Yu Peng & Donald Robinson	Establish a successful modification of the basic Van der Waals equation. [Peng & Robinson, 1976].
1982	Patel and Teja	Suggested modification to Peng Robinson cubic equation of state [Patel & Teja, 1982]
2007	Pazuki	Suggested for heavier hydrocarbon, PR is poorly applicable in predicting liquid molar volume.

2.4 MULTIPHASE FLOW

Multiphase flow is generally known as the simultaneous flow of two or more phases in a reservoir rock. To get the complete picture of reservoir condition, the consideration, and understanding of multi-phase behaviour is important [2].

Due to the intricate interactions between the contributing elements, understanding and modelling the two-phase flow of gas and condensate in porous media are difficult undertakings. Several models and methodologies for production analysis have been developed since the initial research on oil flow in conventional reservoirs [31].

There are three primary flow areas that extend outward from the wellbore that are responsible for fluid flow towards a gas condensate well that is producing from a depleting reservoir. They are:

Region 1: A near well bore area (inner) where both gas and oil flows simultaneously.

Region 2: A condensate build-up area where only gas is mobile, and condensate is practically immobile.

Region 3: Region that contains only single-phase fluid (original reservoir fluid).

These three regions will exist when the reservoir reaches at a pseudo-steady state [4].

Near Well Region (Region 1): In gas condensate wells, these region causes the flow resistance and deliverability loss. The extension of this area and the relative permeability of gas determines the well deliverability. Liquid saturations control the relative permeability of gas. Studies show that the extend of this area increases with time.

The Condensate Build-up Region (Region 2): Here only gas will flow, and the condensate is normally remaining immobile. The condensate saturation can be calculated by CVD experiment. Some empirical equations have been suggested also. The saturation increases towards the well as pressure continues to decrease.

The Single-Phase Gas Region (Region 3): Only single-phase gas exists there in an undersaturated condition. the gas composition is constant in the region.

The conditions for existing various flow regions are summarized in Table 2.2.

Table 2.2: Coexistence of flow regions [4]

Region	Conditions		
	$P_{wf} > P_d$	$P_R < P_d$	$P_{wf} < P_d$ and $P_R > P_d$
1		Exist	Exist
2		May Exist	May Exist
3	Exist		Exist

2.5 FIELD DESCRIPTION

The Kailashtilla field is situated approximately 15 kilometers east of Sylhet town in northeastern Bangladesh. It spans a structure that is 10 kilometers in length and 5 kilometers in width, trending from southwest to northeast. Kailashtilla Field was discovered by Pakistan Shell Oil Company (PSOC) in 1961 and developed by the Bangladesh National Company and is now operated by Sylhet Gas Fields Limited (SGFL).

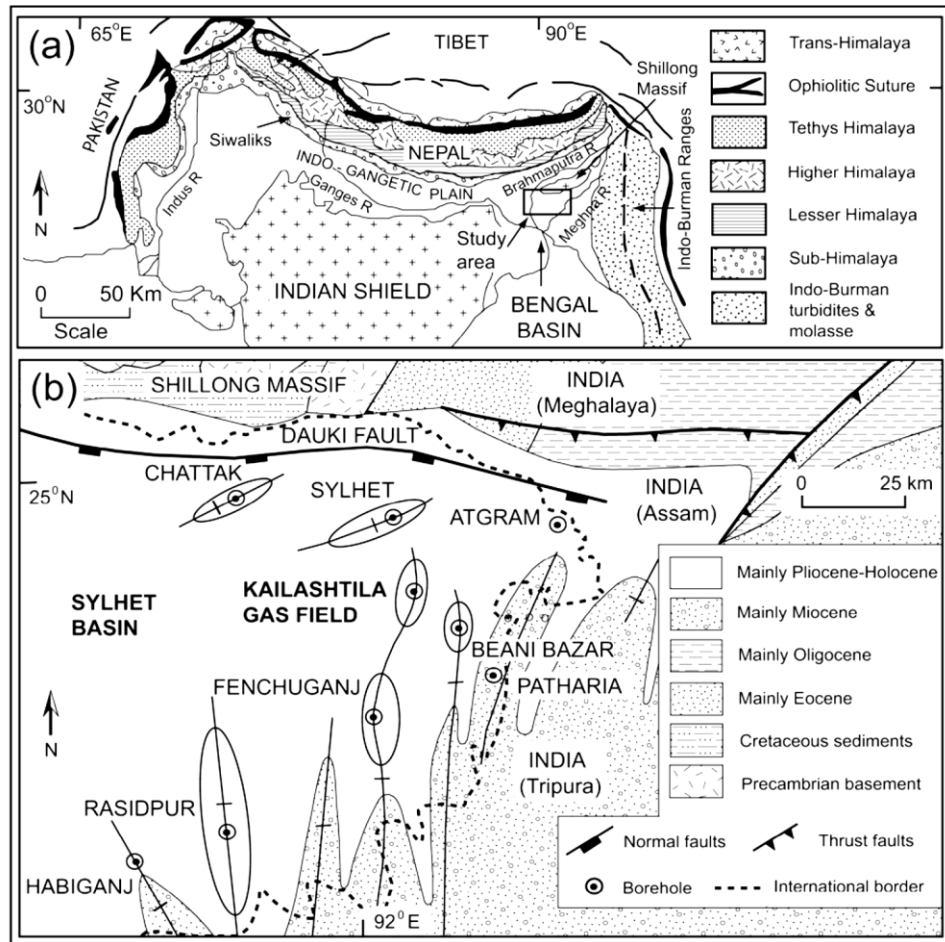


Fig. 2.2: Map of the Bengal Basin and adjoining areas and major geographic features [36].

Gas production with condensate started in 1983. Currently the field produces 29 MMscfd of gas and 402 bbl condensate per day Gas from wells KTL-1 and KTL-5 is being processed through a solid desiccant (silica-gel) plant of 30 MMSCFD capacity. Only 757 Bcf gas has been produced over the last 40-year period from 1983 to 2023 whereas initially gas in place (GIIP) is 3.54 Tcf; reported by RPS Energy in 2009 [37-39]. Middle Gas Sand poses GIIP about 0.72 Tcf. Mahmud et al. suggested drilling one well in MGS and one well in UGS can produce 180 MMscfd plateau for 14 years with 64.71% recoveries.

The Kailashtilla structure is in the Northeast Surma basin of Bangladesh. From regional tectonic history, the north-south trending elongated anticline Kailashtilla structure is quite young and formed during Late Pliocene-Early

Pleistocene time 3, 5 and has developed in the foredeep located west and south of massive orogenic uplifts. Hossain et al., in 2019 conducted Geochemical composition and biomarker parameters on gas condensate samples from this field and examined the origin, maturity and accumulation mechanism of hydrocarbons in the Sylhet structure. It revealed this gas condensate is composed predominantly of methane (85.81 wt.%), ethane (6.68 wt.%), propane (2.13 wt.%), and minor amounts of higher hydrocarbons.

The reservoirs are composed of sandstone and shale and considered to have deposited in the delta or delta front environment. The gas is producing from sand layers of about 7000 to 9000 feet depth of early to late Miocene age. These can be subdivided by Upper Gas Sand (UGS), Middle Gas Sand (MGS), Lower Gas Sand (LGS). Most of the wells of The Kailashtilla field are producing condensate with gas. Intercomp-Kanada Management Limited (1989) reported oil production with gas and water from well KTL-02. [39-41].

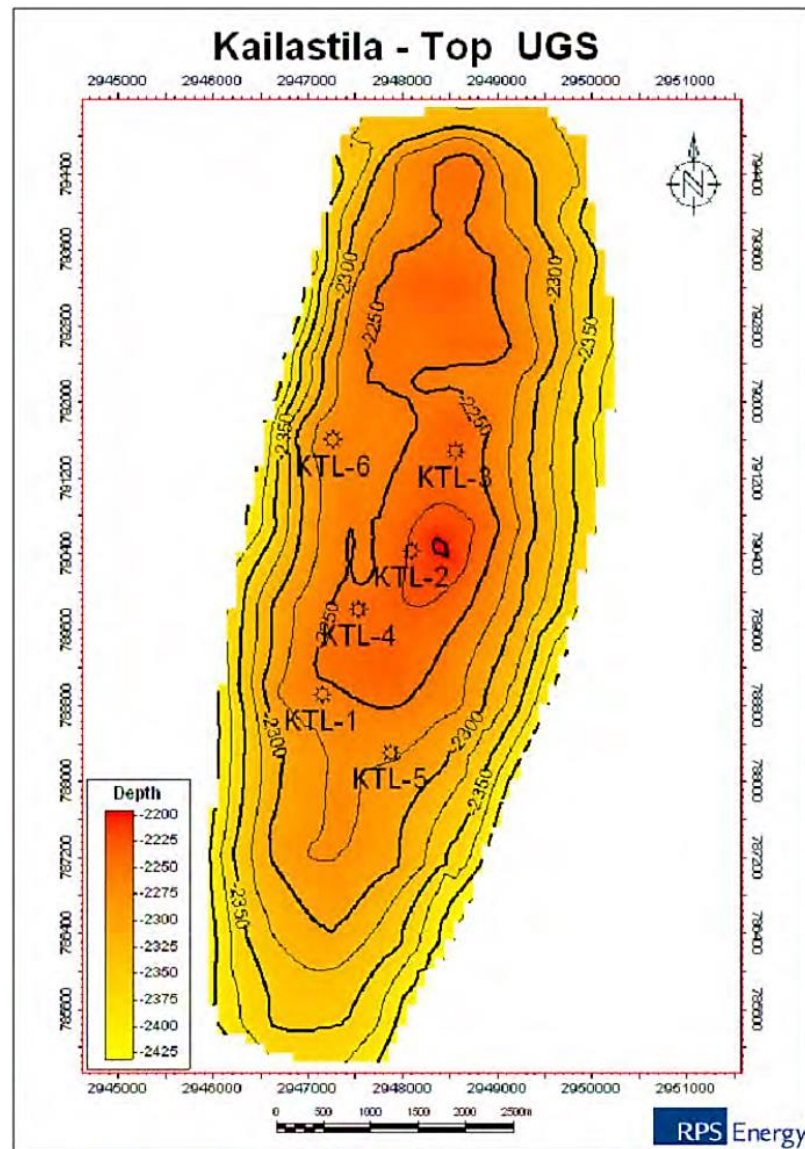


Fig. 2.3 : Depth structure map of UGS [42]

From Well log analysis, Core analysis Md. Mizanur Rahman (2015) reports as Upper Gas Sand poses porosity value 0.21, permeability 501-909 md, water saturation 0.3-0.44.

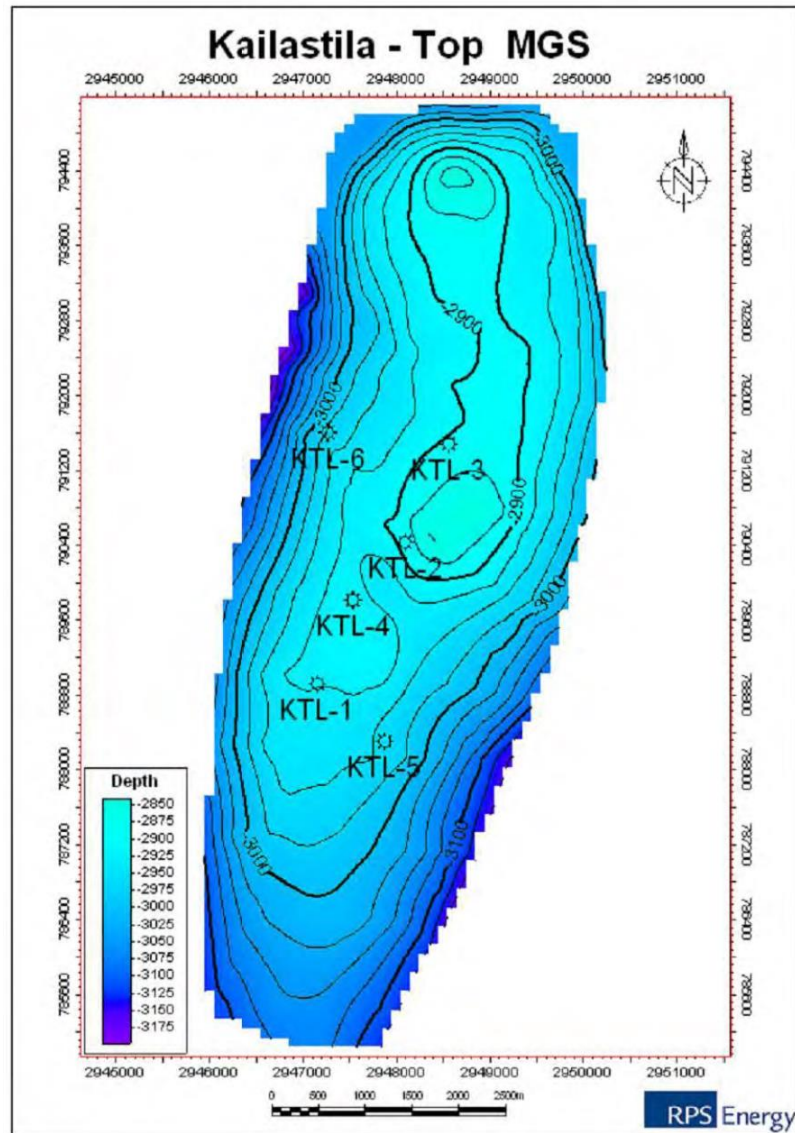


Fig. 2.4: Depth structure map of MGS [42]

For Middle Gas Sand these values are 0.2, 531-753 md and 0.27-0.29. For Lower Gas Sand these values are 0.17-0.20, 206-847 md and 0.37-0.26 [42]. Akter Happy et al. determined the existence of formation cross flow in Kailashtila field which is governed by permeability and skin factor. Gas of Kailashtila has a very high condensate ratio in comparison to other gas fields in the Sylhet region.

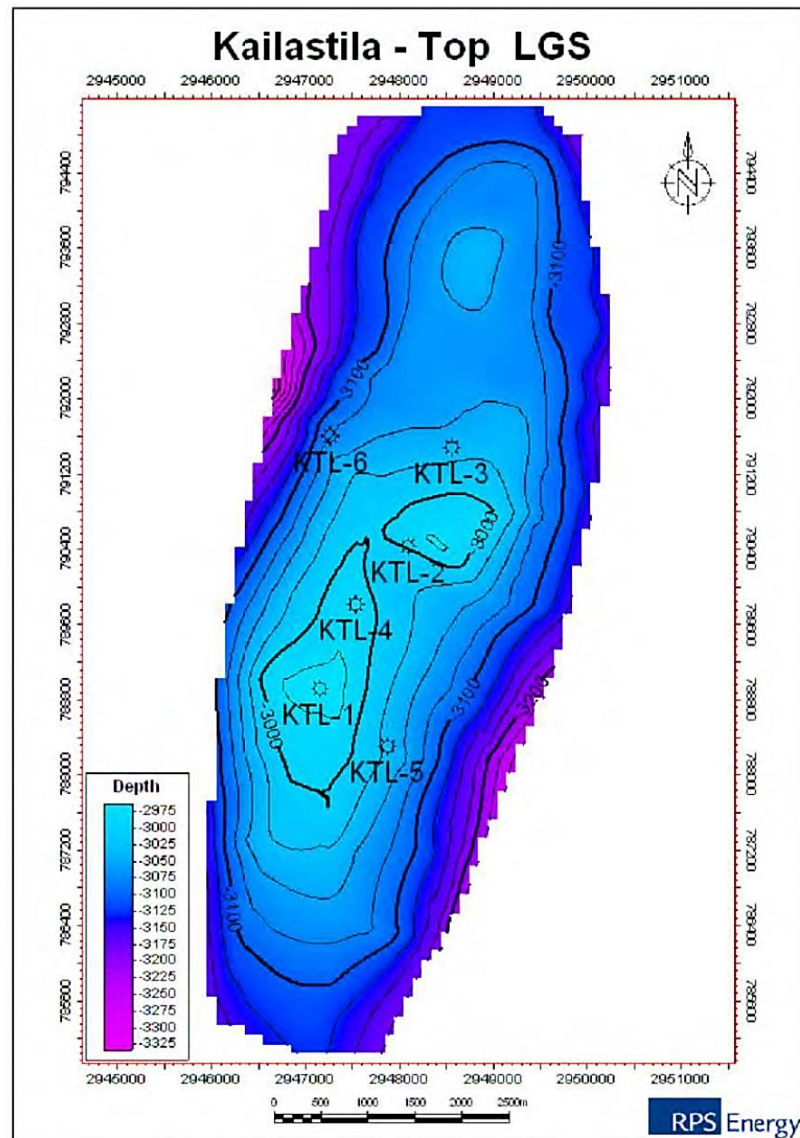


Fig. 2.5: Depth structure map of LGS [42]

The author also works for condensate from Middle Gas Sand. Md. Mizanur Rahman predicted this layer can deliver 19 years at 30.5 MMscfd with recovery factor of 66% which is greater than Upper Gas Sand. The author has used DWSIM software for further analysis. Tangsriwong et al. [43] made a comparison between commercial software Aspen Plus and open-source software DWSIM for modelling chemical processes related to offshore petroleum production facilities. It appeared that these two model's consistent simulation results with real plant data.

2.6 PVT TESTS

In this method, Reservoir fluid samples are taken and sent to a laboratory for a series of tests aimed at identifying the most economical way to produce high-grade products under reservoir pressure and temperature changes to maximize oil and gas field development and production. For example, it is important to understand the circumstances under which the initial one-phase fluid splits into two phases, as well as the composition and properties of each phase. These examinations are referred to as PVT tests, and PVT features are generally expressed as functions of temperature and pressure. The normally used PVT experiments include:

- Composition Analysis
- Constant composition expansion
- Constant volume depletion
- Differential liberation expansion
- Swelling test
- Separator test

2.6.1 Constant Composition Expansion (CCE) / Constant Mass Expansion (CME) Test

The CCE test is typically the first test to be performed on conventional oil or gas condensates after the compositions have been determined in the lab. At reservoir temperature, the test begins at a pressure greater than the bubble point pressure and progressively lowers the pressure (thus the volume being spent at constant composition). The test yields the bubble point, also known as the dew point, and the fluid characteristics that vary with pressure and temperature [44].

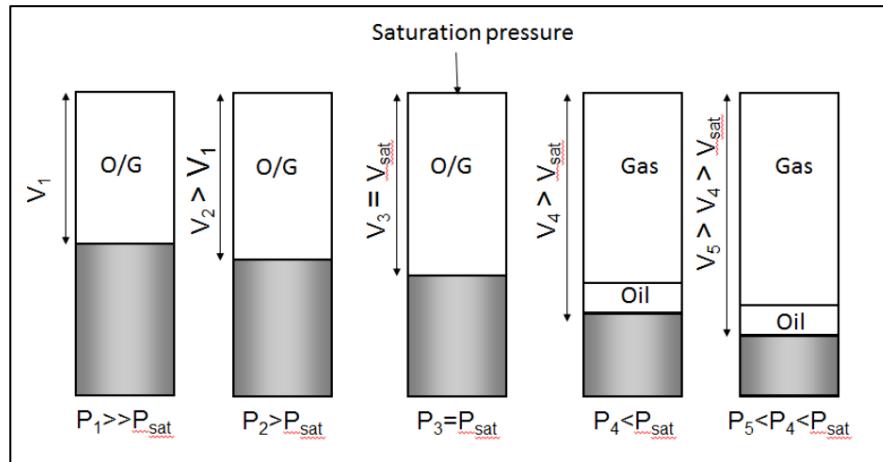


Fig. 2.6: Constant Composition Expansion / Constant Mass Expansion Test [44]

2.6.2 DL (Differential Liberation) Test

The DL test gradually lowers the pressure at a constant temperature, starting at the bubble point pressure (for conventional oil) or dew point pressure (for gas condensate). At every stage, the amounts of gas and oil are monitored, and the gas that has been used up is gathered. Like the CCE test, the goal of the DL test is to comprehend the reservoir fluid's phase behaviour and PVT characteristics under certain reservoir conditions. Additionally, it is to find out how much oil is in the reservoir under standard conditions versus under reservoir conditions, i.e., the gas and oil formation volume factors, B_o and B_g .

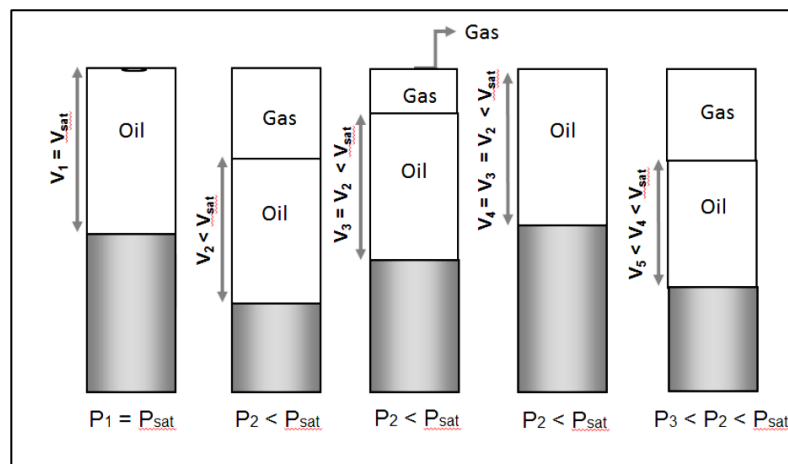


Fig. 2.7: Differential liberation test [44]

2.6.3 CVD (Constant Volume Depletion) Test

The saturation volume at the dew point, or V_{sat} , is measured by the CVD test, which begins at the gas condensate's dew point pressure. The two phases of gas and oil are formed by an increase in volume when the pressure drops. To maintain a constant pressure and the combined volume of the two phases equal to the saturation volume, the gas is exhausted through a valve located at the top of the cylinder (see to the schematic diagram). Both the percentage of liquid dropout of the liquid volume relative to the saturation volume and the percentage of depletion gas relative to the original gas are measured. The PVT characteristics of the volatile oil or gas condensate, as they may vary at each production stage, are acquired [44].

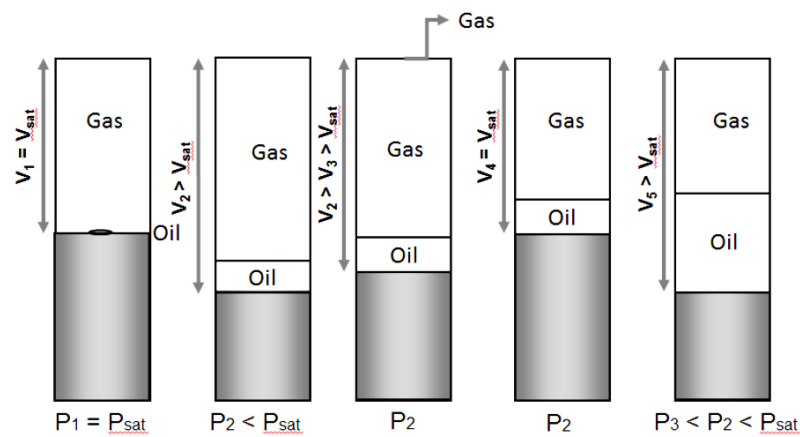


Fig. 2.8: Constant volume depletion [44]

2.6.4 Separator Test

Optimizing the amount of oil produced at the surface is the goal of the separator test. Oil and gas condensate are tested in one or more separators, with the final step being conducted at room temperature and atmospheric pressure.

Within the laboratory cell, a reservoir fluid sample is heated to the reservoir's temperature and pressure to the bubble point. Subsequently, the gas is released and brought back to standard conditions, and the oil is ejected from the cell to the next separator stage. Until stock tank conditions are met, the procedure is

repeated. In the test, the oil formation volume factor, B_o , and the solution GOR are measured.

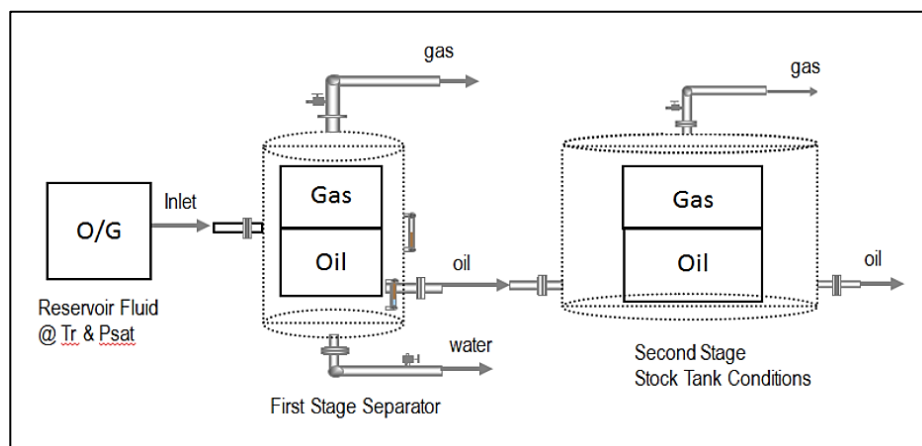


Fig.2.9: Separator test [44]

2.7 CONDENSATE CHARACTERIZATION

The petroleum stream is a mixture of the complicated hydrocarbon chain, but it is not convenient to analyse such a mixture from a compositional perspective since the constituent composition cannot accurately reflect the composition of the stream. The distillation curve is used to identify the streams, which are typically characterized by small petroleum cuts or pseudo-components. When identifying pseudo-components, the most important parameters are the boiling temperatures and specific gravities. Other characteristics, such as molecular weight, critical pressure, temperature, and Watson characterization factor, are needed in the process calculation steps. These characteristics can be predicted with the use of boiling point and specific gravity [44,45]. Since feedstock assays offer a comprehensive and in-depth study of hydrocarbon data, they are crucial to the refining process. Gas condensate differs from distillate, a straw-coloured liquid primarily made of naphtha, in a refinery in that it is more like to the product that is typically obtained by distilling the volatile portion of crude oil. Regarding hydrocarbon components, pentane is the main constituent of the condensate; nevertheless, lighter hydrocarbon, like as methane, ethane, propane, and butane, or higher hydrocarbon up to C_8 maybe

present in the gas condensate [46]. The ASTM distillation is performed in laboratory which then converted into TBP distillation data.

2.7.1 Defining Pseudo-Components

As they are employed in calculations of the thermophysical and thermodynamic parameters of the refinery feed, pseudo components serve as the foundation for characterizing the petroleum fraction in a refining process. Fractionation can detect a limited number of mixtures with a defined range of boiling points, but the actual components are still unknown. The combination has a predetermined cut point or boiling point range, is referred to as a pseudo component, and corresponds to several unknown true components. Each pseudo-component has a specific gravity, molecular weight, and average normal boiling point. Once the normal boiling point and specific gravity are established—which are ascertained from the TBP curve and the gravity vs volume distilled curve—one may treat the pseudo component as stated [47].

2.7.1.1 Generating Pseudo-components:

The petroleum fraction's cuts have qualities including viscosity and API gravity, as well as a defined boiling point range. Pseudo components, which are mixtures of multiple unknown actual components, are used to represent petroleum fractions since it is impossible to determine their exact component makeup. A TBP curve's cut point count specifies how many pseudo components it has; a larger cut point count aids in an accurate reproduction of the TBP curve [48]. A high number of components can cause the computation time to increase even though more are needed to create a smooth property curve. Considering these two facts, a general rule has been proposed.

Table 2.3: Cut point ranges for refining calculations

TBP range	Number of cuts
<37.8°C (100°F)	use actual components (pentenes and lighter)
37.8-427°C(100-800°F)	28
427-649°C(800-1200°F)	8
649-871°C(1200-1600°F)	4

2.8 SUMMARY AND IMPLICATIONS

The research on gas condensate reservoirs, the application of EOS in estimating the phase behaviour of petroleum reservoirs, multi-phase flow modelling, the characterization parameters of petroleum chains, and field descriptions are the main topics of the literature review. The study discovers that condensate reservoir modelling uses EOSs. The study concludes that a specific model is required to monitor the flow conditions close to the wellbore, as well as an appropriate methodology for evaluating the quality and performance of condensate and attempting to close the gap.

Chapter 3 : RESEARCH METHODOLOGY

The study strategy used in this chapter tries to accomplish the goals and objectives mentioned in section 1.3 of Chapter 1. The research design, the stages by which the methodology was [will be] implemented, and the methodology itself are covered in Section 3.1; the study's participants are described in Section 3.2; all of the instruments used in the study are listed in Section 3.3 and their use is justified; Section 3.4 outlines the procedure to be followed and the deadline for completing each stage of the study; Section 3.5 addresses how the data was [will be] analysed; and, finally, Section 3.6 addresses the research's ethical considerations as well as any potential issues or limitations..

3.1 METHODOLOGY AND RESEARCH DESIGN

The next section goes into the design process and research technique.

3.1.1 Methodology

In the analytical process, the careful coordination of all parameters is required to test a gas condensate sample. So, the procedure of sampling, laboratory analysis of the collected sample, testing equipment design, and the design and analysis of the test are critical to the accuracy of the analysis [2,3]. Obtaining a representative formation fluid is very important in testing gas condensate reservoirs. Only this type of sample can truly represent the actual composition and PVT properties of the reservoir.

Testing a condensate reservoir is a special challenge. The retrograde reservoir behaves as if it were formed of two or more concentric regions due to liquid formation. Both liquid and gas comprise the inner region, while the outer region

has a single phase that is gas. The mobility of different fluid in each region is different. And so, conventional composite reservoir analysis can be used.

Fluid properties and a phase diagram for the fluid must be established to analyse a reservoir properly. Darcy's flow law is an empirical relationship that was the first statement of the nature of fluid flow through a porous medium. It has subsequently been ratified in theoretical terms as derivable from the Navier-Stokes equation of motion of a viscous fluid [6,7] For one dimensional, linear, horizontal flow (core flooding experiment), Darcy's law can be expressed in absolute units as

$$q = - \frac{kA}{\mu} \frac{\delta P}{\delta l} \quad \text{Equation 3.1}$$

Here, q = flow rate

k = permeability

A = cross sectional area

μ = viscosity of fluid

To determine the flow of fluid in a black oil reservoir (considering three phase one dimensional flow) the following equations (Equation 3.2- 3.10) are used [6]:

$$\frac{\delta}{\delta t} \left(\frac{\phi S_w}{B_w} \right) + \frac{\delta}{\delta x} \left(\frac{1}{B_w} \mu_w \right) = q_w \quad \text{Equation 3.2}$$

$$\frac{\delta}{\delta t} \left(\frac{\phi S_o}{B_o} \right) + \frac{\delta}{\delta x} \left(\frac{1}{B_o} \mu_o \right) = q_o \quad \text{Equation 3.3}$$

$$\frac{\delta}{\delta t} \left(\frac{\phi S_g}{B_g} + \frac{\phi R_s S_o}{B_o} \right) + \frac{\delta}{\delta x} \left(\frac{1}{B_g} \mu_g + \frac{R_s}{B_o} \mu_o \right) = q_w \quad \text{Equation 3.4}$$

$$S_o + S_w + S_g = 1 \quad \text{Equation 3.5}$$

$$\mu_o = - \frac{K k_{ro}(S_o, S_g)}{\mu_o} \left[\frac{\delta P_o}{\delta x} + \rho_o g \sin \theta \right] \quad \text{Equation 3.6}$$

$$\mu_w = - \frac{K k_{rw}(S_o, S_g)}{\mu_w} \left[\frac{\delta P_w}{\delta x} + \rho_w g \sin \theta \right] \quad \text{Equation 3.7}$$

$$\mu_o = - \frac{K k_{rg}(S_o, S_g)}{\mu_g} \left[\frac{\delta P_g}{\delta x} + \rho_g g \sin \theta \right] \quad \text{Equation 3.8}$$

$$P_o - P_w = P_{cow}(S_w) \quad \text{Equation 3.9}$$

$$P_g - P_o = P_{cog}(S_g) \quad \text{Equation 3.10}$$

These equations are established for the black oil reservoir. This is a system of nine non-linear equations in the nine unknowns. With an appropriate set of boundary conditions and initial conditions, this system can be solved for any location in the reservoir at any time. The boundary conditions are given by the external boundary of the reservoir, together with the well data. The initial conditions are given by the distribution of the fluid saturations and the fluid pressures. A multi-phase flow is considered near the wellbore in a gas condensate reservoir and the objective is targeted to develop a modified flow equation for that region.

3.1.2 Flow Chart:

The following flowsheet describes the work sequence for this thesis

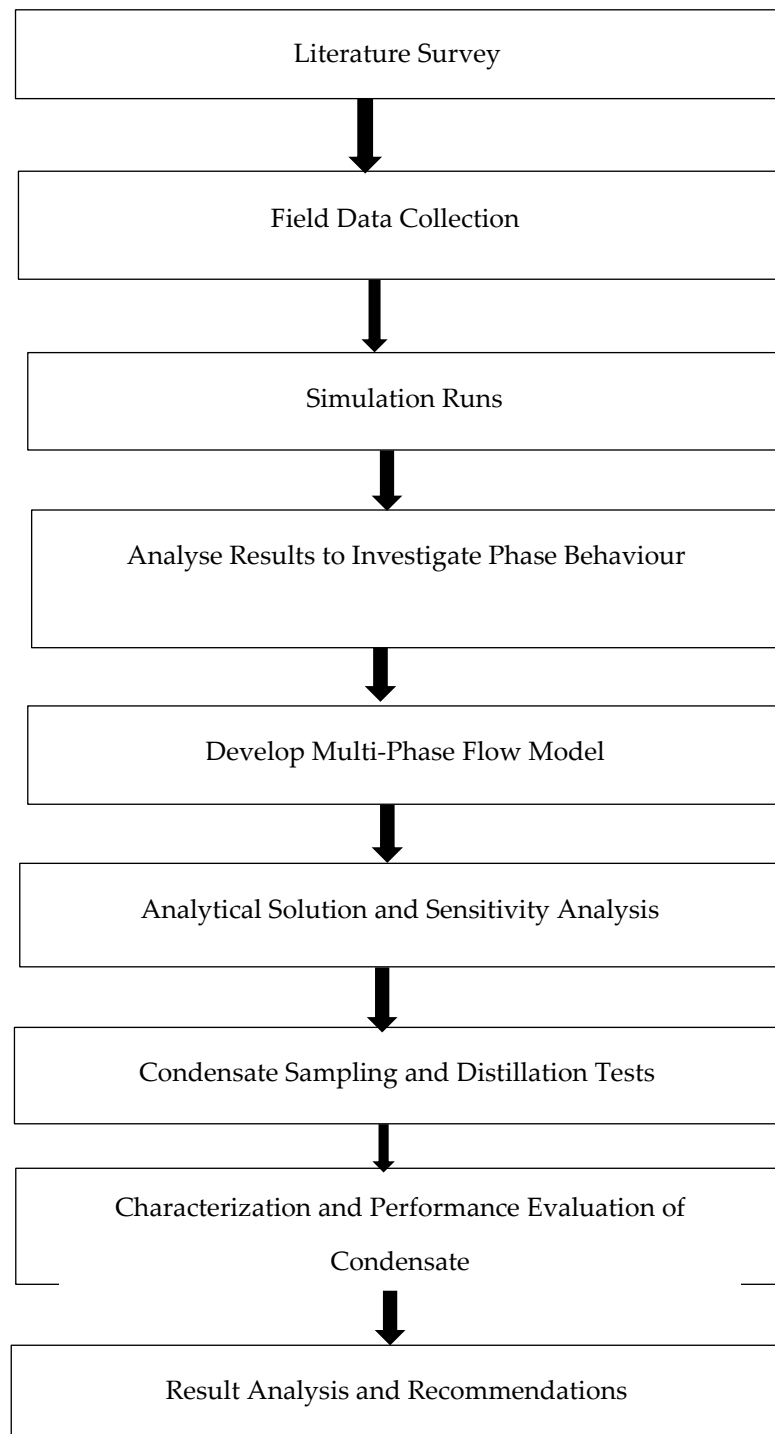


Fig. 3.1: Flow sheet of the research methodology

3.1.2.1 Quantitative

The goal of the study is to identify the fluid and rock characteristics found in the KTL field. After obtaining a representative sample from the field of the studied rock layer, a laboratory experiment is conducted to determine the rock qualities. To ascertain various fluid parameters, samples of the collected fluid from the field are taken using a PVT equipment. After that, simulation is performed to estimate undetermined properties and to generate phase diagram and other property curves. A model is developed to observe the flow response in the wellbore vicinity. Sensitivity tests are performed to observe the response of input parameters. Then the separated liquid sample is tested in an ASTM distillation device to ascertain the distillation qualities.

Table 3.1: Estimated rock, fluid and distillation properties

Sample	Estimated Property
Rock	$\Phi, K, S_w, S_g, P_c, C_t$
Fluid	$B_g, \mu_g, GOR, R_s, \text{Rel Vol}, \gamma_g, \text{Compositional mole fraction}$
Distillation Properties	Density, Distillation Temperature at % Distillate

The Peng-Robinson equation that is used to calculate PVT properties is

$$P = \frac{RT}{V_M - b} - \frac{a\alpha}{v(v+b) + b(b-v)} \quad \text{Equation 3.11}$$

3.1.2.1.1 PVTsim Simulator

PVTsim, a versatile modelling software, allows to estimate fluid properties and experimental PVT data. Table below show the data ranges in the software.

Table 3.2: Input and output parameters of PVTsim

Data	Parameters
Input Data	Compositional Mole Fraction, Saturation Pressure or Temperature, Separator condition, CME, CVD, DLE test data
Output Data	Z-factor, Heat Capacity (Cp), Velocity of Sound, Molecular Weight, Heat Capacity (Cv), Viscosity, Internal Energy Kappa (Cp/Cv), Thermal Conductivity, Enthalpy, JT Coefficient, Interfacial Tension, Entropy. Quality Check, Property curve.

3.1.2.1.2 Model Development

The multi-phase flow model for retrograde gas condensate reservoir is developed considering EOS, conservation of mass law and Darcy's fluid flow equation. The considered equations are

Conservation of mass law:

Mass flow in - Mass flow out = Rate of change of mass in the volume element

$$\bar{\rho}q_M \Big|_{r+dr} - \bar{\rho}q_M \Big|_r = Ah\phi dr \frac{\partial \bar{\rho}}{\partial t} \quad \text{Equation 3.12}$$

An EOS to relate volume or density to pressure and temperature

$$C_t = -1/v \left(\frac{\partial v}{\partial P} \right) \quad \text{Equation 3.13}$$

And Darcy law

$$Q = \frac{KA}{\mu} \frac{\partial P}{\partial r} \quad \text{Equation 3.14}$$

To analyse the sensitivity following equation has been taken into considerations

$$q_M = q_{MW} \cdot \frac{r}{r_w} \cdot e^{D_1(r-r_w)} \quad \text{Equation 3.15}$$

3.1.2.1.3 Conversion between ASTM and TBP Distillation

Since the TBP distillation is a lengthy process, this seems tiresome in some cases. However, the TBP data gives detailed information on the volatile characteristics of crude oil or petroleum fractions. Existing literature has different methods for the conversion between ASTM and TBP distillation

Riazi and Daubert (1980) have developed a relation to performing the inter-conversion of the ASTM method and TBP distillation. API in 1993 also recommends their equation for the conversion in the form (Equation 3.16)

$$TBP = a(ASM\ D86)^b \quad \text{Equation 3.16}$$

Here a and b are constants. The variation of the constants with percent of liquid sample distilled has been included in Appendix A. TBP is calculated at a defined distillate point (like 0, 10, 30, 50, 70, 90, and 95 percent point), where the temperature is expressed in °R. In this method, the error existing between the calculated and measured TBP value is 5°C (41°F).

3.1.2.1.4 Daubert Method

In 1994, Daubert proposed an updated method for the inter-conversion based on the initial and final temperatures of distillation curves. The equations (Equation 3.17) suggested by Daubert are

$$T'_{50} = A_4(T_{50})^{B_4}, \quad T'_{30} = T'_{50} - \Delta T'_3, \quad T'_{10} = T'_{30} - \Delta T'_2, \quad T'_0 = T'_{10} - \Delta T'_1$$

Equation 3.17

Where $\Delta T'_i = A_i(\Delta T_i)^{B_i}$, $\Delta T_1 = T_{10} - T_0$, $\Delta T_2 = T_{30} - T_{10}$, $\Delta T_3 = T_{50} - T_{30}$, $\Delta T_5 = T_{70} - T_{50}$, $\Delta T_6 = T_{90} - T_{70}$, $\Delta T_7 = T_f - T_{90}$

The symbols T and T' stand for ASTM D86, and TBP temperatures, respectively, and are in °F. The subscripts 0 and f stand to represent the initial and final temperatures. A_i and B_i express the constants, and the values are given in Appendix A. The average error between the actual and calculated TBP value for this method is about 3°C (37.4°F).

3.1.2.1.5 DWsim Software

With the use of accurate thermodynamic and unit operations models, DWSIM enables the modelling, simulation, and optimization of both dynamic and steady-state chemical processes. This study employed the tool to assess the energy consumption throughout the distillation process and to characterize the

assay. Here the TBP data, molecular weight and compositional analysis of the stream have been used as input parameters.

3.2 SAMPLES

The reservoir rock and fluid properties, compositional mole fraction for upper, middle, and lower gas sand are collected from online resources. The Flow-After-Flow test and production tests are performed by PetroBangla and Al Mansoori Wireline Service. Gas and condensate samples are collected from separator at separator pressure and temperature. Standard procedures are followed to collect them. Sample Cylinder Shutting Pressure is 690.00 psia and Sample Cylinder Opening Pressure is 560.00 psia. Using SCION 456-GC the compositional weight% of the sample is determined. The condensate samples are then collected to observe the distillation properties. Here ASTM D86 apparatus is used to estimate the temperature at volume % distillate. ASTM D1298 apparatus is used to determine the density of the sample. The distillation and compositional analysis are performed at the quality control laboratory of Super Refinery Pvt. Ltd. (SRL).

3.3 INSTRUMENTS

3.3.1 SCION 456 GC

In this instrument, Hydrogen gas is used as carrier gas. Liquid nitrogen or carbon dioxide has been used to cool down the samples. Samples are collected at a vile and then put into the chamber. The samples are divided into components as it passes through the chromatograph column. As the separated components exit the column, they pass through a detector. The detector responds to the chemical and physical properties of different components. The signals generated by the detector are then analysed by the chromatograph's software.

Table 3.3: Flow/Pressure and Temperature condition [50]

Initial conditions	Pressure (psi)	Hold (min)
Front EFC-24 (Ar)	27.5	10
Middle EFC-24 (Ar)	38.5	10
Total Flow	60 ml/min	
Column Oven Temperature	70 °C	
Valve Oven Temperature	100 °C	

At first, both valves are kept in the (-) position and any flow to FID is kept switched off. Then the hemethanizer is set to 20 milliliters per minute while monitoring the flow at the FID's outflow. Next the H₂ flow is kept off and front EFC-24 flow is adjusted until 30 ml/min of Ar exit the FID. After that valve number two is turned on to the (+) position. The digital manual flow controller is set Set at 30 m/min to match the reference TCD flow and the H₂ Execute launched the procedure as instructed. The system is prepared to determine the best column selection time after the TCD and FID signal have stabilized. At the molecular sieve column, gas/oil mixture is injected containing carbon monoxide, hydrogen, oxygen, nitrogen, and methane. To elute the components from the Hayesep column, valve 2 can be turned to the (+) position once the CO peak has been eluted. The sample delivery time in the two valve is determined against the standard retention time, the peak area is determined, and composition is detected.

3.3.2 ASTM D86 Test Method

In this process, the collected sample (usually 100 ml in amount) is distilled in a flask under specific conditions (ASTM D86, 2007). The flask is connected to an inclined condenser that condenses the rising vapors. A graduated cylinder collects the distilled fractions, and the temperature of the rising vapors is recorded at a specific interval of collected distillate. The initial boiling point (IBP)

refers to the temperature at which the first drop of condensate is collected. When almost the entire sample is distilled (above 95%), the corresponding maximum temperature is called the endpoint (EP).

3.4 PROCEDURE AND TIMELINE

Prior to starting the investigation, the topic's literature background was examined. Next, the Kailashtila gas field was selected as a condensate-producing production. The Sylhet gas field is then used to gather information on the compositional and other characteristics of the rock and fluid. Al Mansoori Wireline Service Ltd. and PetroBangla prepared the field where the pressure test data were also gathered. Next, in order to generate the missing data and double-check the accuracy of the results, another study is conducted using the PVTsim modelling software. Subsequently, a mathematical model is suggested that considers existing and proven theory. The model's validity is validated using reservoir fluid and pressure test data from the KTL field. Following that, SRL conducts an experiment using a sample of gas and condensate. After then, the data are examined to see if they match the goals and conclusions of the research. The process required 2.5 years from the time of data and sample collection to the results.

Table 3.4: Time frame for work

Work Schedule	Time Duration
Literature Survey	1.5 years
Field Data collection	1 month
Simulation	2 weeks
Analysing Phase Behaviour	2 months
Model Development and Sensitivity Analysis	6-7 months
Condensate Performance Evaluation	2 months
Result Analysis and Findings	1 month

3.5 ANALYSIS

First, the research works are reviewed, and the implications and flaws of the works on gas condensate reservoirs, such as modelling, phase behaviour analysis, sampling, and well deliverability of gas condensate wells, are attempted to be ascertained. After taking the suggestions into account, the study concentrated on figuring out the phase behaviour through simulation and real-time experimentation. Next, the data from the pressure transient and well deliverability tests are compared to a suggested model. The study determines a systematic method for approximating the properties of condensate as fuel; hence, the last part of the work examines a methodical approach to characterizing condensate and calculates the energy required to distil the fluid.

3.6 ETHICS AND LIMITATIONS

Thirty years of data was used to analyse phase behaviour. Despite the best efforts, the author was unable to obtain authorization to gather the most recent reservoir and pressure data. The accurate interpretation of the field behaviour is threatened by the lack of recent data. The correctness of the model is then verified using theoretical data. However, it was not feasible to verify the veracity in an actual field. Therefore, it could make people wonder if the model answer will be accepted. Considering the outcomes of simulations and experiments, the condensate's performance was assessed. There is not a sensitivity or economic test carried out to guarantee the accuracy of the results. These represent the study's limitations. The author made every effort to get around these restrictions by running the tests on many instances. To clear up any misunderstandings regarding the accuracy of the data, the error for both expected and experimental outcomes are provided.

Chapter 4 : PHASE BEHAVIOR ANALYSIS OF KAILASHTILA GAS FIELD

This chapter presents the results of the simulation, the experimental PVT properties, and the computation. To provide a look on the field's phase behavior, the fluid's and the rock layer's characteristic curves are displayed.

4.1 ROCK AND FLUID PROPERTIES OF KTL FIELD

The study integrated results generated from IPEC/EXPRO test, core lab tests, production tests, PVT tests gained from KTL well 1, 2 and 3. Three distinct commercial accumulation of hydrocarbon were found at three sand layer namely upper, middle and lower gas sand. All zones contain lean gas while showing a very limited retrograde behavior. Lack of representative fluid composition and complicated validation method have risen the urgency of estimating error between reserve and resource calculation. To evaluate the error, the formation volume factor is taken into considerations where the values are ranges between 0.00443 and 0.00463 Rvol/Svol and 0.00389 and 0.00391 Rvol/Svol for upper and lower gas sand, indicating an error of approximately 4.5%. The LGR was found to range between 9 to 155 bbl/MMscfD. Table 4.1 compiled the various rock properties data for Kailashtila gas field and Table 4.2 shows the compositional fraction for upper and lower sand.

Table 4.1: Kailashtila gas field properties for upper, middle, and lower sand field

Property name	Value		
	UGS	LGS	MGS
Specific Gravity	0.628	0.63	0.63
Reservoir temperature, °F	152	172	171
Initial Reservoir Pressure, psia	3332	4366	4263
Pseudo- reduced temperature	1.691	1.745	-
Pseudo- reduced pressure	5.02	6.583	-
Z factor	0.851	0.954	0.954
Initial Gas formation volume factor, Rvol/Svol	0.00442	0.0039	0.00396
Area, acre	640	640	2725
h_{avg} , ft	179	166	84.2
Porosity	0.2	0.18	0.18
Permeability, md	386.6	287.1	126
Compressibility, 1/psi	0.000155	0.000168	-
Viscosity	0.021	0.02	-
$S_g=1-S_w$	0.84	0.84	0.84
G in place	150.8	168.9	-
P sat	2725	2814	2814
Molecular weight, lb/mol	18.3	18.3	18.3
GWC	Not found	-	Not found
LGR (approx.) bbl/MMscf (lean gas)	11.2	11.7	11.7
Depth, ft	7500	9800	9600

Certain MGS data are deemed comparable to LGS for computational ease.

Table 4.2: Upper and lower sand fluid composition

	UGS	LGS
Compositions	Mole Fraction	Mole fraction
N2	0.0038	0.008
CO2	0.0005	0.0019
C1	0.9403	0.9415
C2	0.0273	0.0271
C3	0.0102	0.0088
i-C4	0.0026	0.0022
n-C4	0.0029	0.0023
i-C5	0.0015	0.0013
n-C5	0.0009	0.0007
C6	0.0014	0.0019
C7	0.0026	0.0035
C8	0.0028	0.0038
C9	0.0013	0.0017
C10	0.0006	0.0008
C11	0.0003	0.0004
C12	0.0002	0.0003
C13	0.0002	0.0003
C14	0.0002	0.0003
C15	0.0004	0.0005
Total	1	1.0073

The sandstones reservoirs in Bangladesh are water wet, though the experimental results were failed to generate results for water cut. The two-phase relative permeability and capillary pressure functions are presented in Table 4.3. Gas saturation and capillary pressure curve is depicted in Fig. 4.1. Gas water relative permeability curve is presented in fig. 4.2.

Table 4.3: The Relative permeability and capillary Pressure function

Sw	Krw	Krow	PCW,psia	KRG	KROG	PCG,Psia
0.16	0	1	53.33334	1	0	0
0.165	0.000001	0.928	38.3333	0.937	0.013	0
0.175	0.000002	0.904	24.9000	0.8871	0.013	0
0.2	0.000004	0.857	12.1737	0.687	0.027	0
0.225	0.000006	0.821	8.3000	0.557	0.043	0
0.25	0.000008	0.785	6.0000	0.443	0.053	0
0.275	0.00001	0.7495	4.0000	0.35	0.07	0
0.3	0.00002	0.714	2.8178	0.251	0.087	0
0.35	0.00009	0.643	1.3000	0.13	0.11	0
0.4	0.00026	0.571	0.6000	0.067	0.143	0
0.45	0.00079	0.5	0	0.03	0.175	0
0.5	0.00308	0.428	0	0.013	0.2	0
0.55	0.017	0.357	0	0.004	0.225	0
0.6	0.056	0.286	0	0	0.25	0
0.7	0.175	0.143	0	0	0.3	0
0.8	0.391	0	0	0	0.37	0
0.9	0.662	0	0	0	0.5	0
1	1	0	0	0	1	0

Fig. 4.1 and 4.2: represents the water wet behavior of the concerned field.

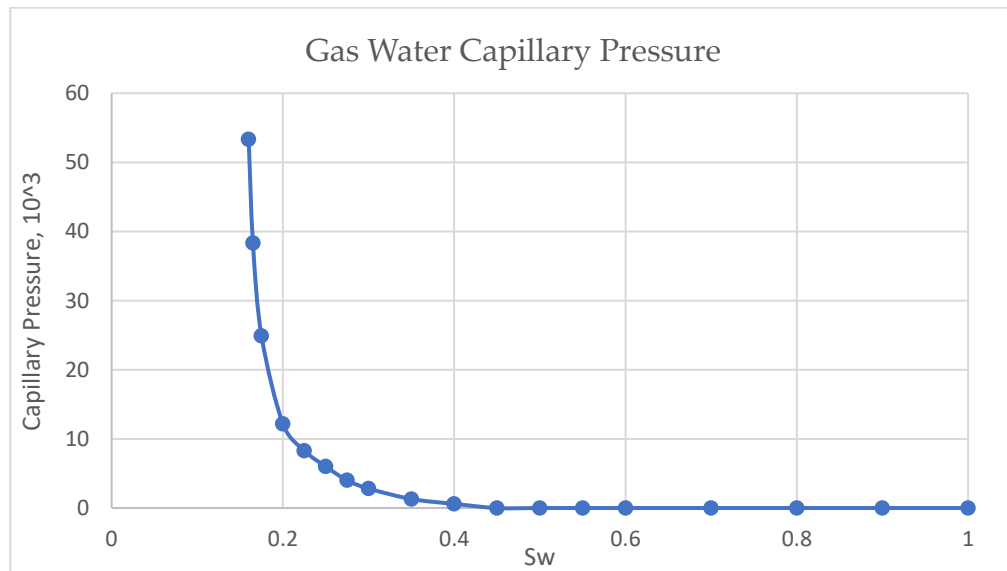


Fig. 4.1: Gas saturation and capillary pressure curve

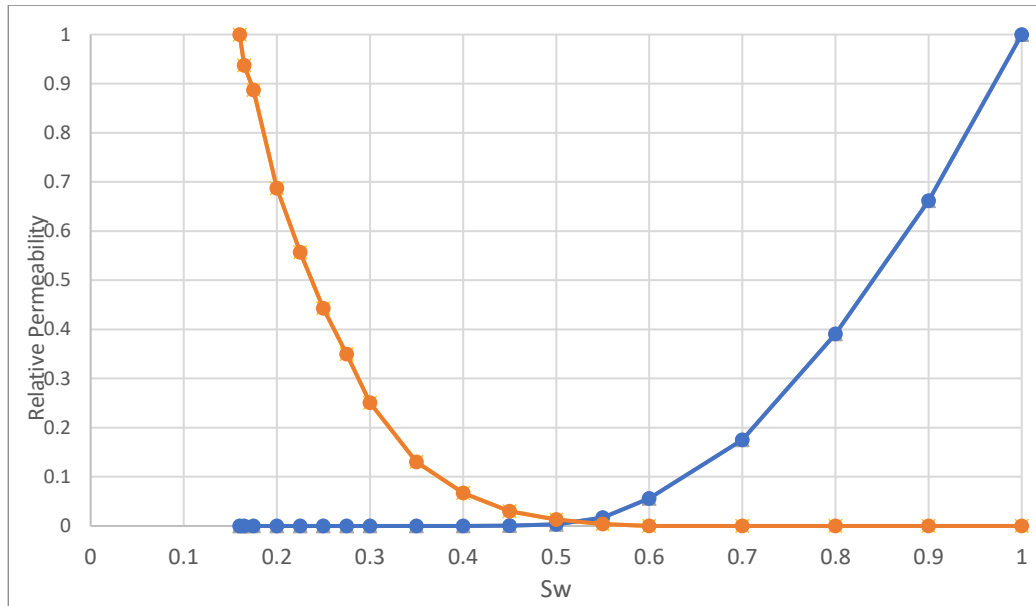


Fig.4.2: Gas water relative permeability curve

The phase diagrams for upper and lower sand are generated using PVTsim software considering the PR Peneloux correction factor for compositional data.

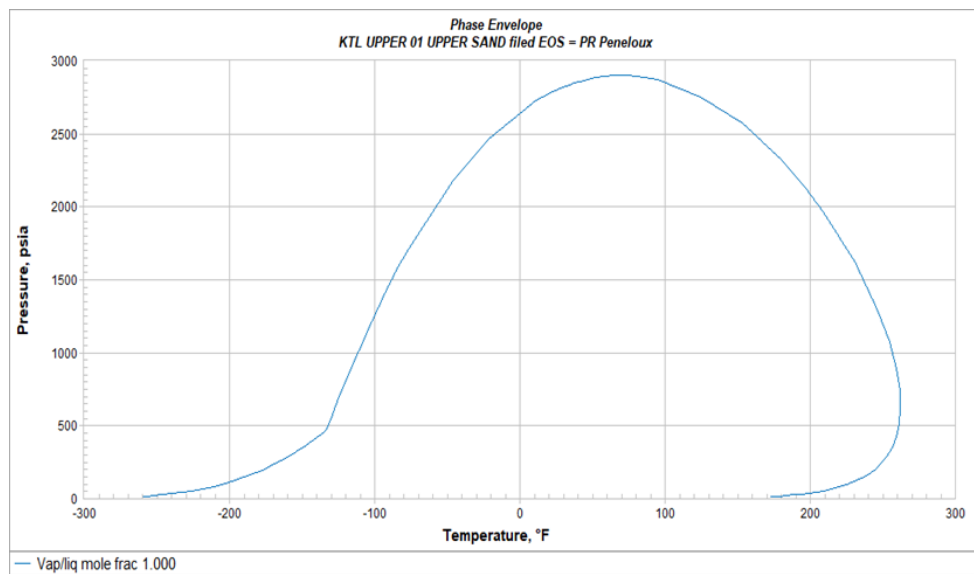


Fig.4.3: Phase diagram for UGS

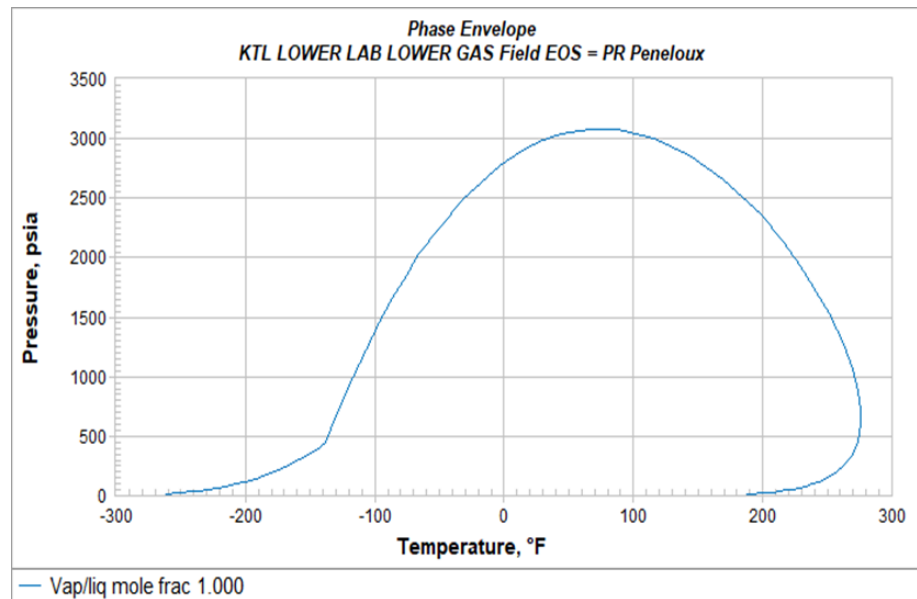


Fig.4.4: Phase diagram for LGS

The phase behavior for upper and lower sand are represented in Fig. 4.3 and 4.4. The temperature ranges between -300°C to the reservoir temperature and pressures are varying between 14.7 psia to reservoir pressure condition for both layers. The critical points could not be located from the curve and so later generated by incorporating empirical equation.

4.1.1 Upper Gas Sand (UGS) Fluid Composition and Properties

The PVT experiment is run to determine phase condition with varying pressure. The IKM's EOS is used to determine the fluid composition at reservoir condition. Using Peng Robinson, Soave Redlich Kong Eos formula the saturation pressure was determined, which is in close agreement with the experimented value. The saturation pressure is calculated as 2725 psia, 500 psi below the original reservoir pressure, is considered as a representative of the reservoir fluid. To estimate the LGR performance with pressure depletion, two additional constant composition tests were run using PVT. The sample recombination ration of 11.2 bbl/ MMscf is matched with core lab test data and the historical production LGR of 11.5 bbl/ MMscf. In the separator run, the pressure and temperature is set to 1000 psi and 50°F.

Table 4.4: Constant Composition Expansion for upper gas sand fluid

IPEC Upper Sand Fluid Composition (PVT EOS simulator)						
Constant Composition Expansion						
Pressure, psia	Vol fraction , liquid	Z factor	Formation Volume Factor, R vol/S vol	Gas gravity, rel. air	liq gravity, rel H2O	Gas Viscosity, cp
3345	0.0000	0.8613	0.0045	0.6916	0.0000	0.0234
3000	0.0000	0.8502	0.0049	0.6916	0.0000	0.0217
2725(P _s)	0.0000	0.8444	0.00536	0.6916	0.006295	0.0203
2500	0.0013	0.8431	0.00583	0.6889	0.6307	0.0192
2000	0.0030	0.8491	0.00735	0.6833	0.6355	0.0171
1500	0.0033	0.8683	0.01001	0.6786	0.6465	0.0153
1000	0.0025	0.9006	0.01558	0.6753	0.6648	0.0141
500	0.0011	0.9448	0.03269	0.6753	0.6898	0.0133
100	0.0001	0.9879	0.17091	0.6829	0.7103	0.0129

4.1.2 Middle Gas sand Fluid (MGS) Composition and Properties

KTL3 is the only completed well in the middle zone and data couldn't be generated during the production tests. Since the estimation of the fluid composition was not successful, the lower gas sand properties are assumed to be same for the mid zone.

4.1.3 Lower Gas sand Fluid (LGS) Composition and Properties

The fluid compositions are found like that of the UGS fluid compositions. No liquid production by zone was determined and so the recombined ratio or LGR was considered to determine the fluid composition. Since the LGR estimated from IPEC/EXPRO and core lab tests has shown a great diversity, material balance, using the total well stream and upper sand composition, is used to generate the lower gas sand fluid composition. The apparent LGR for IPEC/EXPRO and PVT experiment is 11.7 and 13.4 bbl/MMscfd. The dew point pressure is calculated as 2813.5 psia where the separator condition was maintained at 1000 psia and 50°F.

Table 4.5: Constant Composition Expansion for lower gas sand fluid

IPEC US Fluid Composition (PVT EOS simulator)						
Constant Composition Expansion						
Pressure , psia	Vol fraction, liquid	Z factor	Formation Volume Factor, R vol/S vol	Gas gravity, rel. air	liq gravity, rel H2O	Gas Viscosity, cp
4379	0.0000	0.9238	0.00377	0.6987	0.0000	0.0276
4000	0.0000	0.9041	0.00404	0.6987	0.0000	0.0259
3500	0.0000	0.8821	0.0045	0.6987	0.0000	0.0236
2813.5 (P _s)	0.0000	0.8621	0.00547	0.6987	0.0000	0.0205
2500	0.0021	0.8601	0.00615	0.6941	0.5813	0.019
2000	0.0038	0.8656	0.00773	0.6877	0.5905	0.017
1500	0.0039	0.8825	0.01051	0.6826	0.6018	0.0155
1000	0.0029	0.911	0.01628	0.6793	0.6157	0.0143
500	0.0013	0.9502	0.03395	0.6797	0.6321	0.0136
100	0.0001	0.989	0.1767	0.6883	0.6496	0.0132

The PVT properties curve for upper and lower gas sands are shown in Fig. 4.5 and 4.6.

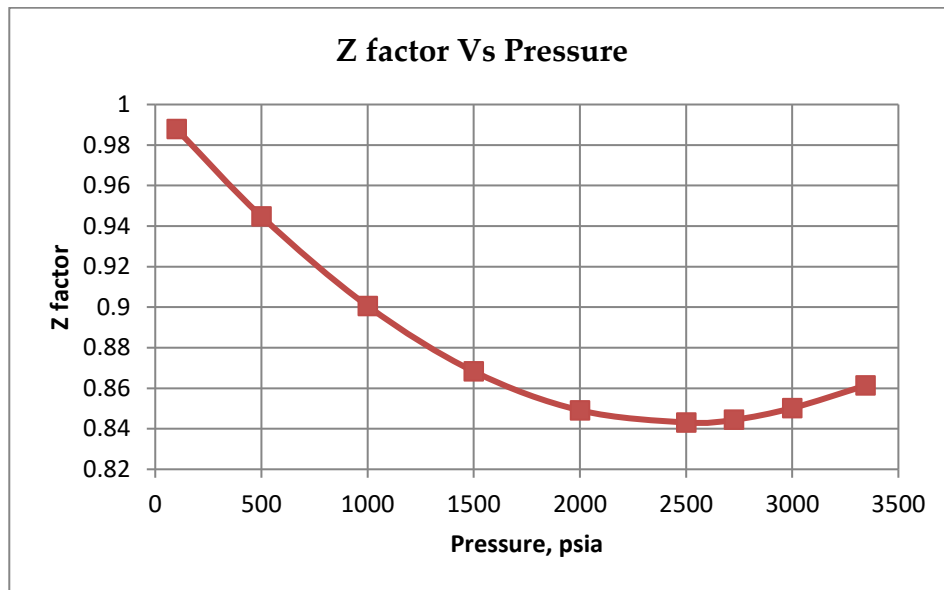


Fig. 4.5: Z factor chart for upper gas sand

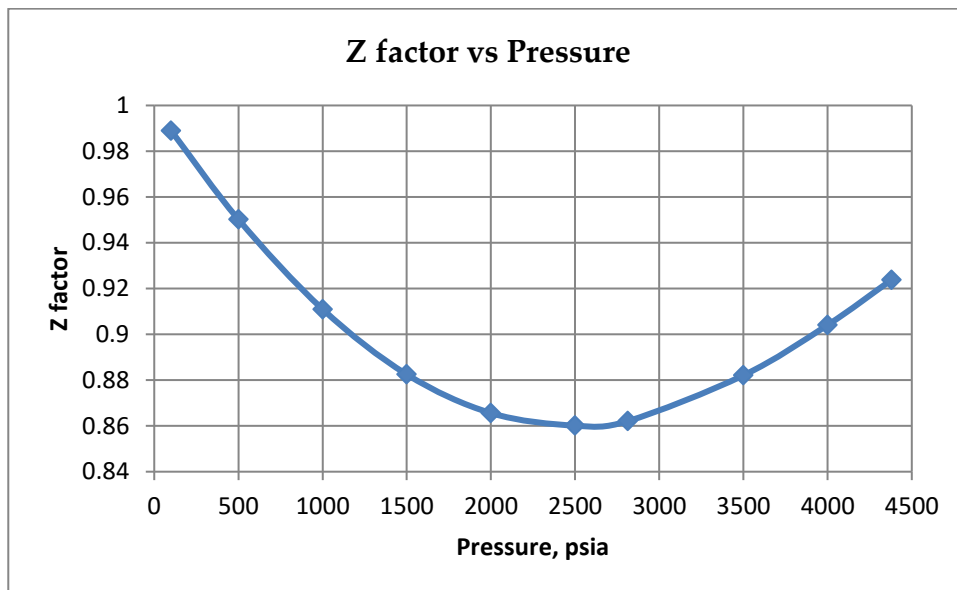


Fig. 4.6: Z factor chart for lower gas sand

Fig. 4.5 and 4.6 shows the variation in gas compressibility factor with pressure, where the values range from 0.86 to 0.98 for upper layer and for lower part 0.92 to 0.99.

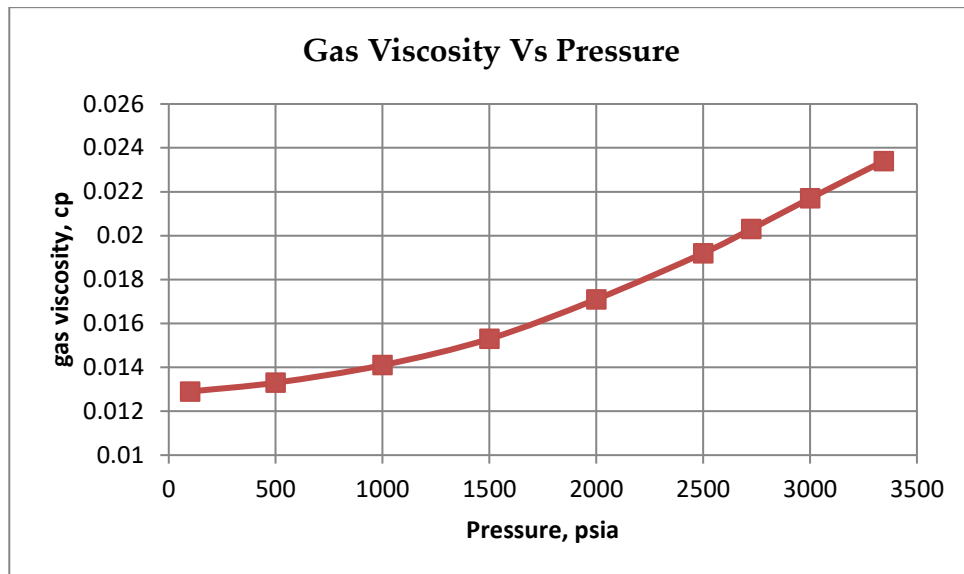


Fig. 4.7: Gas viscosity curve for upper gas sand

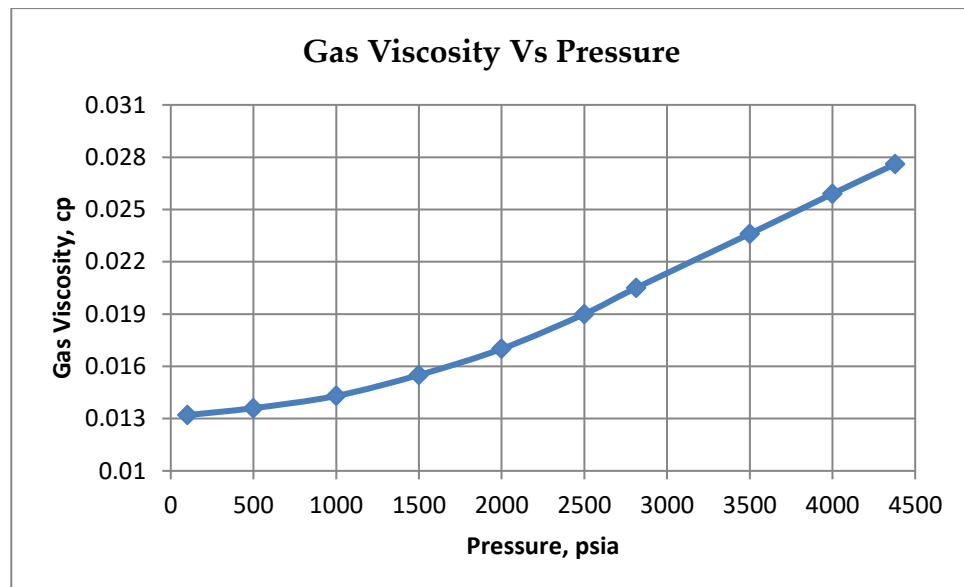


Fig. 4.8: Gas viscosity curve for lower gas sand

Fig. 4.7 and 4.8 represents the viscous nature of upper and lower sand fluid. The values lie between 0.023 to 0.013 and 0.028 to 0.013 for upper and lower part, respectively.

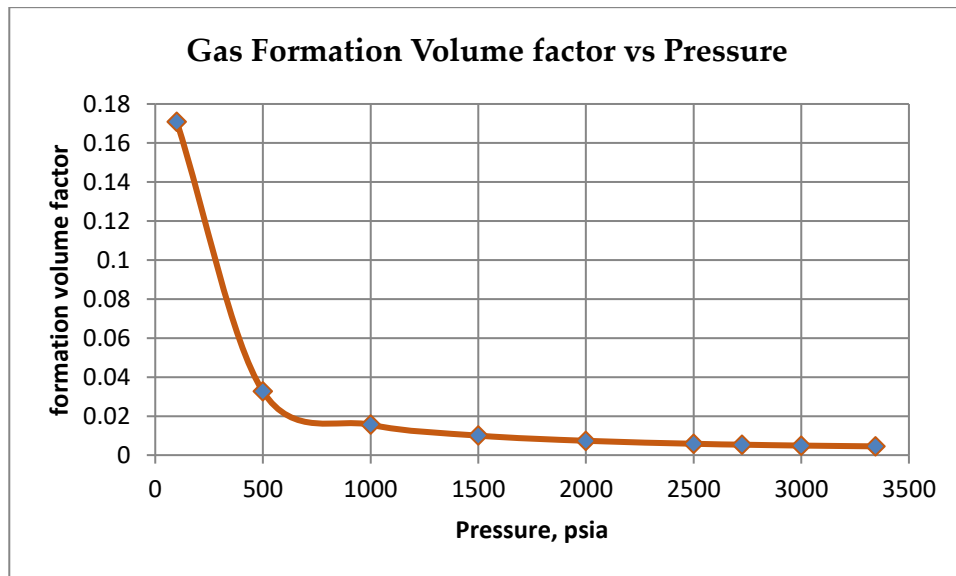


Fig. 4.9: Formation volume factor curve for upper gas sand

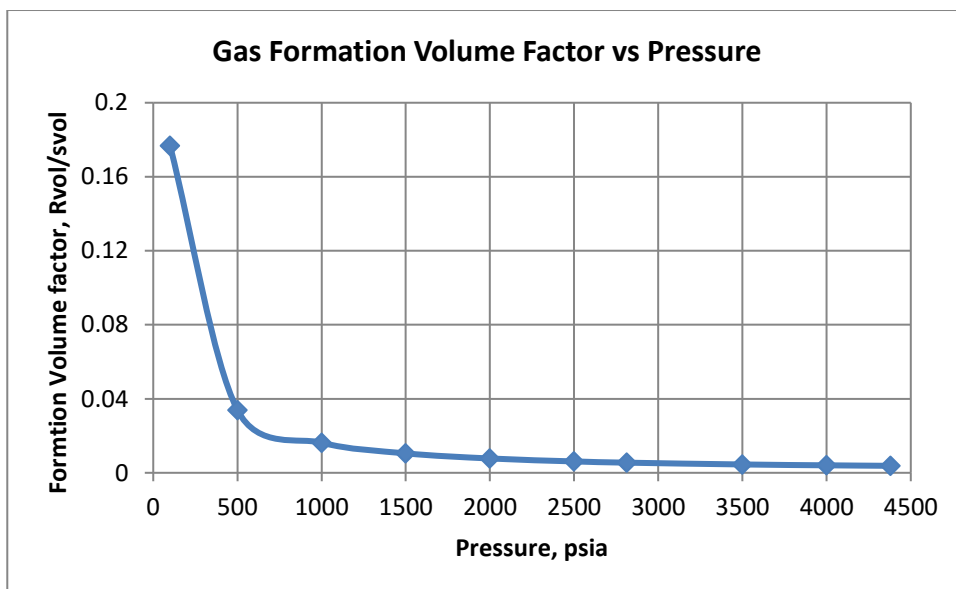


Fig. 4.10: Formation volume factor curve for lower gas sand

Fig .4.9 and 4.10 represents formation volume factor range which is 0.0045 and 0.0037 at the initial stage for two layers respectively and later reduced to 0.17 Rvol/Svol for both.

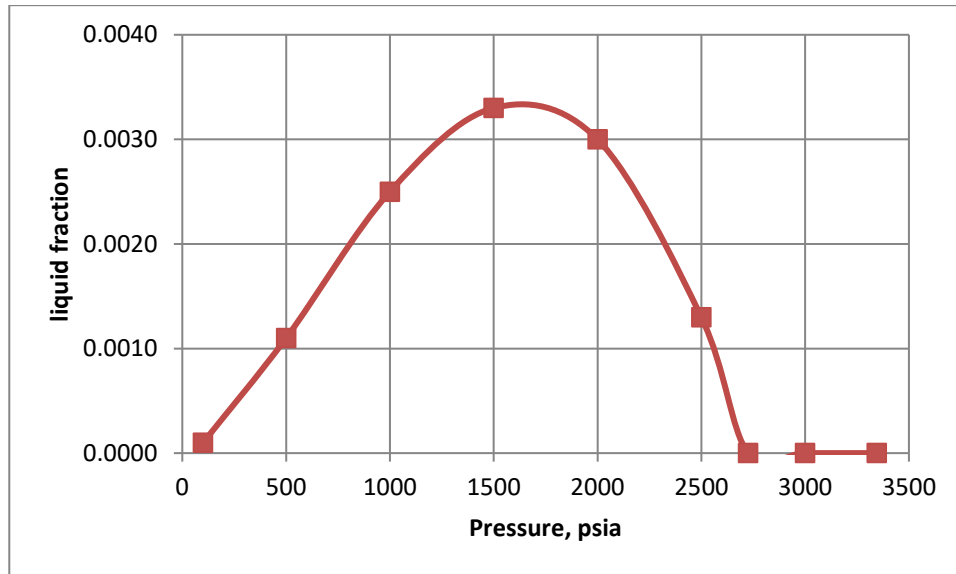


Fig. 4.11: Retrograde liquid curve for upper gas sand

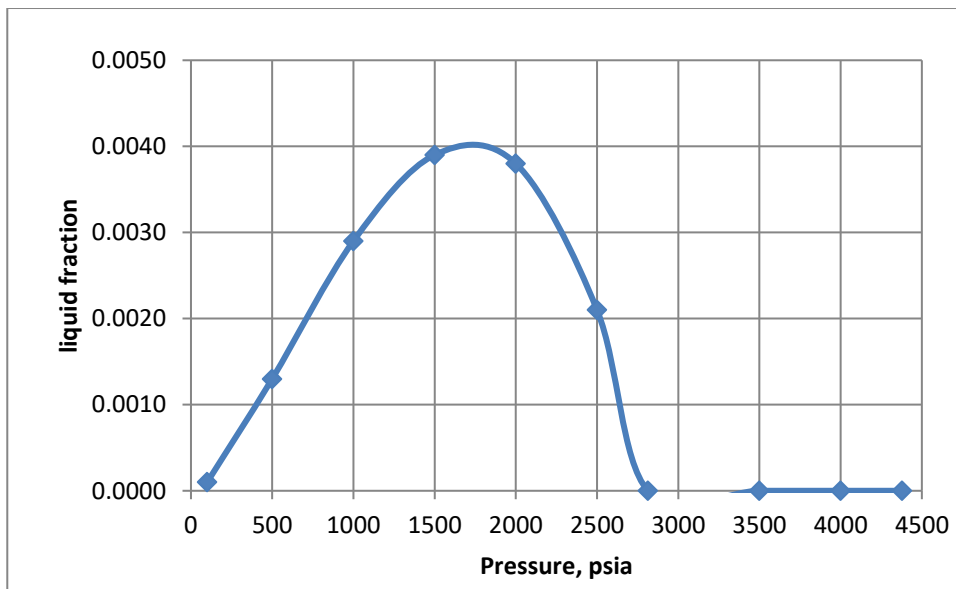


Fig. 4.12: Retrograde liquid curve for lower gas sand

Fig. 4.11 and 4.12 are agreeing the nature of the retrograde behavior of Kailashtila gas field. The value is zero above saturation or dew point pressure but increases slightly later and for upper layer it ranges between 0.0013 to 0.0001 and for lower sand it is 0.0021 to 0.0001 indicating the formation of vary little amount of liquid at reservoir condition.

4.2 SIMULATION RESULTS

To producing best quality product from a petroleum gas/oil reservoir it is necessary to have information on the fluid's behavior under the changes of pressure and temperature. To have these insights several tests are performed at laboratory, which are called PVT tests and the determined properties are called PVT properties. Normally, CCE tests, CVD tests, separator tests, differential liberation (DL) tests are known as PVT tests, performed at integrated PVT apparatus.

In this study, the PVT properties of the fluid are generated through PVT experiment at laboratory as well as by PVTsim software. Since it was not possible to perform all the tests at lab conditions, software was also used to generate all properties. The simulated and experimental results are then compared and both results show a good agreement. For the fluid samples saturation test, separator test, Constant Mass Expansion (CME) and Constant Volume Depletion (CVD) tests are performed, and the phase properties are generated in concurrent at varying pressure steps.

4.2.1 Saturation Test

Since the saturation temperature was unknown, saturation tests are performed to estimate the result. Here, the reservoir temperature, saturation pressure and fluid compositions are used as input data. Peng- Robinson Peneloux equation is considered as the thermodynamic package. The results are presented in Table 4.6 where both temperatures are below the corresponding reservoir temperature.

Table 4.6: Saturation temperature- and pressure for upper and lower sand

Sand Layer	Saturation Temperature at (¹ Bubble / ² Dew)
KTL Upper Sand	2725.00 psia 130.46 °F ²
KTL Lower Sand	2814.00 psia 149.87 °F ²

Additionally, the phase properties and compositional analysis at the saturation stage is generated. Results are shown at Table 4.7 and 4.8. The Z factor value, viscosity, molecular weight is below the initial value and thereby satisfying the

authenticity of the data. Besides the surface tension, heat capacity, enthalpy, and entropy are also estimated at corresponding pressure and temperature.

Table 4.7: Phase properties and composition in mole% for upper sand fluid

Phase Properties at 2725.00 psia 130.46 °F				Composition in mole% at 2725.00 psia 130.46 °F			
	Total	Vapor	Liquid		Total	Vapor	Liquid
Mole%	100.00	100.00	0.00				
Weight%	100.00	100.00	0.00	N2	0.380	0.380	0.117
Volume ,ft ³ /lb-mol	1.99	1.99	1.90	CO2	0.050	0.050	0.045
Volume%	100.00	100.00	0.00	C1	94.030	94.030	53.766
Density,g/cm ³	0.1457	0.1457	0.6432	C2	2.730	2.730	3.326
Z Factor	0.8572	0.8572	0.8174	C3	1.020	1.020	2.077
Molecular Weight	18.12	18.12	76.28	iC4	0.260	0.260	0.735
Enthalpy, J/mol	-814.0	-814.0	-16657.1	nC4	0.290	0.290	0.975
Entropy, J/mol C	-40.34	-40.34	-47.35	iC5	0.150	0.150	0.716
Heat Capacity (Cp), J/mol C	58.72	58.72	169.89	nC5	0.090	0.090	0.485
Heat Capacity (Cv), J/mol C	34.17	34.17	142.62	C6	0.140	0.140	1.156
Kappa (Cp/Cv)	1.719	1.719	1.191	C7	0.260	0.260	3.202
JT Coefficient, C/bar	0.1611	0.1611	-0.0376	C8	0.280	0.280	4.689
Velocity of Sound, ft/s	1628.1	1628.1	2659.8	C9	0.130	0.130	3.150
Viscosity, cP	0.0194	0.0194	0.2730	C10+	0.190	0.190	25.561
Thermal Conductivity, BTU/hr ft F	0.034	0.034	0.101	C10+ Molecular weight	167.427	167.427	199.230
Surface Tension, mN/m		2.411	2.411				

Volume, Enthalpy, Cp and Cv are per mole phase

Table 4.8: Phase properties and composition in mole% for lower sand

Phase Properties at 2814.00 psia 172.00 °F				Composition in mole% at 2814 psia 172.00 °F			
	Total	Vapor	Liquid		Total	Vapor	Liquid
Mole%	100.00	100.00	0.00				
Weight%	100.00	100.00	0.00	N2	0.794	0.794	0.231
Volume, ft ³ /lb-mol	2.30	2.30	2.06	CO2	0.189	0.189	0.152
Volume%	100.00	100.00	0.00	C1	93.463	93.463	49.679
Density, g/cm ³	0.1286	0.1286	0.6473	C2	2.690	2.690	2.991
Z Factor	0.8931	0.8931	0.8009	C3	0.874	0.874	1.615
Molecular Weight	18.44	18.44	83.22	iC4	0.218	0.218	0.564
Enthalpy, J/mol	543.0	543.0	-14106.3	nC4	0.228	0.228	0.695
Entropy, J/mol C	-35.75	-35.75	-34.10	iC5	0.129	0.129	0.559
Heat Capacity (Cp), J/mol C	57.09	57.09	190.85	nC5	0.069	0.069	0.337
Heat Capacity (Cv), J/mol C	35.72	35.72	162.24	C6	0.189	0.189	1.408
Kappa (Cp/Cv)	1.598	1.598	1.176	C7	0.347	0.347	3.818
JT Coefficient, C/bar	0.1598	0.1598	-0.0341	C8	0.377	0.377	5.630
Velocity of Sound, ft/s	1616.9	1616.9	2501.7	C9	0.169	0.169	3.643
Viscosity, cP	0.0188	0.0188	0.2670	C10+	0.263	0.263	28.679
Thermal Conductivity, BTU/hr ft F	0.034	0.034	0.097	C10+ Molecular weight	165.823	165.823	198.114
Surface Tension, mN/m		3.000	3.000				

Volume, Enthalpy, Cp and Cv are per mole phase

4.2.2 Separator Test

The test is started from the saturation pressure and the last stage is performed at surface condition. The objective was to estimate solution GOR and oil formation volume factor. As seen from Table 4.9 and 4.11 total GOR is 112.9 and 0.1 MMscf/stb for upper and lower gas sand fluid, and the formation volume factor ranging between 1 to 1.5 sep bbl/stb.

Table 4.9: Separator test results for UGS

UGS						
Pressure psia	Temp °F	GOR MMScf/stb	Gravity air = 1	Oil Dens g/cm³	FVF sep bbl/stb	Bg sep bbl/stb
2725.00	152.00					0.006
2725.00	130.00	112.9	0.626	0.6430	1.486	
1000.00	50.00	0.0	0.582	0.7427	1.190	
14.70	59.00	0.0	0.757	0.8108	1.000	
Total GOR MMScf/stb			112.9			
Gravity of STO oil °API			43.0130			

The compositional mole % for the liberated gas and residual oil are presented at Table 4.10 and 4.11.

Table 4.10: Compositional mole% for liberated gas and residual oil for UGS fluid

Liberated Gas (mole%)					Residual Oil (mole%)	
Pressure (psia)	2725.00	1000.00	14.70	Combine	Pressure (psia)	14.70
Temp (°F)	130.00	50.00	59.00		Temp (°F)	59.00
N2	0.380	0.284	0.079	0.380	N2	0.000
CO2	0.050	0.052	0.101	0.050	CO2	0.002
C1	94.030	96.045	79.533	94.030	C1	0.476
C2	2.730	2.545	8.783	2.730	C2	0.339
C3	1.020	0.674	5.686	1.020	C3	0.858
iC4	0.260	0.126	1.647	0.260	iC4	0.643
nC4	0.290	0.123	1.896	0.290	nC4	1.088
iC5	0.150	0.044	0.793	0.150	iC5	1.239
nC5	0.090	0.024	0.431	0.090	nC5	0.916
C6	0.140	0.023	0.358	0.140	C6	2.662
C7	0.260	0.029	0.387	0.260	C7	7.811
C8	0.280	0.022	0.236	0.280	C8	11.677
C9	0.130	0.006	0.053	0.130	C9	7.920
C10+	0.190	0.003	0.017	0.190	C10+	64.370
Total	100.000	100.000	100.000	100.000	Total	100.000
Molecular Weight	18.12	16.85	21.94	18.12	Molecular Weight	163.19
Gravity (air=1)	0.626	0.582	0.757	0.626		
C10+ Molwt	167.364	145.225	140.225	167.364	C10+ Molwt	199.170

Table 4.11: Separator test results for LGS

KTL LOWER GAS Field						
Pressure psia	Temp °F	GOR MMScf/stb	Gravity air = 1	Oil Dens g/cm³	FVF sep bbl/stb	Bg sep bbl/stb
2814.00	172.00					0.006
1000.00	50.00	0.1	0.594	0.6698	1.334	
14.70	59.00	0.0	0.860	0.7597	1.000	
Total GOR MMScf/stb			0.1			
Gravity of STO oil °API			54.7619			

Table 4.12: Compositional mole% for liberated gas and residual oil for LGS fluid

Liberated Gas (mole%)				Residual Oil (mole%)	
Pressure (psia)	1000.00	14.70	Combined		
Temp (°F)	50.00	59.00		Pressure (psia)	14.70
N2	0.810	0.220	0.804	Temp (°F)	59.00
CO2	0.189	0.338	0.191	N2	0.000
C1	94.806	74.173	94.604	CO2	0.006
C2	2.662	8.506	2.719	C1	0.448
C3	0.817	6.426	0.872	C2	0.331
iC4	0.189	2.352	0.210	C3	0.976
nC4	0.186	2.759	0.212	iC4	0.923
iC5	0.087	1.548	0.101	nC4	1.592
nC5	0.043	0.783	0.050	iC5	2.427
C6	0.073	1.177	0.083	nC5	1.671
C7	0.077	1.069	0.087	C6	8.774
C8	0.049	0.542	0.053	C7	21.606
C9	0.010	0.087	0.011	C8	26.792
C10+	0.003	0.019	0.004	C9	13.019
Total	100.000	100.000	100.000	C10+	21.432
Molecular Weight	17.20	24.91	17.27	Total	100.000
Gravity (air=1)	0.594	0.860	0.596	Molecular Weight	113.36
C10+ Molwt	139.990	137.717	139.868	C10+ Molwt	166.169

4.2.3 Constant Mass Expansion (CME) Test

This test is started at pressure above the dew point pressure and at reservoir temperature and later pressure is reduced gradually. hence the volume is expanded at constant mass or composition. The relative volume, liquid volume percent, corresponding Z factor and density at each pressure steps is determined. Results are presented at Table 4.13 and 4.15.

Table 4.13: CME test for UGS fluid at reservoir temperature

Constant Mass Expansion at 152.00 °F				
Pressure psia	Rel Vol V/Vd	Liq Vol % of Vd	Z Factor	Density g/cm ³
3345.00	0.7962		0.9042	0.1636
3000.00	0.8727		0.8889	0.1492
2725.00	0.9507		0.8797	0.1370
2579.92	1.0000	0.00	0.8760	0.1302
2500.00	1.0305	0.03		
2000.00	1.2863	0.21		
1500.00	1.7380	0.35		
1000.00	2.6810	0.44		
500.00	5.5848	0.40		
100.00	29.0983	0.18		

The phase properties of upper and lower sand fluids at saturation conditions are tabulated in Table 4.14 and 4.16.

Table 4.14: Phase properties at saturation pressure and reservoir temperature

Phase Properties at 2725.00 psia 152.00 °F	
	Total
Mole%	100.00
Weight%	100.00
Volume, ft ³ /lb-mol	2.12
Volume%	100.00
Density, g/cm ³	0.1370
Z Factor	0.8797
Molecular Weight	18.12
Enthalpy, J/mol	-118.6
Entropy, J/mol C	-38.26
Heat Capacity (Cp), J/mol C	57.55
Heat Capacity (Cv), J/mol C	34.81
Kappa (Cp/Cv)	1.653
JT Coefficient, C/bar	0.1572
Velocity of Sound, ft/s	1635.8
Viscosity, cP	0.0191
Thermal Conductivity, BTU/hr ft F	0.034

Volume, Enthalpy, Cp and Cv are per mole phase

Table 4.15: CME test for LGS fluid at reservoir temperature

KTL LOWER GAS Field			EOS = PR Peneloux	
Constant Mass Expansion at 172.00 °F				
Pressure psia	Rel Vol V/Vd	Liq Vol % of Vd	Z Factor	Density g/cm³
4379.00	0.6593		0.9781	0.1950
4000.00	0.7040		0.9540	0.1827
3500.00	0.7810		0.9261	0.1646
2814.00	0.9418		0.8979	0.1365
2636.17	1.0000	0.00	0.8931	0.1286
2500.00	1.0517	0.05		
2000.00	1.3126	0.28		
1500.00	1.7692	0.46		
1000.00	2.7164	0.55		
500.00	5.6264	0.49		
100.00	29.1890	0.21		

Table 4.16: Phase properties at saturation pressure and reservoir temperature

Phase Properties at 2814.00 psia 172.00 °F	
	Total
Mole%	100.00
Weight%	100.00
Volume, ft ³ /lb-mol	2.16
Volume%	100.00
Density, g/cm ³	0.1365
Z Factor	0.8979
Molecular Weight	18.44
Enthalpy, J/mol	435.6
Entropy, J/mol C	-36.54
Heat Capacity (Cp), J/mol C	57.55
Heat Capacity (Cv), J/mol C	35.82
Kappa (Cp/Cv)	1.606
JT Coefficient, C/bar	0.1461
Velocity of Sound, ft/s	1647.7
Viscosity, cP	0.0194
Thermal Conductivity, BTU/hr ft F	0.034

Volume, Enthalpy, Cp and Cv are per mole phase

Results generated from CME tests are displayed through curve. The density curve, Z factor and relative volume curve is displayed here.

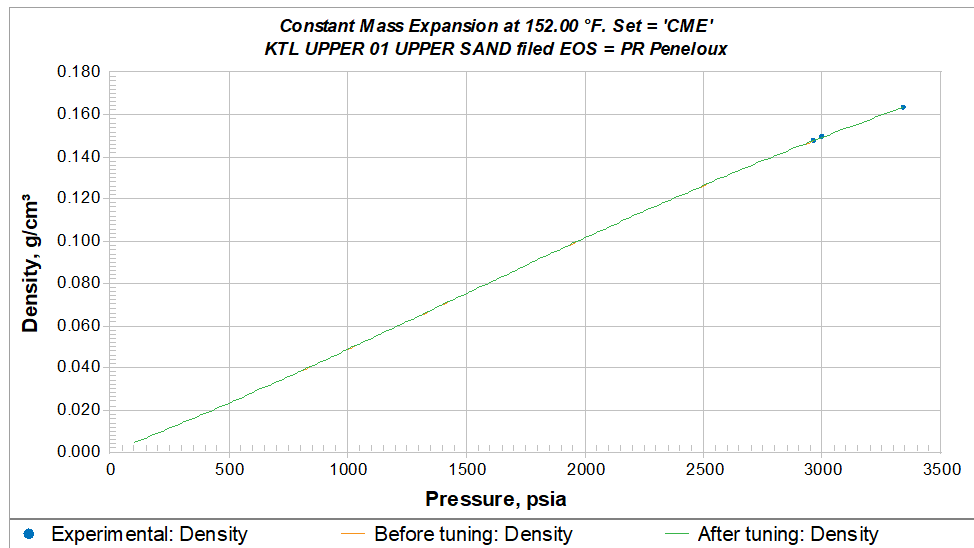


Fig. 4.13: Density Vs Pressure for UGS

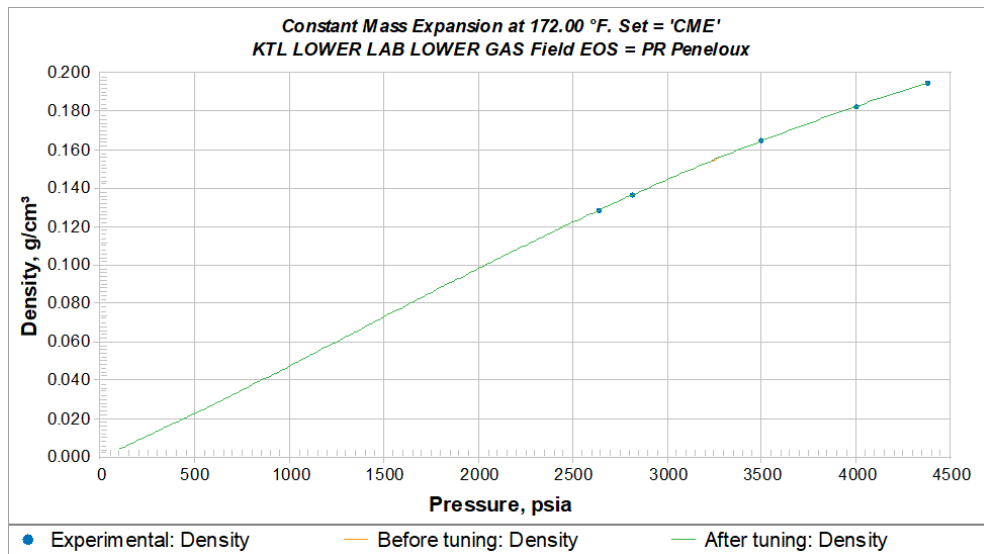


Fig. 4.14: Density Vs Pressure for LGS

Fig. 4.13 and 4.14 are representing the density variation with pressure. For UGS the value is slightly higher than 0.16 and for lower sand fluid it almost touches 0.20 at Y axis.

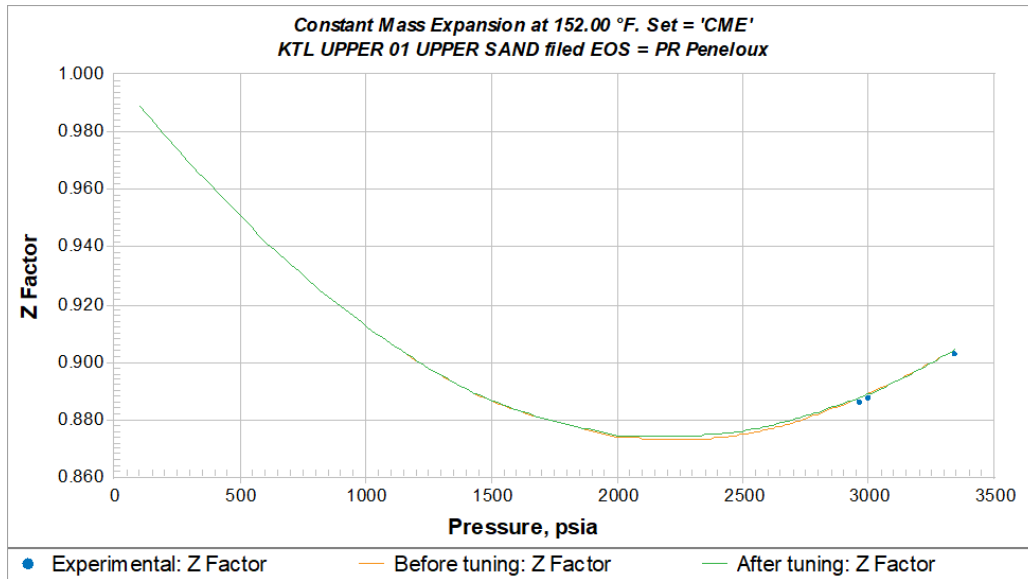


Fig. 4.15: Z factor Chart for UGS

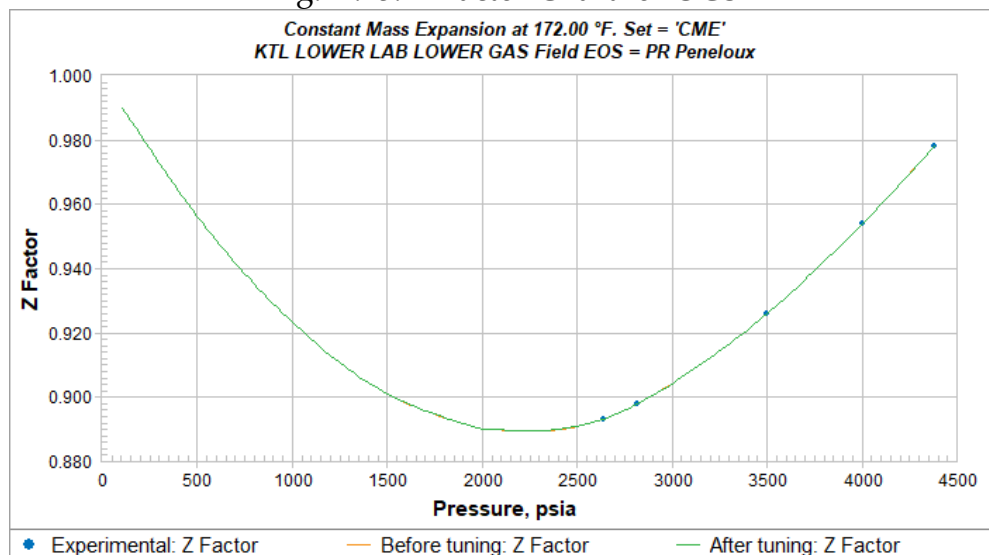


Fig. 4.16: Z factor Chart for LGS

In Fig. 4.15 and 4.16, changes of the compressibility factor with pressure variation is shown. For UGS the value lies between 0.87 to 0.9 and for LGS fluid it lies between 0.89 to 0.97. Data are then tuned to give the curve a perfect shape and extrapolates the value above the given pressure range.

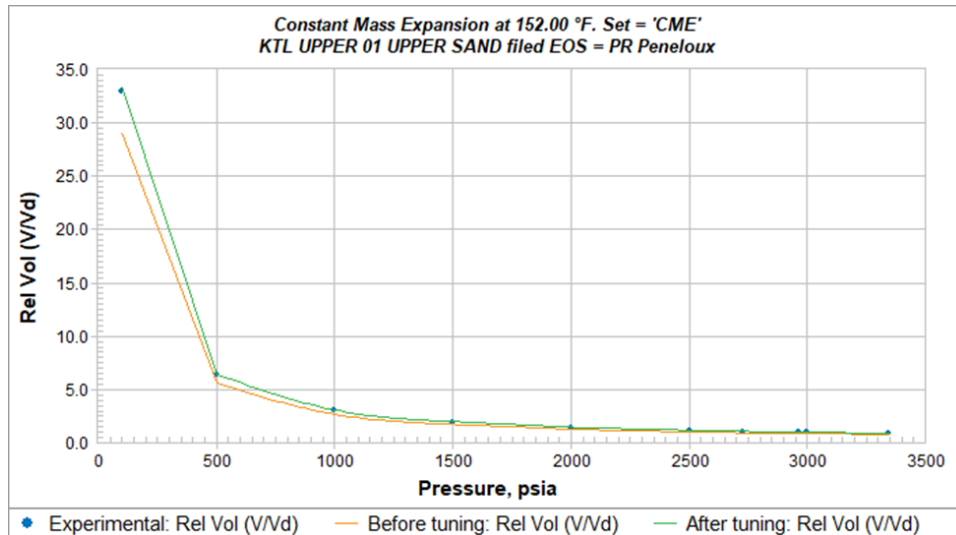


Fig. 4.17: Relative volume (%) curve for UGS

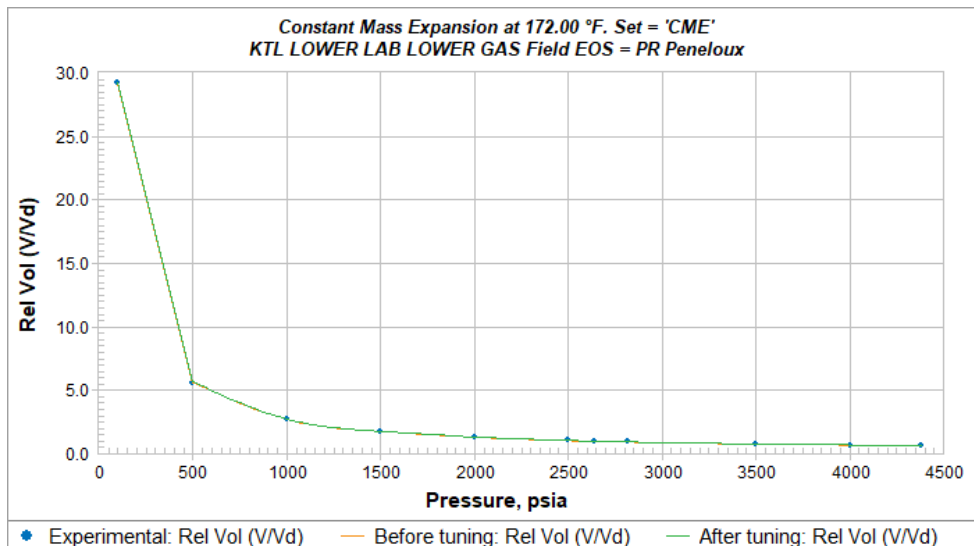


Fig. 4.18: Relative volume (%) curve for LGS

The relative volume for both fluid samples are below 0.1 and later increased to 30 with decreasing pressure as seen from Fig. 4.17 and 4.18.

4.2.4 CVD Test

This test is started from the dew point pressure for gas condensate sample and it measured the saturation volume at dew point. The two phase z factor is determined. Results are shown at Table 4.17 and 4.19.

Table 4.17: CVD test at reservoir temperature for UGS

KTL Upper Gas Sand					
Constant Volume Depletion at 152.00 °F					
Pressure psia	Liq Vol % of Vd	%Prod Mole	Z Factor Gas	Z Factor Two Phase	Viscosity cP
2725.00		0.00	0.877		0.019
2579.92	0.00	0.00	0.876	0.876	0.019
2500.00	0.03	2.96	0.875	0.875	0.018
2000.00	0.20	22.25	0.874	0.873	0.017
1500.00	0.31	42.42	0.887	0.885	0.015
1000.00	0.36	62.59	0.913	0.908	0.014
500.00	0.33	81.92	0.951	0.939	0.013
100.00	0.22	96.42	0.989	0.950	0.013

The fluid compositional mole % from produced stream at decreasing pressure stages are shown at Table 4.18 and 4.20.

Table 4.18: Produced well stream fluid composition mole%

Produced Well Stream (mole%)							
Pressure (psia)	2579.92	2500.00	2000.00	1500.00	1000.0 0	500.00	100.00
Temp (°F)	152.00	152.00	152.00	152.00	152.00	152.00	152.00
N ₂	0.380	0.380	0.381	0.381	0.381	0.381	0.379
CO ₂	0.050	0.050	0.050	0.050	0.050	0.050	0.050
C ₁	94.030	94.045	94.142	94.244	94.327	94.296	93.800
C ₂	2.730	2.730	2.729	2.730	2.733	2.739	2.738
C ₃	1.020	1.020	1.018	1.016	1.017	1.023	1.033
iC ₄	0.260	0.260	0.259	0.258	0.258	0.260	0.267
nC ₄	0.290	0.290	0.288	0.287	0.286	0.290	0.300
iC ₅	0.150	0.150	0.148	0.147	0.146	0.149	0.160
nC ₅	0.090	0.090	0.089	0.088	0.087	0.089	0.097
C ₆	0.140	0.140	0.137	0.133	0.129	0.133	0.163
C ₇	0.260	0.259	0.250	0.238	0.225	0.233	0.329
C ₈	0.280	0.278	0.265	0.244	0.221	0.227	0.380
C ₉	0.130	0.129	0.119	0.103	0.086	0.085	0.180
C ₁₀₊	0.190	0.180	0.125	0.082	0.053	0.046	0.125
Total	100.000	100.000	100.000	100.000	100.00 0	100.00 0	100.00 0
Molecular Weight	18.12	18.10	17.97	17.85	17.76	17.77	18.23
Gravity (air=1)	0.626	0.625	0.620	0.616	0.613	0.614	0.629

Viscosity (cP)	0.0185	0.0183	0.0165	0.0151	0.0139	0.0131	0.0125
C10+ Molwt	167.427	165.659	155.705	148.842	144.918	142.932	143.589

Table 4.19: CVD test at reservoir temperature for LGS

KTL LOWER GAS Field			EOS = PR Peneloux		
Constant Volume Depletion at 172.00 °F					
Pressure	Liq Vol % of Vd	%Prod	Z Factor	Z Factor	Viscosity
psia		Mole	Gas	Two Phase	cP
2814.00		0.00	0.898		0.019
2636.17	0.00	0.00	0.893	0.893	0.019
2500.00	0.05	4.92	0.891	0.891	0.018
2000.00	0.27	23.80	0.890	0.889	0.017
1500.00	0.41	43.42	0.901	0.898	0.015
1000.00	0.46	63.05	0.923	0.917	0.014
500.00	0.41	82.01	0.956	0.942	0.013
100.00	0.26	96.40	0.990	0.942	0.013

Table 4.20: Produced well stream fluid composition mole%

Produced Well Stream (mole%)							
Pressure (psia)	2636.1 7	2500.0 0	2000.0 0	1500.00	1000.0 0	500.00	100.00
Temp (°F)	172.00	172.00	172.00	172.00	172.00	172.00	172.00
N2	0.794	0.795	0.796	0.797	0.798	0.797	0.790
CO2	0.189	0.189	0.189	0.189	0.189	0.189	0.188
C1	93.463	93.490	93.622	93.751	93.840	93.782	93.143
C2	2.690	2.690	2.690	2.691	2.695	2.701	2.698
C3	0.874	0.873	0.871	0.870	0.871	0.877	0.886
iC4	0.218	0.218	0.217	0.216	0.216	0.219	0.225
nC4	0.228	0.228	0.227	0.225	0.225	0.229	0.237
iC5	0.129	0.129	0.127	0.126	0.125	0.128	0.138
nC5	0.069	0.069	0.068	0.068	0.067	0.069	0.075
C6	0.189	0.188	0.183	0.178	0.175	0.182	0.220
C7	0.347	0.345	0.332	0.316	0.302	0.318	0.441
C8	0.377	0.374	0.353	0.326	0.301	0.317	0.517
C9	0.169	0.166	0.152	0.133	0.115	0.119	0.244
C10+	0.263	0.246	0.172	0.114	0.079	0.073	0.200
Total	100.00 0	100.00 0	100.00 0	100.000	100.00 0	100.00 0	100.00 0
Molecular Weight	18.44	18.40	18.23	18.07	17.97	18.00	18.62
Gravity (air=1)	0.637	0.635	0.629	0.624	0.620	0.622	0.643
Viscosity (cP)	0.0188	0.0183	0.0167	0.0153	0.0143	0.0134	0.0129
C10+ Molwt	165.82 3	163.91 9	156.50 6	150.618	146.87 7	144.87 9	146.24 7

The compositional analysis for residual oil left at separator is also performed and compiled at Table 4.21 for both fluid samples.

Table 4.21: Residual oil % at CVD Test for UGS and LGS

Residual Oil (mole%)			
UGS		LGS	
Pressure (psia)	100.00	Pressure (psia)	100.00
Temp (°F)	152.00	Temp (°F)	172.00
N2	0.004	N2	0.008
CO2	0.003	CO2	0.010
C1	2.802	C1	2.668
C2	0.333	C2	0.292
C3	0.353	C3	0.256
iC4	0.190	iC4	0.131
nC4	0.284	nC4	0.180
iC5	0.324	iC5	0.217
nC5	0.246	nC5	0.145
C6	1.061	C6	1.043
C7	4.491	C7	4.205
C8	10.122	C8	9.288
C9	10.982	C9	9.574
C10+	68.805	C10+	71.983
Total	100.000	Total	100.000
Molecular Weight	156.62	Molecular Weight	157.60
C10+ Molwt	182.955	C10+ Molwt	180.691

The generated results are presented through Fig. 4.19 – Fig. 4.26.

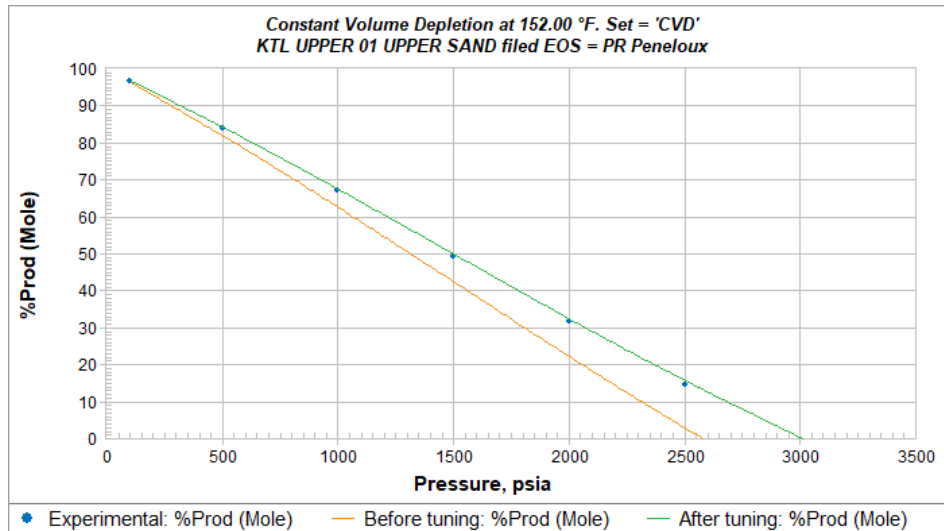


Fig. 4.19: Percent production curve for UGS

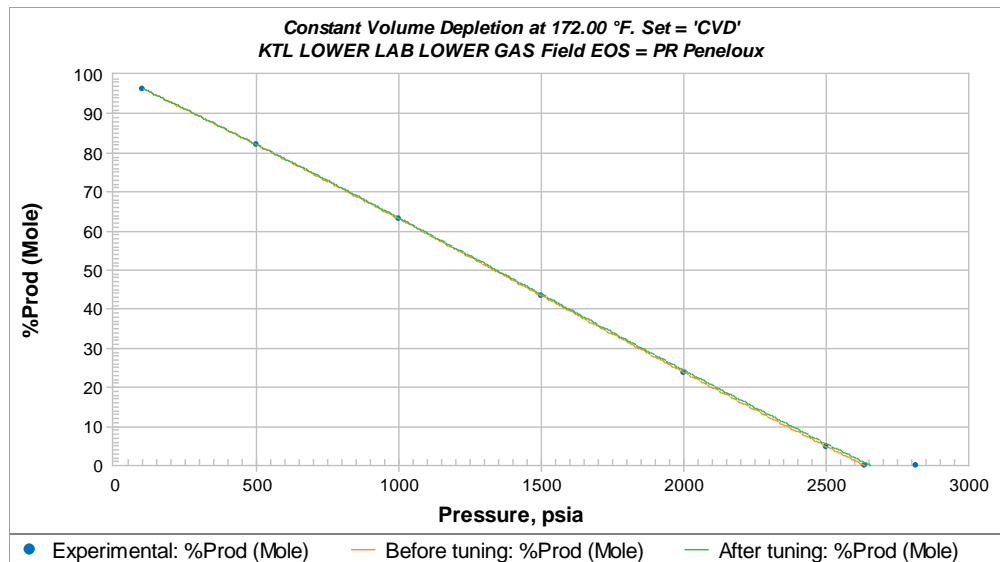


Fig. 4.20: Percent production curve for LGS

In Fig. 4.19 and 4.20 the production percentage is shown for the two samples. The experimental test results are tuned and the both curves are in good agreement. As seen from the figures, with reducing pressure at constant temperature the rate is increased from 0 to almost 97%.

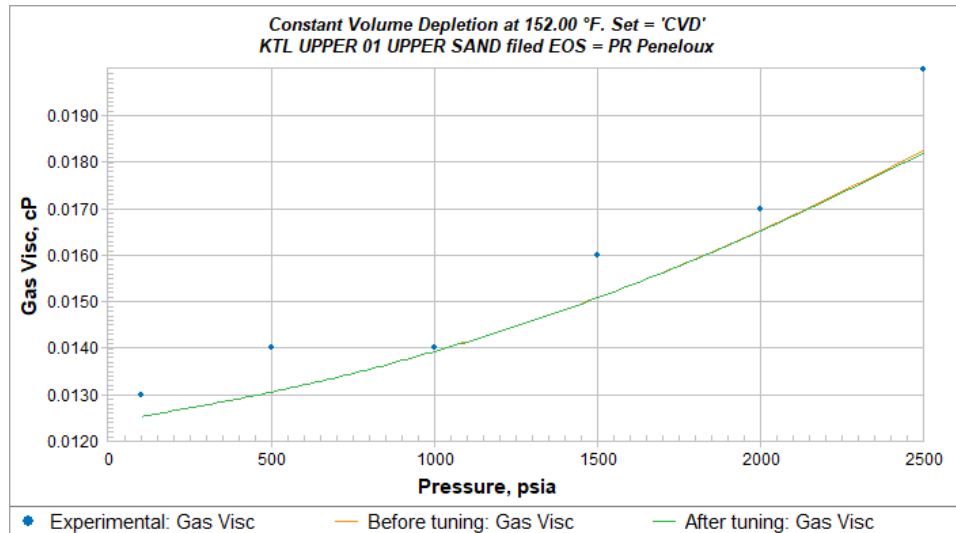


Fig. 4.21: Gas viscosity curve for UGS

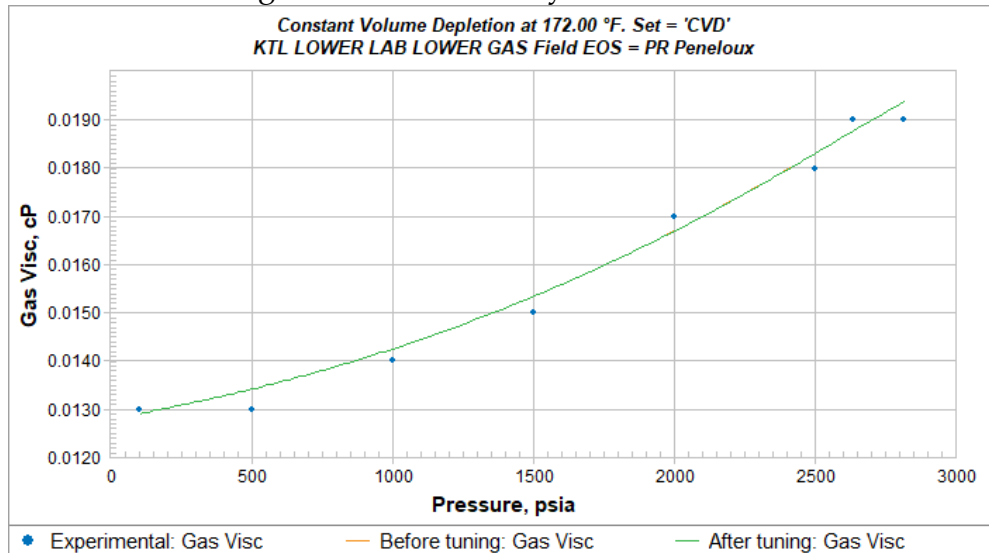


Fig. 4.22: Gas viscosity curve for LGS

In Fig. 4.21 and 4.22 the viscosity changes are represented. The value is ranged between 0.013 to 0.019 for both samples.

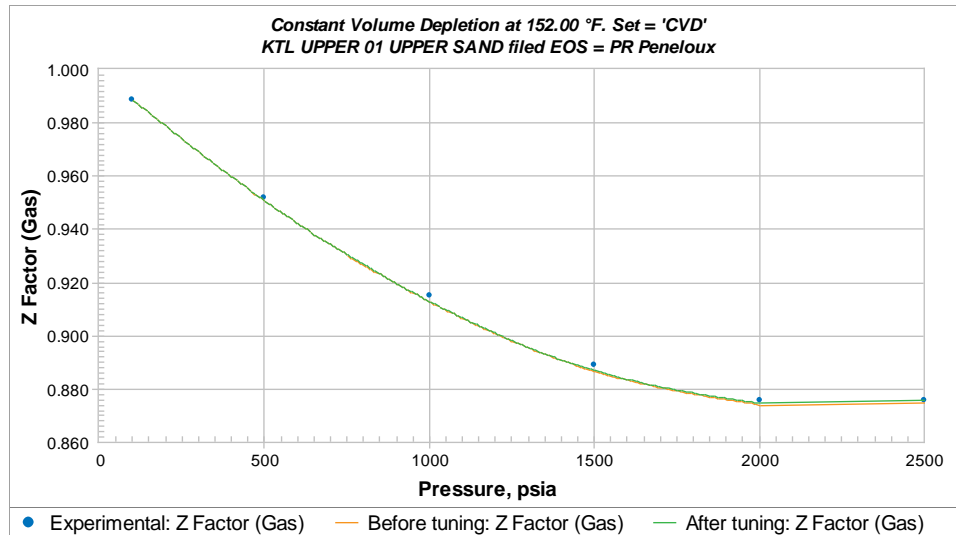


Fig. 4.23: Z factor chart for UGS

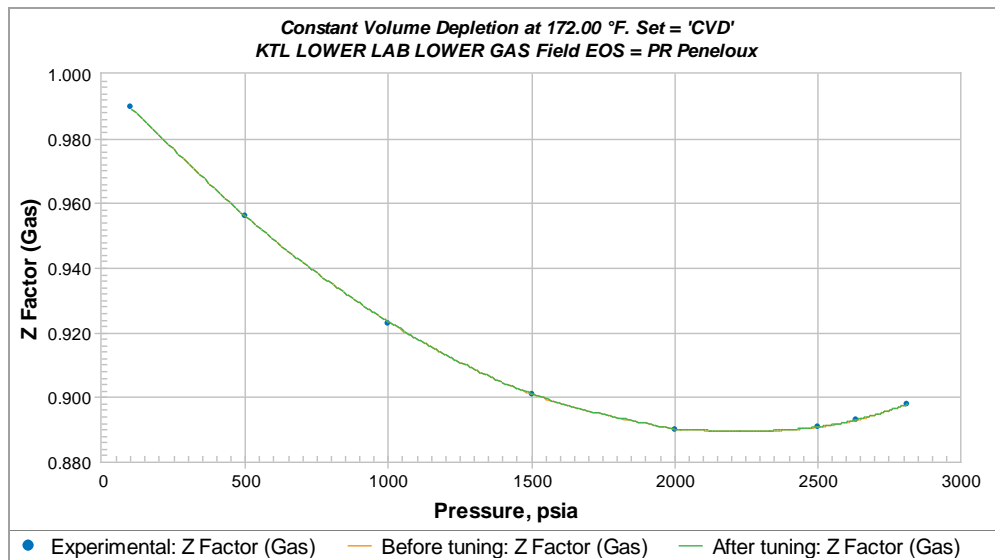


Fig. 4.24: Z factor chart for LGS

From Fig 4.23 and 4.24 the Z factor range is observed as 0.877 to 0.989 for UGS fluid and 0.898 to 0.99 for LGS fluid.

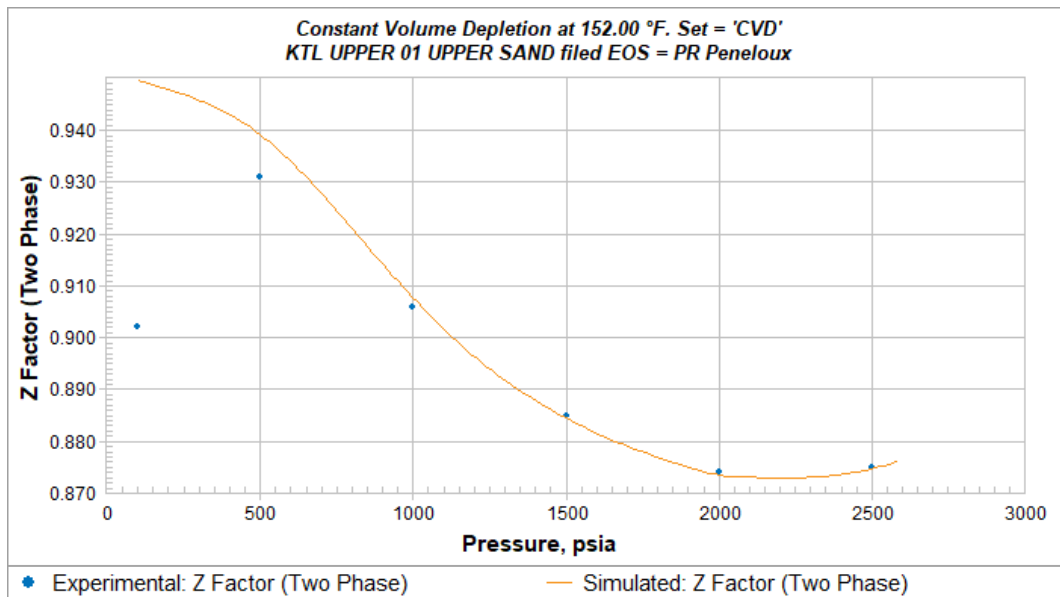


Fig. 4.25: Two phase Z factor curve for UGS

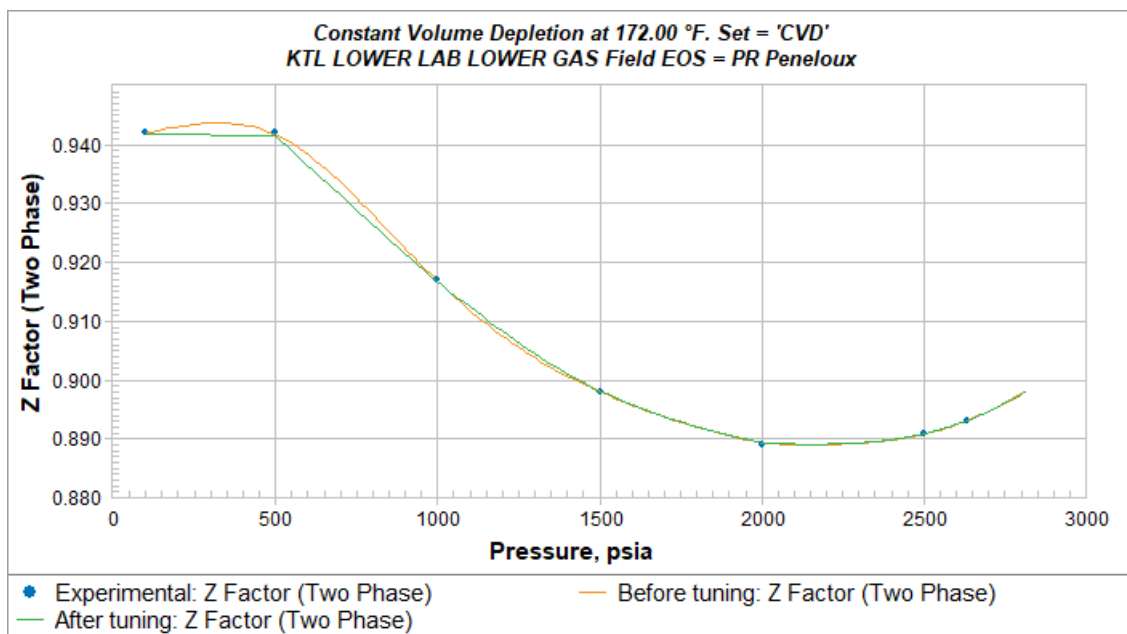


Fig. 4.26: Two-phase Z factor curve for UGS

The two-phase z factor value is presented via Fig. 4.25 and 4.26. Data is obtained below the saturation stage, started with 0.876 for UGS sample and ended up in 0.95, and for LGS sample it ranges between 0.893 to 0.942.

Chapter 5 :MULTI-PHASE FLOW

MODELLING

This chapter develops a mathematical model for a gas condensate reservoir, which is given in section 5.1. In section 5.2, an analytical approach is evaluated and in section 5.3 the sensitivity of the model is examined using actual field data.

5.1 RESERVOIR MODEL FOR MULTI-PHASE FLOW IN NEAR WELL-BORE REGION

To develop the model some basic assumptions are introduced to combine the principle of mass conservation, equation of motion for fluid flow through porous media and an equation of state (EOS). To allow radial flow in the vicinity of well, the equation will be in radial form. An attempt has been made to sought to find an analytical solution applying initial and boundary condition. For a lean gas reservoir, where condensate banking problem is existing the region is divided into three part as seen from figure that are Region 1, 2 and 3. At Region 1 , two-phase non Darcy flow is considered, at Region 2 single phase flow is considered with little amount of liquid droplet is forming and at Region 3 only single phase gas flow will exist.

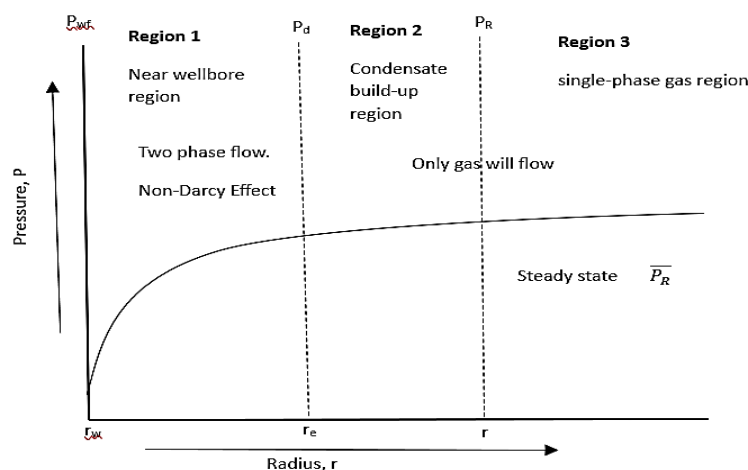


Fig. 5.1: Flow regions for a radial well producing from a gas condensate reservoir

Assumptions:

Assumptions are made only for Region 1

- The reservoir is considered homogeneous in all rock properties and isotropic with respect to permeability.
- Fluid flow is radial from the reservoir to the wellbore (-X direction)
- The producing well is completed across entire formation thickness thereby ensuring fully radial flow.
- Multi-phase flow is considered near well bore for a retrograde condensate reservoir and the fluid is compressible.
- Pseudo-steady state and non- Darcy effect is considered since the multi flow will exist.

5.1.1 Partial Differential Model for Region 1, i.e. for near well bore region

Assuming a small control volume, which is a porous media, is fixed in space and the flow is in -X direction (opposite to conventional X axis) and the net generation of matter is zero. The flow through a volume element of thickness 'dr' situated at a distance r from the center of the radial cell. Then from the principle of mass conservation,

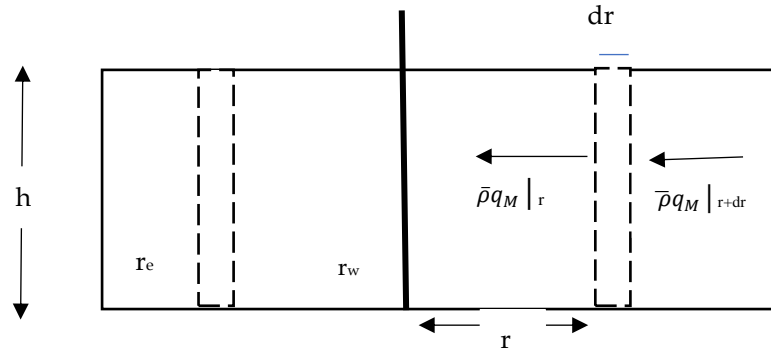


Fig. 5.2: Radial multi-phase flow near well bore

Mass flow in - Mass flow out = Rate of change of mass in the volume element

$$\bar{\rho} q_M |_{r+dr} - \bar{\rho} q_M |_r = Ah\phi dr \frac{\partial \bar{\rho}}{\partial t}$$

Where, Multi-phase /Total flow rate is q_M and

$$q_M = q_g + q_c; \quad q_g = \text{flow rate of gas, } q_c = \text{flow rate of condensate}$$

$\bar{\rho}$ = average density, h = reservoir thickness, ϕ = porosity, A = area of the reservoir

$$\text{Now, } \bar{\rho} q_M \Big|_{r+dr} - \bar{\rho} q_M \Big|_r = V \phi dr \frac{\partial \bar{\rho}}{\partial t}$$

The left-hand side of the equation can be written as

$$\rho q_M \Big|_r + \frac{\delta}{\delta r} (q_M) dr - \rho q_M \Big|_r = V \phi dr \frac{\partial \bar{\rho}}{\partial t}$$

Which simplifies the equation into

$$\frac{\delta}{\delta r} (\bar{\rho} q_M) = V \phi \frac{\partial \bar{\rho}}{\partial t} \quad \text{Equation 5.1}$$

An EOS relates volume or density to pressure and temperature. We can assume isothermal condition since heat capacity of fluid is generally negligible to that of rock. Then from the definition of compressibility C_t ,

$$C_t = -1/V \left(\frac{\partial V}{\partial P} \right)$$

Considering the relationship between density and volume the right-hand side of the equation can be written as

$$C_t = \frac{1}{\bar{\rho}} \frac{\partial \bar{\rho}}{\partial P}$$

$$\text{Or, } C_t \bar{\rho} \partial P = \partial \bar{\rho}$$

Now differentiating both sides with respect to time, we get

$$C_t \bar{\rho} \frac{\partial P}{\partial t} = \frac{\partial \bar{\rho}}{\partial t}$$

Inserting the value of $\frac{\partial \bar{\rho}}{\partial t}$ in Equation 5.1 we get,

$$\frac{\partial}{\partial r} (\bar{\rho} q_M) = \phi V \bar{\rho} C_t \frac{\partial P}{\partial t}$$

Applying chain-rule in the right-hand side,

$$\bar{\rho} \frac{\partial}{\partial r} (q_M) + q_M \frac{\partial}{\partial r} (\bar{\rho}) = \phi V \bar{\rho} C_t \frac{\partial P}{\partial t} \quad \text{Equation 5.2}$$

From the definition of density, we know,

$$\bar{\rho} = \frac{m_t}{V} = \frac{m_t}{A \times h} = \frac{m_t}{2\pi r h \times h}, \text{ here } m_t = \text{total mass of the fluid}$$

Inserting the value of $\bar{\rho}$ in Equation 5.2

$$\begin{aligned} \left(\frac{m_t}{2\pi r h \times h} \right) \frac{\partial}{\partial r} (q_M) + q_M \frac{m_t}{2\pi h \times h} \frac{\partial}{\partial r} \left(\frac{1}{r} \right) &= \phi V \bar{\rho} C_t \frac{\partial P}{\partial t} \\ \left(\frac{m_t}{2\pi r h \times h} \right) \frac{\partial}{\partial r} (q_M) + q_M \frac{m_t}{2\pi h \times h} \frac{\partial}{\partial r} \left(\frac{1}{r} \right) &= \phi V \frac{m_t}{2\pi r h \times h} C_t \frac{\partial P}{\partial t} \end{aligned}$$

Cancelling out $\frac{m_t}{2\pi r h \times h}$ from both sides,

$$\frac{1}{r} \frac{\partial q_M}{\partial r} + q_M \frac{\partial}{\partial r} \left(\frac{1}{r} \right) = \phi V \frac{1}{r} C_t \frac{\partial P}{\partial t}$$

Substituting $\frac{\partial P}{\partial r} \frac{\partial r}{\partial t}$ in place of $\frac{\partial P}{\partial t}$ at the right-hand side,

$$\frac{1}{r} \frac{\partial q_M}{\partial r} + q_M \frac{\partial}{\partial r} \left(\frac{1}{r} \right) = \phi V C_t \frac{1}{r} \frac{\partial P}{\partial r} \frac{\partial r}{\partial t} \quad \text{Equation 5.3}$$

An equation of motion relates velocity and pressure gradients within the control volume. Because of the complexity of the flow paths within the porous media, empirical equation must be used for the equation of motion. Fluid flow is generally modeled by Darcy's law. Incorporating Darcy's law for radial, horizontal flow in the right side of the equation for $\frac{\partial P}{\partial r}$, we get

$$\frac{\partial q_M}{\partial r} + q_M \frac{\partial}{\partial r} \left(\frac{1}{r} \right) = \phi V C_t \frac{1}{r} \frac{q_M}{K_T} \frac{\mu_T}{A} \frac{\partial r}{\partial t} ;$$

here μ = fluid viscosity, K = Permeability

Since, Volume, V = Area, $A \times$ thickness, h , the left hand-side can be written as,

$$\frac{\partial q_M}{\partial r} + q_M \frac{\partial}{\partial r} \left(\frac{1}{r} \right) = \phi (A \times h) C_t \frac{1}{r} \frac{q_M}{K_T} \frac{\mu_T}{A} \frac{\partial r}{\partial t}$$

$$\frac{\partial q_M}{\partial r} + q_M \frac{\partial}{\partial r} \left(\frac{1}{r} \right) = \phi h C_t \frac{1}{r} \frac{q_M}{K_T} \frac{\mu_T}{r} \frac{\partial r}{\partial t}$$

Again, volumetric flow rate q_M = mass flow rate, $U_T \times \text{Area}$, A . Inserting the value of q_M at right-hand side,

$$\frac{\partial q_M}{\partial r} + q_M \frac{\partial}{\partial r} \left(\frac{1}{r} \right) = \phi h C_t \frac{1}{r} \frac{U_T \times A}{K_T} \frac{\mu_T}{r} \frac{\partial r}{\partial t}$$

$$\frac{\partial q_M}{\partial r} + q_M \frac{\partial}{\partial r} \left(\frac{1}{r} \right) = \phi h C_t \frac{U_T \times 2\pi r h}{K_T} \frac{\mu_T}{r} \frac{\partial r}{\partial t}, \quad \text{Area, } A = 2\pi r h$$

$$\text{So, } \frac{\partial q_M}{\partial r} + q_M \frac{\partial}{\partial r} \left(\frac{1}{r} \right) = \phi h C_t \frac{U_T \times 2\pi h}{K_T} \mu_T \frac{\partial r}{\partial t}$$

Now multiplying both sides by $1/r$

$$\frac{1}{r} \left(\frac{1}{r} \right) \frac{\partial q_M}{\partial r} + q_M \left(\frac{1}{r} \right) \frac{\partial}{\partial r} \left(\frac{1}{r} \right) = 2\pi \phi h \cdot h C_t U_T \frac{\mu_T}{K_T} \frac{1}{r} \frac{\partial r}{\partial t} \quad \text{Equation 5.4}$$

Presenting $D = 2\pi \phi h \cdot h C_t U_T \frac{\mu_T}{K_T} \frac{1}{r}$ in the right hand side, Equation 5.4 can be written as

$$\frac{1}{r} \left(\frac{1}{r} \right) \frac{\partial q_M}{\partial r} + q_M \left(\frac{1}{r} \right) \frac{\partial}{\partial r} \left(\frac{1}{r} \right) = D \frac{\partial r}{\partial t}; \quad [\text{here } D \text{ is a dimensionless term}]$$

$$\frac{1}{r} \frac{\partial}{\partial r} (q_M \cdot \frac{1}{r}) = D \frac{\partial r}{\partial t}$$

To replace the term $\frac{\partial r}{\partial t}$ by $\frac{\partial q_M}{\partial t}$, we apply the definition of mass flow rate $U_T = \frac{q_M}{A}$, and differentiating it with respect to r and t we get, $\frac{\partial r}{\partial t} = \frac{2t}{A} \frac{\partial q_M}{\partial t}$. Inserting the value in the right-hand side of the equation

$$r \cdot \frac{\partial}{\partial r} (q_M \cdot \frac{1}{r}) = D_1 t \frac{\partial q_M}{\partial t} \quad \text{Equation 5.5}$$

Here D_1 is a dimensionless term,

where $D_1 = 2 \varphi h C_g U_T \frac{\mu_T}{K_T} \frac{1}{r}$.

This is the proposed partial differential equation for radial flow of multi-phase fluid at region (1) in a porous medium.

5.2 ANALYTICAL SOLUTION

The equation is simplified to find an analytical solution and therefore it is needed first to linearize the equation. It is assumed the well is produced at pseudo-steady state near wellbore region, and at a constant rate q_M at the wellbore, $r = r_w$. Since, the reservoir is considered retrograde, condensate will form at reservoir condition near wellbore and therefore it will affect the flow rate in this region. Starting with equation (v)

$$r \cdot \frac{\partial}{\partial r} (q_M \cdot \frac{1}{r}) = D_1 t \frac{\partial q_M}{\partial t}$$

Applying chain-rule in the left-hand side,

$$r \cdot \frac{1}{r} \frac{\partial}{\partial r} (q_M) + q_M \cdot r \cdot \frac{\partial}{\partial r} (\frac{1}{r}) = D_1 t \frac{\partial q_M}{\partial t}$$

Differentiating $\frac{1}{r}$ with respect r,

$$\frac{\partial}{\partial r} (q_M) + q_M \cdot r \cdot (\frac{-1}{r^2}) = D_1 t \frac{\partial q_M}{\partial t}$$

$$\frac{\partial q_M}{\partial r} - \frac{q_M}{r} = D_1 t \frac{\partial q_M}{\partial t}$$

Since $q_M = V/t$, we get $\frac{\partial q_M}{\partial t} = - \frac{V}{t^2}$, considering total volume as constant. Now inserting the value of $\frac{\partial q_M}{\partial t}$ in the right-hand side,

$$\frac{\partial q_M}{\partial r} - \frac{q_M}{r} = - D_1 \frac{V}{t}$$

To replace the negative sign at the right-hand side we again incorporate the $V/t = q_M$

$$\frac{\partial q_M}{\partial r} - \frac{q_M}{r} = D_1 * q_M$$

$$\frac{\partial q_M}{\partial r} = D_1 * q_M + \frac{q_M}{r}$$

$$\frac{\partial q_M}{\partial r} = (D_1 + \frac{1}{r}) q_M$$

$$\frac{\partial q_M}{q_M} = (D_1 + \frac{1}{r}) \partial r$$

Integrating both sides we get,

$\ln q_M = D_1 r + \ln r + K_1$; here K_1 is the integration constant

$$\ln q_M = \ln e^{D_1 r} + \ln r + \ln e^{K_1} = \ln (e^{D_1 r} \cdot r \cdot e^{K_1})$$

$$\text{or, } q_M = e^{D_1 r} \cdot r \cdot e^{K_1}$$

Equation 5.6

Now, Let's say, $e^{K_1} = K$, then Equation 5.6 becomes

$$q_M = K \cdot e^{D_1 r} \cdot r$$

Equation 5.7

Assuming boundary condition as

at $r = r_w$, $q_M = q_{MW}$ when $P = P_w$,

and at $r = r_e$, $q_M = q$ when $P = \bar{P}$,

So, from Equation 5.7, we get, $K = \frac{q_{MW}}{e^{(D_1 r_w)} r_w}$

And inserting the value of K in Equation 5.7

$$\begin{aligned} q_M &= \frac{q_{MW}}{e^{(D_1 r_w)} r_w} e^{D_1 r} \cdot r \\ \text{Or, } q_M &= q_{MW} \cdot \frac{r}{r_w} \cdot e^{D_1 (r - r_w)} \end{aligned} \quad \text{Equation 5.8}$$

This is the proposed solution for Equation 5.8. This solution will be valid at near well bore condition where $r = r'$, and $P = P'$ i.e. at a little distance from wellbore where condensate banking problem will exist.

In dimensionless form Equation 5.8 can be written as

$$q_{MD} = r_D \cdot e^{D_1 (r - r_w)}$$

Here, Dimensionless flow $q_{MD} = \frac{q_M}{q_{MW}}$, and Dimensionless radius, $r_D = \frac{r}{r_w}$.

In the later part of the study the behavior of q_M will be observed for a particular well.

5.3 SENSITIVITY ANALYSIS

The study is performed for three well namely Well 1, 2 and 3 for Kailashtila gas field which has been found as gas condensate reservoir in the previous chapter. Data are taken from long string, short string and production tests performed are performed within the field. The three well are producing fluid from three different gas layer, well 1 from lower gas sand, well 2 from upper gas sand and well 3 from middle gas sand. KTL 2 and 3 have formation evaluation and deliverability data limited to completion zone production test data. Then the results are analyzed to get an overview of the flow behavior of the discussed field. Initial pressure for each zone was determined in 1962 by Shell upon well completion. Pressures were later estimated in 1985 for upper gas zone and in 1988 for lower gas zone by IPEC. The formation data gathered from different tests are compiled at Table 5.1.

Table 5.1: Well data for KTL well 1, 2 and 3

	Well 1	Well 2	Well 3
Input Data	long string test	Production test	long string test
Formation volume factor	0.003764	0.00442	0.00396
Porosity	0.2	0.2	0.18
Viscosity, cp	0.025	0.021	0.02
Total compressibility, 1/psi	0.000155	0.000155	0.000168
Reservoir thickness, ft	159	179	84.2
Well radius, ft	0.3	0.3	0.3
Permeability, md	287.1	386.6	126
Area, acres	640	640	2725

5.3.1 Well 1

A series of production tests were performed on completed intervals by IPEC at KTL 1 during late 1984 and early 1985. Test data provide estimate on zone deliverability, well capacity, wellbore damage. The well was dually completed in the lower (9810 ft to 9870 ft) and upper gas sands (7487 ft to 7547 ft). Tubing

restrictions found at 7600 ft, 2300 ft above the perforated interval. This difference affected the pressure transient test results.

Table 5.2: Kailashtila well no. 1 lower gas sand deliverability
(Based on long string tests, dated January 1985)

Test	Q, MscfD	del m(P) 10 ⁷
1.	8502	2.725
2.	9629	3.933
3.	11530	5.265
4.	14165	8.0703
5.	14566	8.169
a=1108	b= 0 .3017	r _{inv} = 735 ft

The flow after flow tests are conducted to generate results in terms of pressure squared terms. For simplified and laminar-inertial-turbulent, the pressure squared approach is used to obtain absolute open flow (AOF). The reservoir production rate and sand-face pressure are considered to conduct the tests. The well was flowed for approximately 6 hours in different chokes and shut in for approximately 24 hrs.

Table 5.3: Deliverability test results in terms of pressure squared

Average Reservoir Pressure, \bar{P} , psia	3515
Sand-face Pressure, P_{fs} , psia	3499.3
Bottomhole flowing pressure, P_{wf} , psia	3479.3
C [(MMscfd/10 ⁶)/psi ²ⁿ]	850
n	0.781
del P, ($\bar{P}^2 - P_{wf}^2$)	249696.5
q_{MW} , MMscfD	13.957192
U, ft/s	0.133179262
D1	3.83772E-11

Using the available data, the flow rate q_M is obtained for different value of r using Equation (viii). Here wellbore radius is 0.3 ft, and radius of investigation is 735 ft. The maximum value of r is therefore considered as 735 ft. Additionally, for

different value of q_M , bottomhole flowing pressure, P_{wf} and reservoir pressure is determined until it becomes equal to that the average reservoir pressure. Results are shown at Table 5.4. The bottomhole flowing pressure P_{wf} is assumed to be 20 psi less than the sand-face pressure. Mass flow rate, UT is determined from the reservoir flow rate and D1 is calculated from reservoir fluid properties obtained for each sand layer. For the average reservoir pressure and bottomhole pressure given, the corresponding flow rate, q_{MW} is determined using pressure squared method, which is taken as the actual value of flow rater. The calculated flow rate, q_M is then compared with q_{MW} and relative error is measured using the equation: $\text{Relative error} = \frac{|measured\ value - actual\ value|}{actual\ value}$

Table 5.4: Calculated value of q_M , relative error, P_{wf} and P_R

r	r/r _w	q_M	Relative Error	$aq+bq^2$	P_{wf}^2	P_{wf}	P_R^2	P_R
0.3	1	13.957	0	15523.13	12339701.9	3512.791	11575523.1	3481.53007
0.5	1.666667	23.26167	0.666667	25937.18	12329287.8	3511.309	11585937.2	3483.02536
0.7	2.333333	32.56633	1.333333	36403.47	12318821.5	3509.818	11596403.5	3484.52751
1	3.333333	46.52333	2.333333	52200.86	12303024.1	3507.567	11612200.9	3486.79356
3	10	139.57	9	160520.6	12194704.4	3492.092	11720520.6	3502.29198
4.3	14.33	200.05	13.33	233729.8443	12121495.16	3481.593767	12339258.33	3512.72805
5	16.66667	232.6167	15.66667	274064.4	12081160.6	3475.796	11834064.4	3518.46457
9	30	418.71	29	516824.1	11838400.9	3440.698	12076824.1	3552.79504
11	36.66667	511.7567	35.66667	646040.1	11709184.9	3421.869	12206040.1	3570.93385
13	43.33333	604.8033	42.33333	780480.1	11574744.9	3402.168	12340480.1	3589.7087
15	50	697.85	49	920144.1	11435080.9	3381.58	12480144.1	3609.10966
17	56.66667	790.8967	55.66667	1065032	11290192.9	3360.088	12625032.1	3629.1267
20	66.66667	930.4667	65.66667	1292159	11063065.7	3326.119	12852159.3	3660.28521

It has been observed the pressure reaches its average value before radius 5 ft and the actual value is 4.3 ft. Then another calculation is performed for different value of r and corresponding q_M is measured keeping the average reservoir pressure same. The objective is to observe the flow rater change after the steady state condition has been achieved and data are presented in Table 5.5.

Table 5.5: Flow rate at different point in reservoir (steady state condition)

r, ft	q_M , MMscfD	P_R , psia
0.3	13.957	3481.53
0.5	23.2616667	3485.253
0.7	32.5663333	3490.472
1	46.5233333	3497.941
3	139.57	Reach average \bar{P}_R =3515
5	232.616667	
9	418.71	
11	511.756667	
13	604.803333	
15	697.85	
17	790.896667	
20	930.466667	
30	1395.7	
50	2326.16667	
100	4652.33333	
300	13957	
500	23261.6667	
700	32566.3333	
735	34194.65	

5.3.2 Well 2

The deliverability test conducted in KTL 2 consisted of 3 drawdown tests over a 24-hour period, each with an 8-hour buildup followed by a final 4 hour drawdown and 4 hour buildup. The gauge pressures were subjected to questions due to some malfunctioned.

Table 5.6: Kailashtila well no.2 upper gas sand deliverability
(Based on production tests, dated October 1988)

Test	q , MscfD	del m(P) 10^6
1.	14000	26.06
2.	18180	42.4
3.	22200	63.62
4.	75051	72.45
a=14.8	b= 0.1284	$r_{inv} = 600\text{ft}$

Same approach as KTL well 1 is applied here. Results are obtained from the tests conducted by Al Mansoori Wire Lines Services and shown in Table 5.6. The well was tested across various intervals and was completed in the Upper Gas Sand from 7390 ft to 7430 ft. The radius of investigation for well 2 was not determined from tests and for calculation purpose it is assumed as 600 ft. Four after Four test deliverability results are displayed in Table 5.7.

Table 5.7: Deliverability test results in terms of pressure squared

Average Reservoir Pressure, \bar{P} , psia	3332
Sandface Pressure, P_{fs} , psia	3222.4
Bottomhole flowing pressure, P_{wf} , psia	3202.4
$C [(MMscfd/10^6)/psi^{2n}]$	165
n	0.5
$\Delta P, (\bar{P}^2 - P_{wf}^2)$	846858.24
q_{MW} , MMscfD	151.8411
U , ft/s	2.529076556
$D1$	5.11806E-10

Then calculation is performed to obtain flow rate, reservoir pressure and bottomhole flowing pressure for different r value. The relative error is also measured. All results are combined in Table 5.8.

Table 5.8: Calculated value of q_M , relative error, P_{wf} and P_R

r	r/r_w	q_M	Error	$aq+bq^2$	P_{wf}^2	P_{wf}	P_R^2	P_R
0.3	1	151.841	0	5207.597	11097016.4	3331.218	10258011.6	3202.813
0.5	1.666667	253.0683	0.666667	11968.61	11090255.4	3330.204	10264772.6	3203.868
0.7	2.333333	354.2957	1.333333	21361.04	11080863	3328.793	10274165	3205.334
1	3.333333	506.1367	2.333333	40383.61	11061840.4	3325.935	10293187.6	3208.3
3	10	1518.41	9	318507.5	10783716.5	3283.857	10571311.5	3251.355
5	16.66667	2530.683	15.66667	859773.7	10242450.3	3200.383	11112577.7	3333.553
9	30	4555.23	29	2731733	8370491.14	2893.18	12984536.9	3603.406
11	36.66667	5567.503	35.66667	4062426	7039798.16	2653.262	14315229.8	3783.547
13	43.33333	6579.777	42.33333	5656261	5445962.92	2333.659	15909065.1	3988.617
15	50	7592.05	49	7513239	3588985.4	1894.462	17766042.6	4214.978
17	56.66667	8604.323	55.66667	9633358	1468865.62	1211.968	19886162.4	4459.39
20	66.66667	10122.73	65.66667	-	-	-	23559733.8	4853.837

Here the average pressure is achieved at 5 ft and then the second calculation is performed at the steady state to obtain flow rate at various point in reservoir as shown in Table 5.9.

Table 5.9: Flow rate at different point in reservoir (steady state condition)

r, ft	q_M , MMscfD	P_R , psia
0.3	151.841	3202.813
0.5	253.068333	3203.868
0.7	354.295667	3205.334
1	506.136667	3208.3
3	1518.41	3251.355
5	2530.68333	Reach average \bar{P}_R =3332
9	4555.23	
11	5567.50333	
13	6579.77667	
15	7592.05	
17	8604.32333	
20	10122.7333	
30	15184.1	
50	25306.83333	
100	50613.66667	
200	101227.3333	
300	151841	
400	202454.6667	
500	253068.3333	
600	303682	

5.3.3 Well 3

Production data from KTL 3 is the only available option to gather information about middle gas zone. Tests consisted with an initial 2 hour cleanup, a 2 hour build up, a 6 hour extended drawdown, a 6 hour extended buildup and a three rate flow-after-flow drawdown (each rate extending 4 hours) and a final 4 hour buildup. The accuracy of the deliverability relationship was affected by thermal transient found in the KTL 3 production test. This caused the gauge pressure to reduce below actual level and so the AOFPP estimates are considered directionally low. Production data are displayed in Table 5.10.

Table 5.10: Kailashtila well no. 3 Middle Gas Sand Deliverability
(Based on production tests, dated January 1989)

Test	q, MMscfD	del m(P) 10 ⁶
1.	32.7	58.368
2.	11.3	10.756
3.	22.2	30.427
4.	27.3	43.1878
a=509.1	b= 0.03907	r _{inv} = 530 ft

The initial reservoir pressure was 4263 psi. When the tests are performed by Al Mansoori Wire Lines Services in 2007, the average pressure is observed as 3463 psia and the sand-face pressure is obtained as 3132 psia as shown in Table 5.11.

Table 5.11: Deliverability test results in terms of pressure squared

Average Reservoir Pressure, \bar{P} , psia	3463
Sand-face Pressure, P_{fs} , psia	3132.82
Bottomhole flowing pressure, P_{wf} , psia	3112.82
C [(MMscfd/10 ⁶)/psi ²ⁿ]	728.75
n	0.599
del P, ($\bar{P}^2 - P_{wf}^2$)	2302720.648
q_{MW} , MMscfD	4.712
U, ft/s	4.44717E-07
D1	5.84811E-17

Flow rate, P_{wf} and P_R is measured using Equation (viii) and represented in Table 5.12.

Table 5.12: Calculated value of q_M , relative error, P_{wf} and P_R

r	r/r _w	q_M	Error	aq+bq ²	P_{wf}^2	P_{wf}	P_R^2	P_R
0.3	1	4.712	0	2399.74667	11989969.3	3462.653	9692048.1	3113.205
0.5	1.666667	7.853333	0.6667	4000.54164	11988368.5	3462.422	9693648.89	3113.463
0.7	2.333333	10.99467	1.3333	5602.10769	11986766.9	3462.191	9695250.46	3113.72
1	3.333333	15.70667	2.3333	8005.90254	11984363.1	3461.844	9697654.25	3114.106
3	10	47.12	9	24075.5389	11968293.5	3459.522	9713723.89	3116.685
5	16.66667	78.53333	15.6667	40222.2836	11952146.7	3457.188	9729870.64	3119.274
9	30	141.36	29	72747.0981	11919621.9	3452.481	9762395.45	3124.483
11	36.66667	172.7733	35.6667	89125.1679	11903243.8	3450.108	9778773.52	3127.103
13	43.33333	204.1867	42.3333	105580.346	11886788.7	3447.722	9795228.7	3129.733
15	50	235.6	49	122112.633	11870256.4	3445.324	9811760.98	3132.373
17	56.66667	267.0133	55.6667	138722.027	11853647	3442.913	9828370.38	3135.023
20	66.66667	314.1333	65.6667	163780.698	11828588.3	3439.271	9853429.05	3139.017
30	100	471.2	99	248562.61	11743806.4	3426.924	9938210.96	3152.493
100	333.3333	1570.667	332.333	896011.847	11096357.2	3331.12	10585660.2	3253.561
226.5	755	3557.56	754	2305632.825	9686736.175	3112.352	11995281.18	3463.42

Here, average reservoir pressure has been achieved at 227 ft which is 3463 psia.

Since the original reservoir pressure was 4263 psia, the calculation was continued to see at what condition it will achieve value and found at 611 ft radius the pressure will be the same as the initial condition. So, this calculation is performed beyond r_{inv} .

Table 5.13: Flow rate at reservoir pressure

r, ft	q_M , MMscfD	P_R , psia
0.3	4.712	3113.205438
0.9	14.136	3113.977007
1	15.70666667	3114.105691
5	78.53333333	3119.274056
9	141.36	3124.483229
15	235.6	3132.37306
20	314.1333333	3139.017211
30	471.2	3152.492817
50	785.3333333	3180.182057
100	1570.666667	3253.561157
226.5	3557.56	Reach average \bar{P}_R =3463 psia
490	7696.266667	
500	7853.333333	
530	8324.533333	

Results are showed in curves.

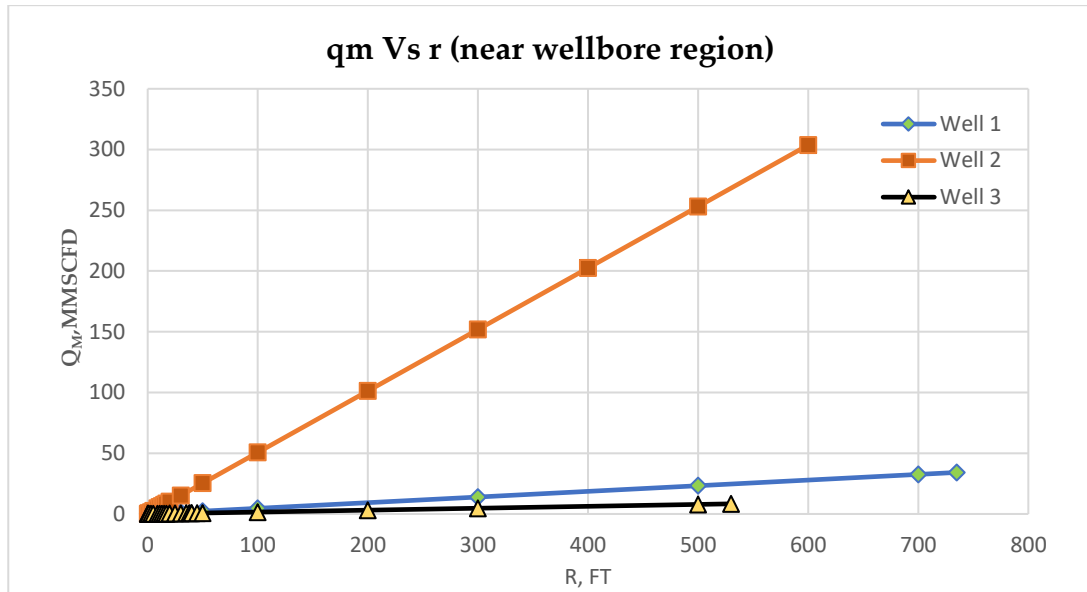


Fig. 5.3: Flow rate at different location in reservoir for Well 1, 2 and 3

The curves as seen from Fig. 5.3 are perfectly linear for each well. Since the value of the exponential term in the equation $q_M = q_{MW} \cdot \frac{r}{r_w} \cdot e^{D_1(r-r_w)}$ is estimated as 1, it becomes analogous to straight line equation, $Y=mX$; where $Y = q_M$, $X = q_{MW} \cdot \frac{r}{r_w}$ and $m = e^{D_1(r-r_w)}$. This relationship is valid for the data gathered for the three well. Each curve is displayed over the investigated zone and the flow rate for well 2 is higher than others.

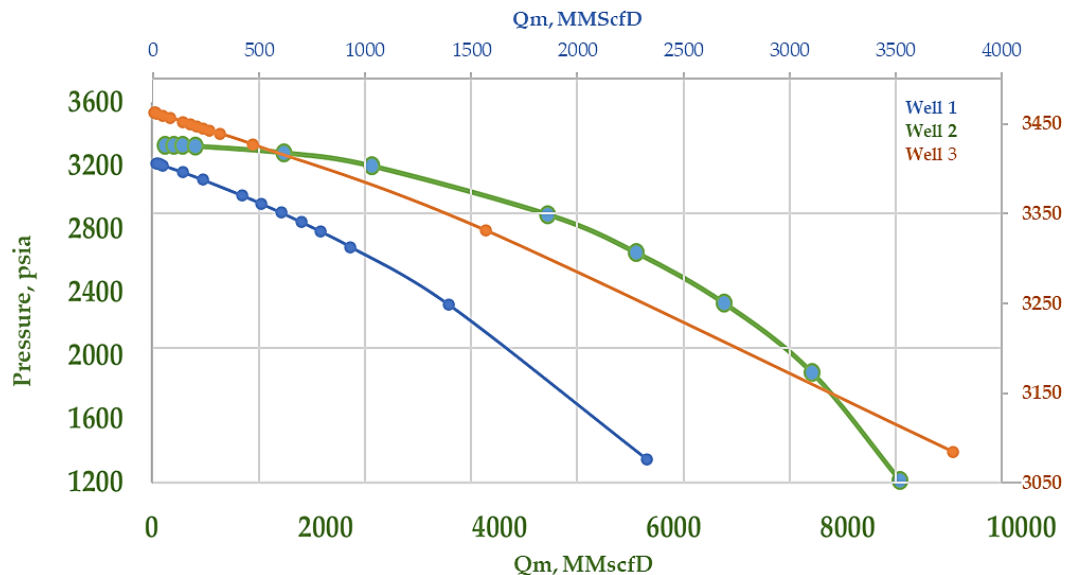


Fig. 5.4: Inflow performance curve for Well 1,2 and 3

In Fig. 5.4 the relationship between P_{wf} and q_M is shown which otherwise known as Inflow performance curve. For well 3 the curve is a straight line. For each well

the curves are downward sloping with increasing flow rate and satisfies the common trend of Inflow performance relationship. So, it can be said that data obtained from the calculation can be marked as valid.

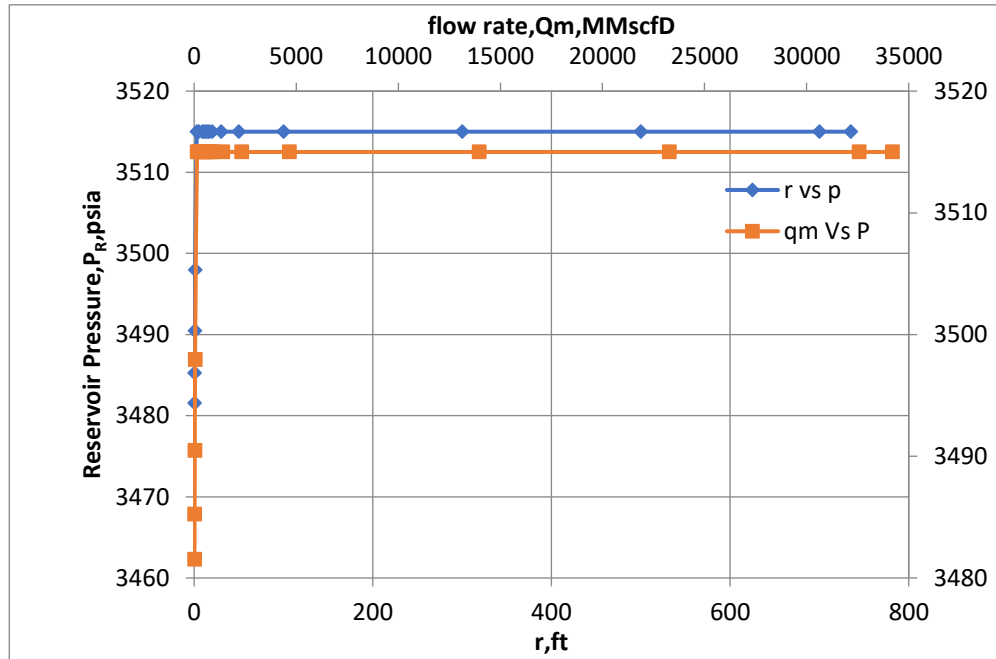


Fig. 5.5: Reservoir pressure as a function of flow rate and radius for Well 1

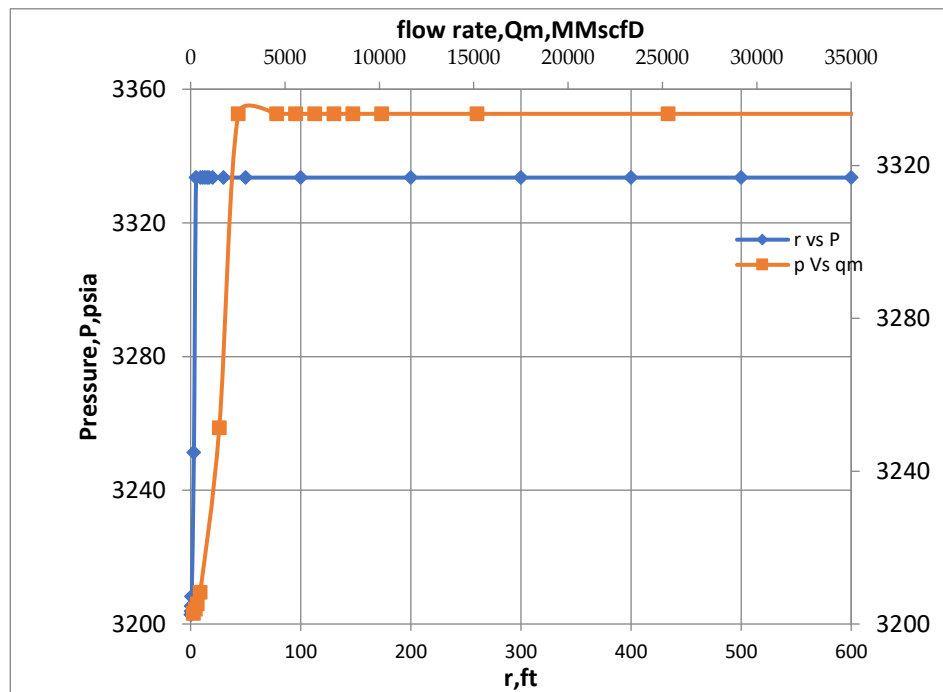


Fig. 5.6: Reservoir pressure as a function of flow rate and radius for Well 2

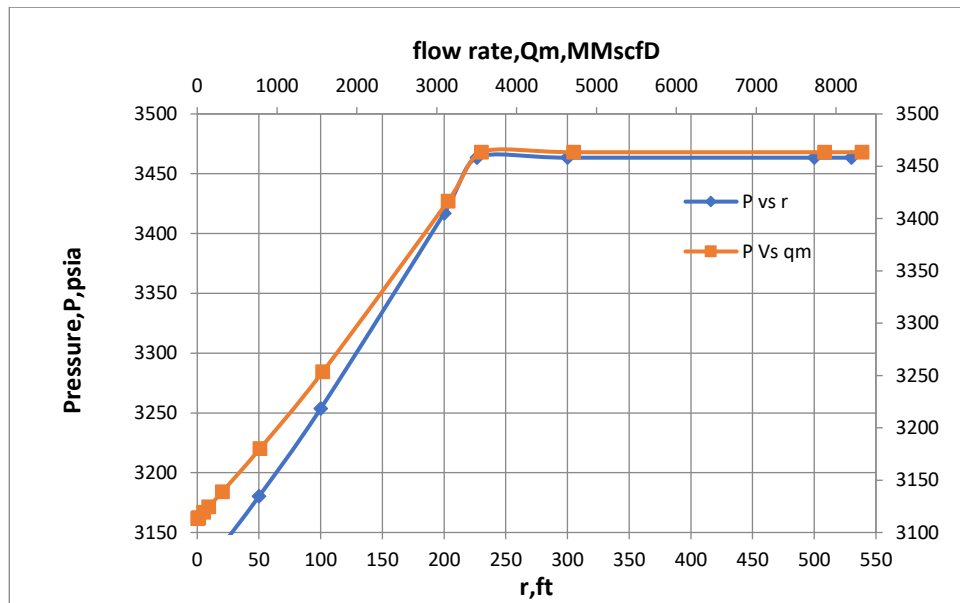


Fig. 5.7: Reservoir pressure as a function of flow rate and radius for Well 3

For wells 1, 2, and 3, the reservoir pressure has been displayed as a function of flow rate and radius at Figs. 5.5, 5.6, and 5.7. The reservoir pressure is shown on the Y axis, and the flow rate and radius are on the X axis. After reaching the average reservoir pressure, the curves plateaued. Following a period of stable pressure, the flow rate increases as the radius increases, representing the flow rate at various reservoir points. The determined value can be regarded as valid for the specified condition since the trend satisfies the natural relationship between reservoir pressure and radius for typical reservoirs. The curve for Well 1 is perfectly straight, however there has been some non-linear behavior seen in Wells 2 and 3.

Chapter 6 : Characterization and Performance Evaluation of KTL Condensate

This chapter estimates the properties of condensate that is recovered from the KTL field's well stream. Section 6.1 presents the sampling process; Section 6.2 presents the distillation and simulated data; and Section 6.3 presents the distillation setup and pertinent calculations.

6.1 CONDENSATE SAMPLING

Several samples of gas and condensate have been collected for compositional and phase behavior analysis as well as for performing distillation tests. The compositional data are generated by natural gas analyzer and gas chromatograph. Phase behavior studies are performed by PVTsim simulation software and then results are compared with data generated from PVT experiments. The ASTM Distillation test is performed in laboratory and then DWSIM software is used to observe the performance and energy efficiency of distillation column and feed. The compositional analysis and results are summarized in this chapter.

Samples of gas and condensate are taken at separator temperature and pressure from KTL field separators. After analysis, the samples are generated as a compositional weight percentage. Software is then used to recombine the gas and condensate sample findings from the compositional analysis to produce the compositional properties of the recombined fluid. The results are shown in Table 6.1.

Table 6.1: Compositional analysis of gas, condensate, and recombined fluid

Gas		Condensate		Recombined Fluid	
Compositions	weight%	Compositions	weight%	Component	weight %
N2	0.927	N2	0.0001	N2	0.585
CO2	0.798	CO2	0.0001	CO2	0.32
C1	84.84	C1	0.14	C1	93.463
C2	4.98	C2	0.1395	C2	2.929
C3	2.38	C3	1.95149	C3	0.97
i-C4	0.78	i-C4	1.4129	iC4	0.246
n-C4	0.841	n-C4	2.725	nC4	0.272
i-C5	0.535	i-C5	0.97057	iC5	0.136
n-C5	0.353	n-C5	14.083	nC5	0.156
i-C6	0.688	i-C6	2.4067	C6	0.151
n-C6	0.281	n-C6	1.1177	nC6	0.062
C6(cyclo)	1.273	C6(cyclo)	10.1625	c-C6	0.31
i-C7	0.211	i-C7	6.3938	nC7	0.06
n-C7	0.062	n-C7	1.30395	c-C7	0.016
C7(cyclo)	0.331	C7(cyclo)	7.8207	nC8	0.075
i-C8	0.429	i-C8	15.325	c-C8	0.116
n-C8	0.0513	n-C8	1.824	C7	0.016
C8(cyclo)	0.2169	C8(cyclo)	1.97066	C8	0.042
C9	0.004	n-C9	10.24348	C9	0.028
C10	0.003	i-C10	2.04585	C10-C11	0.024
C11	0.002	i-C11	7.32566	C12	0.023
C12	0.003	n-C12	10.102	C13	7.10E-06
Total	99.9892	Total	99.46466	C14	9.50E-07
				C15	1.00E-06
				C16	8.10E-07
				C17	9.00E-07
				C18	7.20E-07
				C19-C21	1.50E-06
				Total	100

6.1.1 Property Estimation

Then the critical properties, density, and Normal Boiling Point of each component of the recombined fluid is generated by PVTsim software as seen from Table 6.2. These data are then matched with real filed data to compare the presence of any kind of differences between real and simulated results.

Table 6.2: Critical properties and Normal Boiling Point (NBP) of recombined fluid

Component	Liquid Density g/cm ³	Crit T °F	Crit P psia	Acentric factor -	Normal Tb °F	Wt av Mol wt	Crit V ft ³ /lb-mol
N2		-232.51	492.32	0.04	-320.35	28.014	1.44
CO2		87.89	1069.87	0.225	-109.3	44.01	1.51
C1		-116.59	667.2	0.008	-258.79	16.043	1.59
C2		90.05	708.35	0.098	-127.39	30.07	2.37
C3		205.97	615.76	0.152	-43.69	44.097	3.25
iC4		274.91	529.06	0.176	10.85	58.124	4.21
nC4		305.69	551.1	0.193	31.19	58.124	4.08
iC5		369.05	490.85	0.227	82.13	72.151	4.9
nC5		385.61	489.38	0.251	96.89	72.151	4.87
C6	0.664	453.65	430.59	0.296	155.75	86.178	5.93
nC6	0.664	453.65	430.59	0.296	155.75	86.178	5.93
c-C6	0.783	536.45	590.78	0.213	177.35	84.162	4.93
nC7	0.69	512.69	396.79	0.351	209.21	100.205	6.92
c-C7	0.813	627.89	552.6	0.237	245.21	98.189	5.65
nC8	0.708	564.17	360.05	0.394	258.17	114.232	7.88
c-C8	0.837	705.29	516.34	0.236	299.93	112.216	6.57
C7	0.738	506.009	427.16	0.3374	197.51	96	7.62
C8	0.765	544.807	397.63	0.3743	242.15	107	7.81
C9	0.781	612.787	343.44	0.4498	288.05	130	9.11
C10-C11	0.7951	650.851	320.84	0.495	360.26	144.034	9.85
C12	0.7597	687.461	288.67	0.5484	407.03	161	11.64
C13	0.825	728.141	284.4	0.5925	441.05	175	11.6
C14	0.836	762.385	271.34	0.6384	475.61	190	12.54
C15	0.842	796.681	259.01	0.6863	510.53	206	13.65
C16	0.849	829.831	248.91	0.7331	541.13	222	14.76
C17	0.845	858.523	239.35	0.7757	571.73	237	15.93
C18	0.848	885.442	232.53	0.8146	595.13	251	16.95
C19-C21	0.8603	923.708	225.49	0.868	631.1	270.988	18.34

Additionally, the formation heating temperature, molecular weight, and associated parameters of EOS is generated and represented through Table 6.3.

Table 6.3: Heat of formation, molecular weight parameters for recombined fluid

Component	M & C (SRK) C1 -	M & C (SRK) C2 -	M & C (SRK) C3 -	C _{pen} ft ³ /lb- mol	C _{pen} T ft ³ /lb- mol°F	H _{ref} J/mol	T _f °F
N2	0.543	-0.052	-0.338	-6.78E-02	0	8330.8	
CO2	0.865	-0.439	1.345	-2.63E-02	3.91E-05	19459.1	
C1	0.586	-0.721	1.29	-8.33E-02	0	2.6	
C2	0.718	-0.764	1.64	-9.27E-02	0	9761.1	
C3	0.786	-0.746	1.845	-0.1	0	19519.6	
iC4	0.24	3.836	-8.045	-0.12	0	29278.1	
nC4	0.879	-0.94	2.267	-0.1	0	29278.1	
iC5	0.828	0	0	-9.93E-02	0	39036.6	
nC5	1.028	-2.562	6.248	-8.20E-02	0	39036.6	
C6	0.93	0	0	2.23E-02	0	48795.1	
nC6	1.083	-1.28	2.618	2.23E-02	0	48795.1	
c-C6	0.191	2.73	-3.867	-7.77E-02	0	47392.6	43.79
nC7	-0.162	6.242	-8.826	4.05E-02	0	58553.6	-130.99
c-C7	0.843	0	0	-6.23E-02	0	57151.1	17.33
nC8	1.074	0.066	-0.272	0.11	0	68312.1	-70.15
c-C8	0.842	0	0	-3.22E-02	0	66909.6	58.01
C7				0.11	8.61E-05	55628.2	-159.273
C8				0.17	3.52E-05	63280.8	-119.872
C9				0.25	-2.07E-04	79281.8	-58.751
C10-C11				0.31	-3.14E-04	88893.6	-31.249
C12				0.25	-7.88E-04	100848.3	-3.511
C13				0.4	-5.23E-04	110588	15.19
C14				0.43	-6.31E-04	121023.4	32.277
C15				0.44	-7.74E-04	132154.5	47.874
C16				0.44	-9.06E-04	143285.6	61.331
C17				0.4	-1.10E-03	153721	72.389
C18				0.38	-1.23E-03	163460.7	81.594
C19-C21				0.37	-1.35E-03	177114.7	92.89

The phase envelope of the recombined fluid, as well as samples of gas and condensate, are developed using this data. The reservoir condition is considered for recombined fluid, while the separator condition is considered for gas and condensate samples.

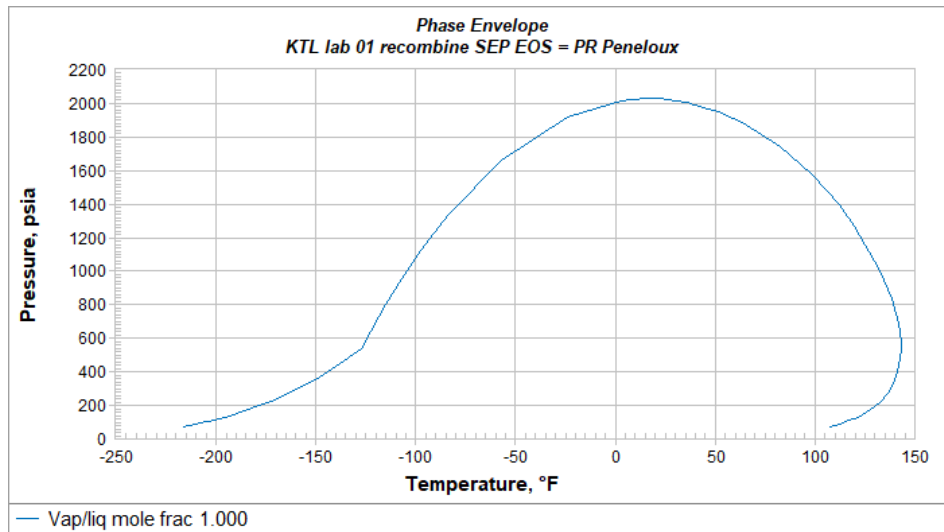


Fig. 6.1: Phase diagram of recombined fluid

Since the dew point temperature in Fig. 6.1 is higher than the reservoir condition, the fluid there displays the lean gas reservoir phase diagram trend rather than the retrograde trend of the field.

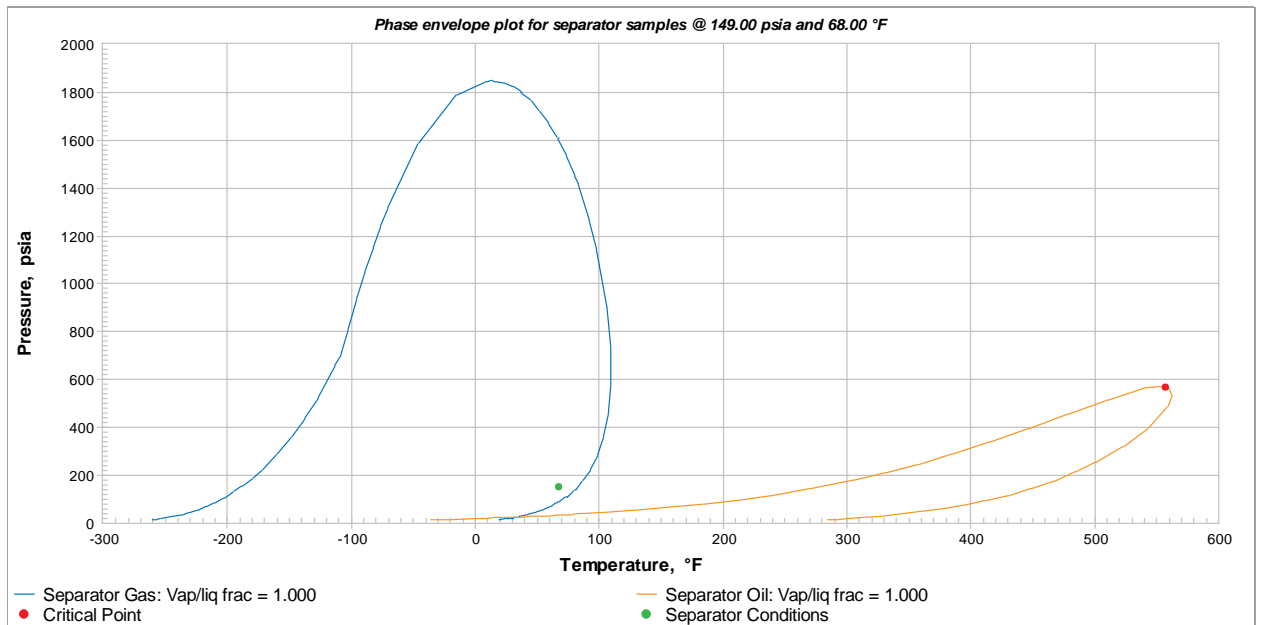


Fig. 6.2: Phase diagram of gas and condensate in separator condition

The phase diagrams for gas and condensate are displayed in Fig. 6.2. The condensate phase diagram's critical point is produced. The points where the two-phase transition converges into one are indicated by the intersection of both curves at temperatures below 100 °C and pressures below 100 psia. Since the

separator condition is in the gas phase, a higher temperature is needed to reach the liquid phase's critical state.

Since the critical points of the recombined fluid cannot be located from the phase diagram, EOS's have been used to find the values, which yields temperature higher than the reservoir temperature as seen from Table 6.4. In an isothermal condition, where the reservoir temperature is below the fluid critical temperature, the pressure is decreased on a regular basis. These prerequisites are met, causing the reservoir to exhibit retrograde nature. Thus, the reservoir may be referred to as retrograde.

Table 6.4: Critical pressure and temperature of KTL recombined fluid

KTL condensate lab	EOS = PR Peneloux
Critical Point	
Critical Temperature, °F	553.67
Critical Pressure, psia	562.04

The phase properties and compositional mole % of the recombined fluid at critical condition are shown in Table 6.5.

Table 6.5: Phase properties and composition mole% at critical conditions

Phase Properties at 562.04 psia 553.67 °F		Composition in mole%	
	Total	N2	0.000
Mole%	100.00	CO2	0.000
Weight%	100.00	C1	0.851
Volume, ft ³ /lb-mol	6.93	C2	0.452
Volume%	100.00	C3	4.316
Density, g/cm ³	0.2241	iC4	2.371
Z Factor	0.3584	nC4	4.573
Molecular Weight	97.01	iC5	1.312
Enthalpy, J/mol	43927.1	nC5	19.037
Entropy, J/mol C	109.36	C6	2.724
Heat Capacity (Cp), J/mol C	583.60	nC6	1.265
Heat Capacity, (Cv), J/mol C	254.53	c-C6	11.777
Kappa (Cp/Cv)	2.293	nC7	6.223
JT Coefficient, C/bar	1.2463	c-C7	1.295
Velocity of Sound, ft/s	385.6	nC8	6.677
Viscosity, cP	0.0546	c-C8	13.320
Thermal Conductivity, BTU/hr ft F	0.033	C7	1.853
		C8	1.796
		C9	7.685
		C10+	12.471
		Total	152.322

Volume, Enthalpy, Cp and Cv are per mole phase.

To observe the phase behavior of the recombined fluid the UGS reservoir condition is taken into consideration since the property found analogous to that of UGS fluid. The CVD test and separator test have been performed. From CVD test results seen from Table 6.6, the liquid phase is found to exist from 1333.74 psia pressure.

Table 6.6: CVD experiment for recombined fluid

KTL		LAB		Recombined GAS-COND		EOS = PR Peneloux		
Constant Volume Depletion at 152.00 °F								
Pressure	Liq	Vol	%Prod	Z	Factor	Z	Factor	Viscosity
psia	% of Vd		Mole	Gas		Two Phase		cP
2500.00			0.00	0.878				0.018
2000.00			0.00	0.875				0.017
1500.00			0.00	0.886				0.015
1333.74	0.00		0.00	0.893		0.893		0.015
1000.00	0.02		26.55	0.911		0.911		0.014
500.00	0.02		64.76	0.950		0.949		0.013
100.00	0.01		93.23	0.989		0.988		0.013

The well stream fluid compositions and residual oil compositions start from the dew point pressure 1333.74 are shown in Table 6.7.

Table 6.7: Produced well stream and residual oil mole % from CVD experiment

Produced Well Stream (mole%)					Residual Oil (mole%)	
Pressure (psia)	1333.74	1000.00	500.00	100.00	Pressure (psia)	100.00
Temp (°F)	152.00	152.00	152.00	152.00	Temp (°F)	152.00
N2	0.585	0.585	0.585	0.585	N2	0.007
CO2	0.321	0.321	0.321	0.321	CO2	0.021
C1	93.497	93.519	93.525	93.472	C1	2.879
C2	2.929	2.930	2.930	2.929	C2	0.362
C3	0.968	0.967	0.968	0.968	C3	0.335
iC4	0.245	0.244	0.245	0.245	iC4	0.177
nC4	0.270	0.270	0.270	0.270	nC4	0.258
iC5	0.135	0.135	0.135	0.136	iC5	0.277
nC5	0.146	0.146	0.146	0.146	nC5	0.372
C6	0.150	0.149	0.149	0.151	C6	0.990
nC6	0.062	0.061	0.061	0.062	nC6	0.407
Benzene	0.032	0.031	0.031	0.032	Benzene	0.234
c-C6	0.275	0.273	0.273	0.278	c-C6	2.366
nC7	0.015	0.015	0.015	0.015	nC7	0.253
Toluene	0.001	0.001	0.001	0.001	Toluene	0.014
c-C7	0.083	0.082	0.081	0.086	c-C7	2.220
nC8	0.013	0.012	0.012	0.013	nC8	0.542
m-Xylene	0.003	0.003	0.003	0.003	m-Xylene	0.154
o-Xylene	0.002	0.002	0.002	0.002	o-Xylene	0.133
c-C8	0.035	0.034	0.033	0.038	c-C8	2.455
nC9	0.017	0.016	0.015	0.018	nC9	1.761
nC10	0.001	0.001	0.001	0.001	nC10	0.271
nC11	0.001	0.001	0.000	0.001	nC11	0.475
nC12	0.002	0.002	0.001	0.003	nC12	3.489
cC10	0.002	0.002	0.002	0.003	cC10	1.526
1-m-Napht	0.002	0.001	0.001	0.003	1-m-Napht	3.403
cC11	0.003	0.001	0.001	0.002	cC11	20.294
C7	0.032	0.031	0.031	0.032	C7	0.440
C8	0.114	0.113	0.113	0.116	C8	1.699
C9	0.032	0.031	0.031	0.032	C9	0.601
C10+	0.029	0.022	0.019	0.034	C10+	51.588
Total	100.000	100.000	100.000	100.000	Total	100.000
Molecular Weight	17.99	17.96	17.95	18.01	Molecular Weight	155.65
Gravity (air=1)	0.621	0.620	0.620	0.622	C10+ Molwt	185.571
Viscosity (cP)	0.0147	0.0140	0.0131	0.0126		
C10+ Molwt	164.844	160.097	156.522	164.851		

Next, a separator test is performed to obtain gas liquid ratio and formation volume factor at separator conditions. Results are shown in Table 6.8. The total GOR is estimated 0.2 MMscf/STB.

Table 6.8: Separator test for recombined fluid

KTL	LAB	Recombined GAS-COND		EOS = PR Peneloux		
	Separator Test					
Pressure, psia	Temp °F	GOR MMScf/stb	Gravity air = 1	Oil Dens g/cm³	FVF sep bbl/stb	Bg, sep bbl/stb
1333.74	152.00					0.012
690.00	70.00	0.2	0.606	0.6809	1.199	
140.00	89.00	0.0	0.710	0.7193	1.066	
14.70	59.00	0.0	1.117	0.7456	1.000	
Total GOR MMScf/stb		0.2				
Gravity of STO oil °API		58.2689				

The composition of the gas liberated from separator is displayed in Table 6.9.

Table 6.9: Liberated gas mole % for recombined fluid.

Liberated Gas (mole%)				
Pressure (psia)	690.00	140.00	14.70	Combined
Temp (°F)	70.00	89.00	59.00	
N2	0.589	0.205	0.042	0.588
CO2	0.321	0.629	0.942	0.322
C1	94.046	84.187	50.161	94.009
C2	2.928	7.431	17.137	2.942
C3	0.952	3.405	13.730	0.962
iC4	0.234	0.885	4.111	0.237
nC4	0.254	0.976	4.595	0.257
iC5	0.118	0.433	1.977	0.119
nC5	0.122	0.446	1.985	0.124
C6	0.098	0.322	1.273	0.099
nC6	0.040	0.133	0.524	0.041
Benzene	0.019	0.068	0.273	0.019
c-C6	0.157	0.534	2.105	0.158
nC7	0.006	0.018	0.063	0.006
Toluene	0.000	0.001	0.003	0.000
c-C7	0.024	0.073	0.247	0.024
nC8	0.003	0.007	0.022	0.003
m-Xylene	0.000	0.001	0.003	0.000
o-Xylene	0.000	0.001	0.002	0.000
c-C8	0.005	0.013	0.039	0.005
nC9	0.002	0.004	0.010	0.002
nC10	0.000	0.000	0.000	0.000
nC11	0.000	0.000	0.000	0.000
nC12	0.000	0.000	0.000	0.000
cC10	0.000	0.000	0.000	0.000
1-m-Napht	0.000	0.000	0.000	0.000
cC11	0.000	0.000	0.000	0.000
C7	0.014	0.044	0.157	0.015
C8	0.053	0.149	0.495	0.053
C9	0.014	0.033	0.100	0.014
C10+	0.001	0.002	0.004	0.001
Total	100.000	100.000	100.000	100.000
Molecular Weight	17.55	20.55	32.34	17.56
Gravity (air=1)	0.606	0.710	1.117	0.606
C10+ Molwt	144.991	143.866	142.770	144.982

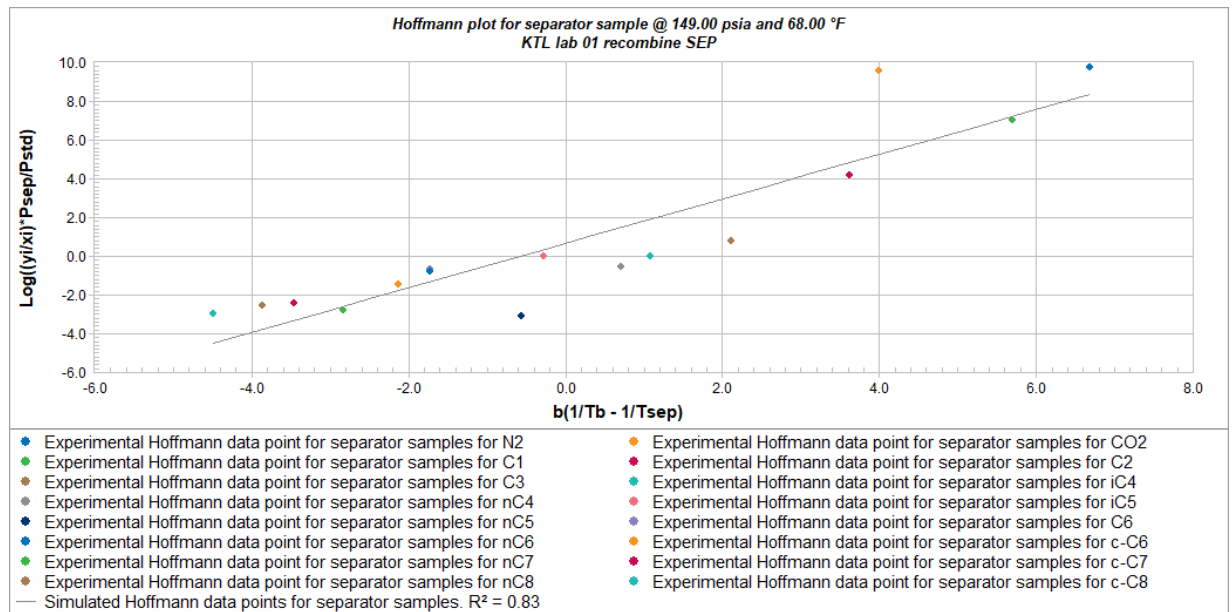


Fig. 6.3: Hoffman plot recombined fluid at separator condition

The Hoffman plot in Fig. 6.3 used to analyze the reservoir boundaries like homogeneous or bounded condition and estimating reservoir parameters. For example, by analyzing the slope and intercept of the straight-line segments, permeability and skin factor can be estimated. Here the Y axis represents dimensionless pressure and X axis a dimensionless temperature. The experimented curve is not perfectly straight, and the deviation is $R^2 = 0.83$. The data are used for estimating other properties.

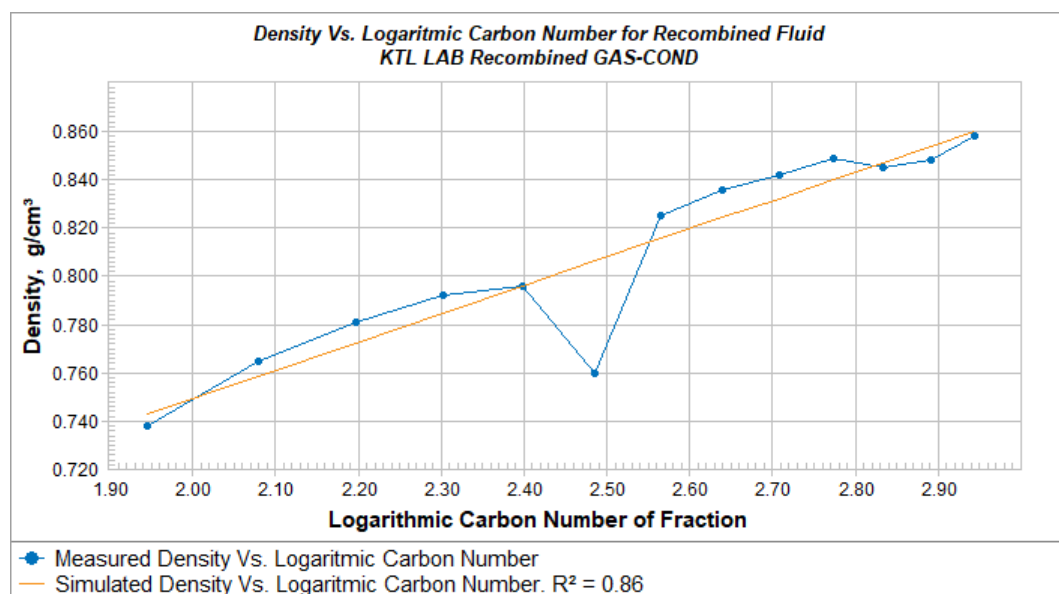


Fig. 6.4: Density vs. logarithmic carbon number for recombined fluid

Fig. 6.4 provides an insight into the composition of the recombined fluid by showing how the density varies with the size (carbon number) of hydrocarbon molecules. Variations in density with carbon number indicates transitions between gaseous and liquid phases.

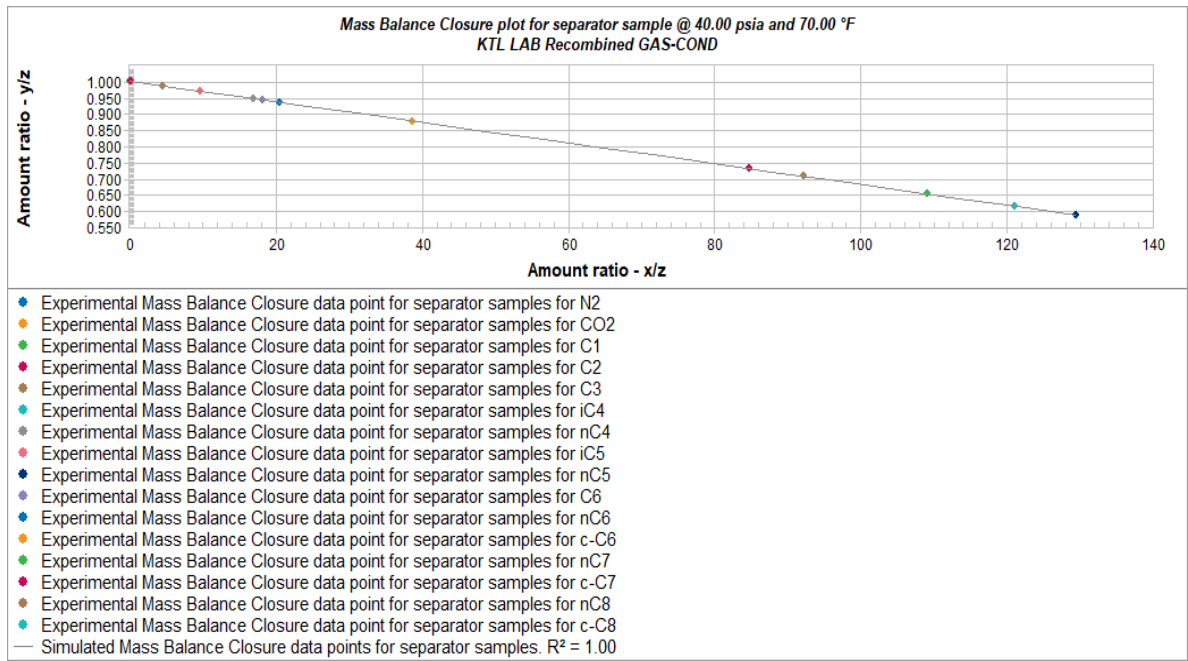


Fig. 6.5 Mass balance closure plot for recombined fluid at separator condition. The mass balance closure plot shown in Fig. 6.5 offers insight into the dependability of simulations by evaluating the precision and consistency of mass balance computations in the context of fluid production from reservoir. In this case, the R^2 value drops to 1 since the simulated and experimental values perfectly match. Consequently, more research on reservoir characteristics can be done using this data.

The second part of this experiment is done on condensate sample at Super Refinery (Pvt.).

6.2 CONDENSATE CHARACTERIZATION

The Petroleum stream constitutes a mixture of the complex hydrocarbon chain. Small petroleum cuts or pseudo-components generally characterize the streams, which are identified from the distillation curve [45,46]. Feedstock assay data are essential in the refining process because the assay provides an extensive and detailed analysis data of hydrocarbon [51].

As the rule of thumb, the high degree of fractionation gives detailed and accurate information on the component distribution. TBP curve (Fig. 6.6), a graphical representation of the average boiling point of components against the volume percent of the distilled sample, has a smooth shape for many components, and small distillation steps [45].

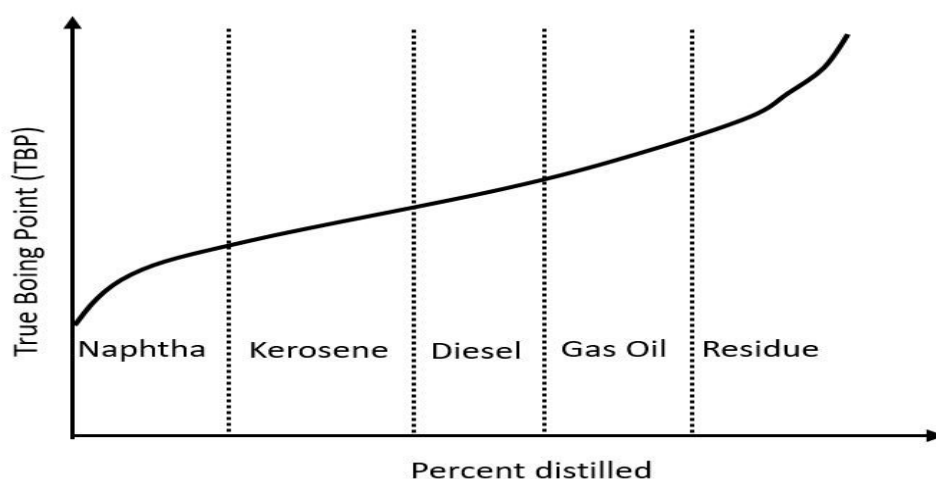


Fig. 6.6: Typical TBP curve of a petroleum mixture [49]

Here ASTM D86 test is performed to gather distillation data and ASTM D1298 to estimate density. The study initially carried out laboratory tests to establish the boiling point and specific gravity. The calculated findings of the physical characteristics of the condensate sample as well as distillation results are tabulated in Data and shown in Table 6.10.

Table 6.10: Distillation data for KTL condensate

Volume %	ASTM°C (KTL)	DAUBERT°C	Field name	KTL
0	48	11.23731	VABP	263.84
10	84	61.974034	MeABP	244.827
30	100	92.206098	K	11.43882
50	114	114.51526	SG	0.778
70	136	143.19988	MW	23.25854
90	210	218.07942	API gravity	50.37661
95	259	329.57423	ν_{210}	0.371
EP.	310		ν_{100}	0.679
Density @32(kg/L)	0.844			

Empirical correlations are used to determine the necessary physical parameters for calculations involving the refining process. The actual boiling point (TBP) curve is constructed using Daubert's new approach, and the extrapolation of the Daubert curves results in the greatest recovery at the final distillation point. Then, utilizing Peng Robinson's thermodynamic model, DWSIM software helps create pseudo-components and their associated attributes using the generated TBP data.

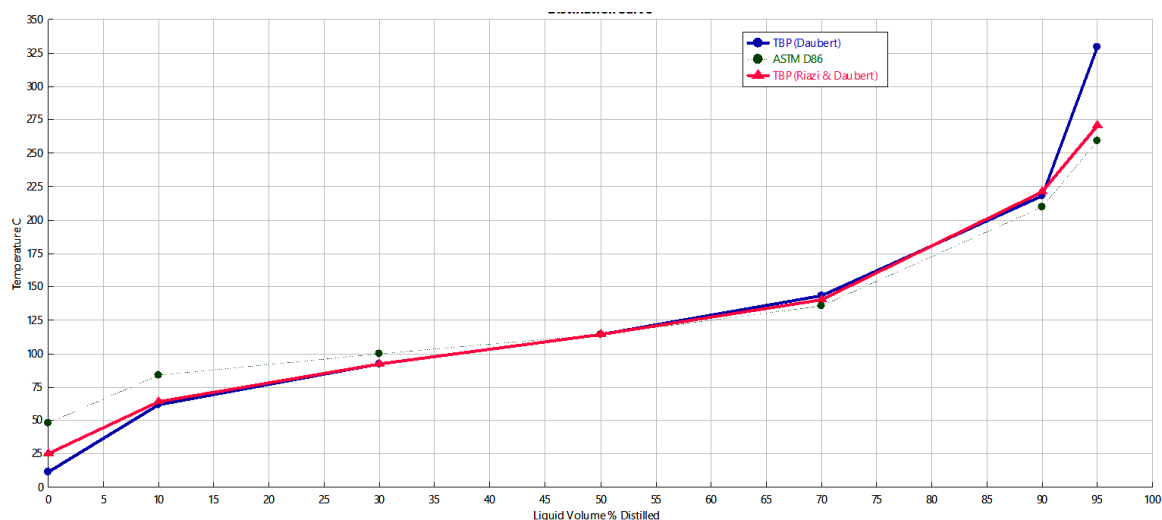


Fig. 6.7: ASTM and TBP curve for KTL condensate

In this study, the ASTM data are transformed into TBP data using the Riazi/API method and Daubert correlation. The differences in the curves are seen in Fig. 6.7. The ultimate boiling point is greater than the real ASTM data in the figure, however the IBP is lower than the ASTM IBP point for both TBP procedures. Additionally, the final boiling point is substantially higher according to the Daubert estimate than it is according to the Riazi calculation. Because a TBP distillation test has a higher degree of separation than an ASTM distillation test, the findings are different. Daubert's approach has a substantially higher endpoint (EP) temperature for KTL condensate. This is due to the KTL's smaller weight and the presence of more volatile components at the curve's conclusion.

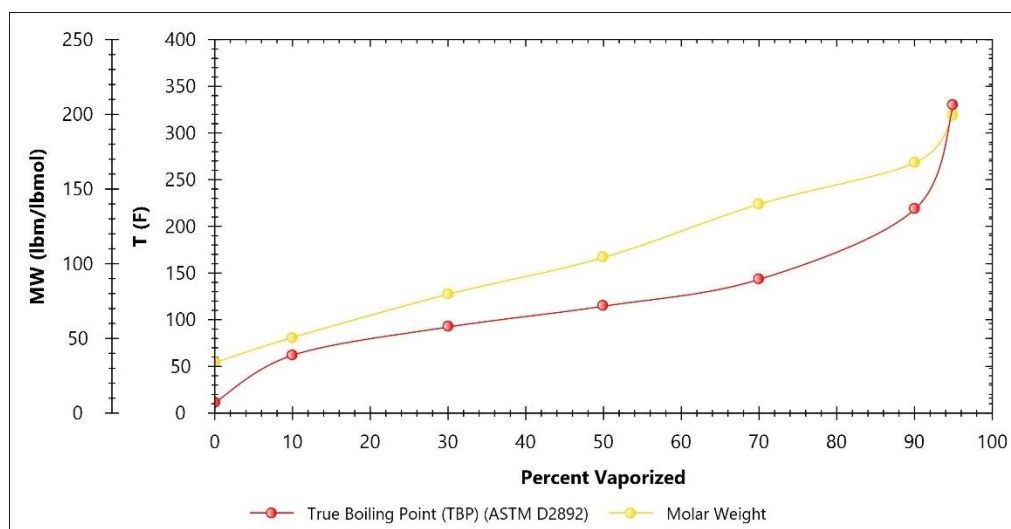


Fig. 6.8: TBP and Molecular weight curve for KTL condensate

In Fig. 6.8 the variation of molecular weight and boiling point temperature with % vaporized is displayed which assists in understanding the number of volatile components present at a particular fraction and thus aid in refining optimization.

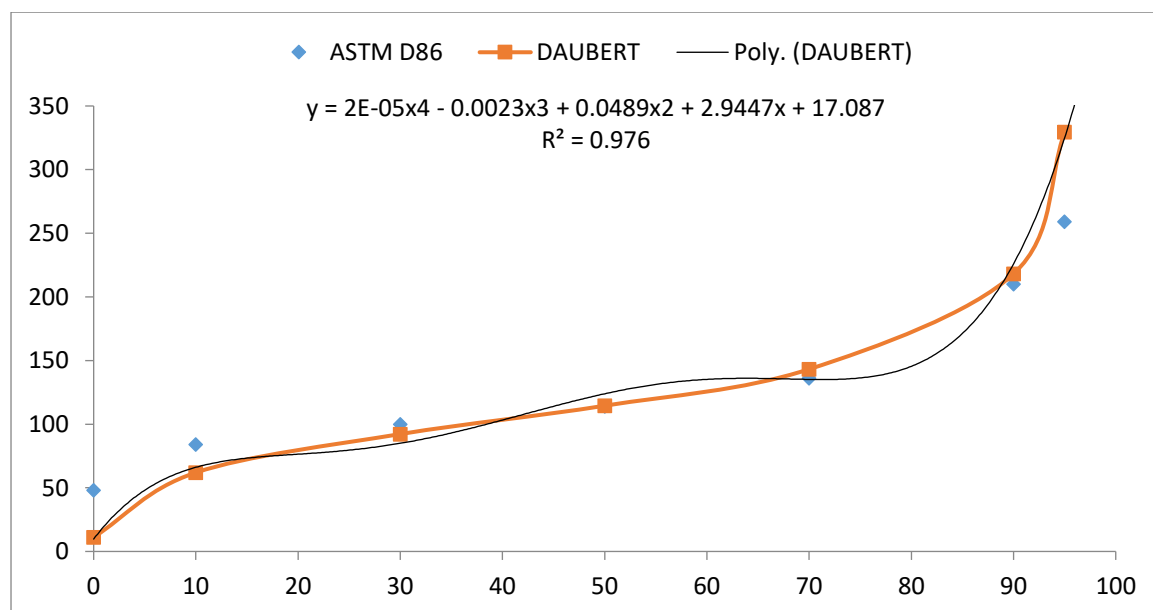


Fig. 6.9: Daubert's TBP extrapolation curve

The extrapolation of the curve to the final point (100%) is necessary to acquire the average boiling point of the last cut, which is needed to construct pseudo-components. The extrapolation produces a fourth-order equation with a correlation parameter of 0.976 in the case of the KTL sample (Fig. 6.9).

The petroleum fraction in a refining process is characterized using pseudo components as the foundation. Fractionation cannot identify the precise

components, such as aromatic, naphthene's, and paraffin; it can identify a specific number of mixture points. The combination has a predetermined cut point or boiling point range, is referred to as a pseudo component, and corresponds to several unknown true components.

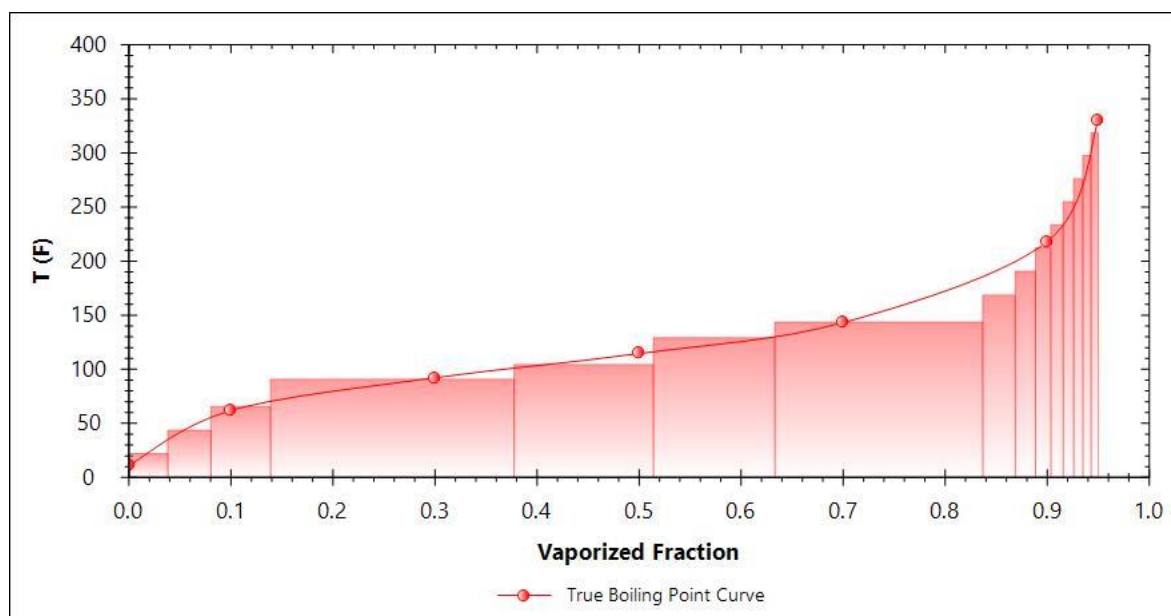


Fig. 6.10: Representation of TBP curve for pseudo components
Pseudo Cuts for the condensate sample is generated through software. Fig. 6.10 shows the cuts that correspond to a particular temperature and represent the cumulative percentage of vaporized fraction. This makes it easier to understand the hydrocarbon distribution within a particular boiling range and for this experiment it ranges from 48 to 310 °C. Subsequently, the thermodynamic and physical properties of each cut are generated and represented in Table 6.11.

Table 6.11: Physical properties of pseudo cuts

Name	Molar fraction	NB P C	SG	API	MW lb/lbm ol	Tc F	Pc lbf/f t2	Ac	Visc 1 ft2/s	Visc 2	PR Vshift ci/bi	SRK Vshif t
C_2061_ NBP_44	0.09582 1	21. 914 4	0.71 1228	33. 960 1	333.88	111 662	0.13 1645	2.63 E-06	4.88E -06	1.06 1625	1.23155 7	0.763 154
C_2061_ NBP_91	0.09554 6	43. 572 3	0.72 8057	38. 773 5	363.33 2	108 073	0.14 8008	2.67 E-06	4.11E -06	1.02 3699	1.18881 7	0.787 455
C_2061_ NBP_129	0.09671 1	65. 587 8	0.74 4127	54. 066 3	392.73 1	104 398	0.15 0812	2.76 E-06	3.65E -06	0.93 6009	1.09741 4	0.758 724
C_2061_ NBP_169	0.26606 2	90. 887 1	0.76 1436	82. 2	425.89 9	100 210	0.16 8542	2.90 E-06	3.34E -06	0.79 6883	0.95416 3	1.231 557
C_2061_ NBP_212	0.14537 3	104 .53	0.77 0303	86. 911 2	443.52 9	979 85. 4	0.17 8144	3.00 E-06	3.25E -06	0.78 5076	0.94039 6	1.188 817
C_2061_ NBP_255	0.08735 3	129 .32 2	0.78 5653	128 .80 3	475.13 8	940 29. 6	0.19 5655	3.21 E-06	3.18E -06	0.61 9012	0.77110 1	0.771 101
C_2061_ NBP_297	0.14271 9	143 .81 1	0.79 4201	136 .34	493.36 9	917 77. 8	0.20 5923	3.36 E-06	3.18E -06	0.60 8312	0.75872 4	0.940 396
C_2061_ NBP_22	0.02260 2	168 .71 7	0.80 8231	137 .58 6	524.31 5	880 22. 6	0.22 3365	3.66 E-06	3.24E -06	0.63 9728	0.78745 5	0.954 163
C_2061_ NBP_66	0.01290 7	190 .71 4	0.81 9976	151 .91 5	551.25 5	848 35. 2	0.23 896	3.97 E-06	3.35E -06	0.61 7499	0.76315 4	1.097 414
C_2061_ NBP_105	0.00905 5	212 .21 9	0.83 0925	164 .52 9	577.26 1	818 39. 9	0.23 1128	4.33 E-06	3.51E -06	0.60 8144	0.75245 2	0.789 8
C_2061_ NBP_144	0.00700 7	233 .59	0.84 1322	174 .72 3	602.79 7	789 82. 7	0.24 5072	4.74 E-06	3.71E -06	0.60 6007	0.74861 7	0.775 142
C_2061_ NBP_191	0.00575 3	254 .90 4	0.85 1249	182 .71 9	627.97 4	762 51	0.25 9001	5.21 E-06	3.96E -06	0.61 1743	0.75279 6	0.762 326
C_2061_ NBP_234	0.00491 3	276 .18 9	0.86 0753	188 .93 1	652.84 2	736 38. 4	0.27 2957	5.76 E-06	4.25E -06	0.62 2657	0.76232 6	0.752 796
C_2061_ NBP_276	0.00431 3	297 .45 6	0.86 987	193 .74 9	677.42 9	711 40. 2	0.28 695	6.39 E-06	4.60E -06	0.63 6736	0.77514 2	0.748 617

6.2.1 Atmospheric Distillation

The first significant procedure in a refinery, atmospheric distillation, often divides crude oil into its component fraction for additional processing. At 350 to 390 °C and atmospheric pressure, the feed is typically introduced into the column. The recombined fluid composition is used in this study as a feedstock for distillation, and the operation is simulated to observe the conditions of the distillate and bottom product. Furthermore, the energy efficiency of the condensate duty, reboiler duty, and column are monitored. The outcomes are then examined and contrasted with actual filed data that was obtained from the refinery.

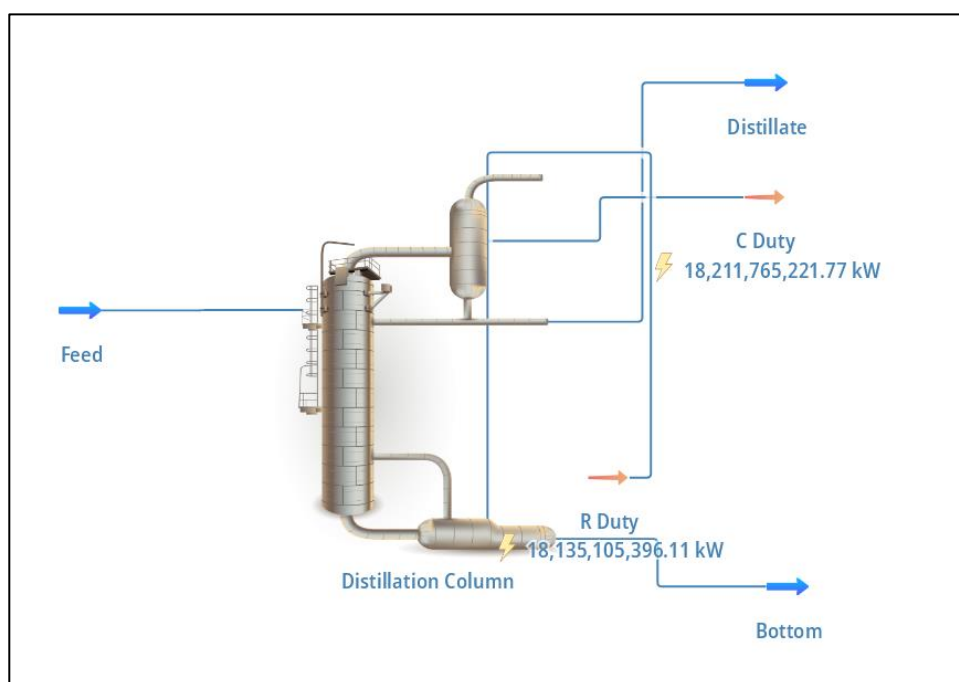


Fig. 6.11: Atmospheric distillation for KTL condensate

Here a single distillation column, a condenser for the top product and a reboiler is used for the bottom product as seen from Fig. 6.11. The top column pressure is maintained at 2.0 -2.5 barg and bottom pressure is maintained at 2.2 -2.7 barg. The feed is introduced at 360°C at stages 6. Feed flow rate is maintained as 170 m³/hour. The values are kept like that of the distillation of Eastern Refinery Limited (ERL). Peng Robinson equation has been selected as the thermodynamic

package. The column pressure drop has set 0.5 bar, and theoretically 12 stages have been chosen to distillate the products. The calculated pressure and temperature for each stage are shown in Table 6.12.

Table 6.12: Property table for distillation column

Distillation Column Type: Distillation Column			
Condenser Pressure Drop: 0.5 bar		Column Pressure Drop: 2 bar	
Condenser Duty: 1.82118E+10 kW		Reboiler Duty: -1.81351E+10 kW	
Number of Stages: 12			
Stage_Pressure_1	1.01325 bar	Stage_Temperature_1	140.401 C
Stage_Pressure_2	1.19507 bar	Stage_Temperature_2	130.62 C
Stage_Pressure_3	1.37689 bar	Stage_Temperature_3	137.187 C
Stage_Pressure_4	1.5587 bar	Stage_Temperature_4	148.574 C
Stage_Pressure_5	1.74052 bar	Stage_Temperature_5	181.509 C
Stage_Pressure_6	1.92234 bar	Stage_Temperature_6	222.534 C
Stage_Pressure_7	2.10416 bar	Stage_Temperature_7	242.482 C
Stage_Pressure_8	2.28598 bar	Stage_Temperature_8	250.874C
Stage_Pressure_9	2.4678 bar	Stage_Temperature_9	255.853 C
Stage_Pressure_10	2.64961 bar	Stage_Temperature_10	259.838 C
Stage_Pressure_11	2.83143 bar	Stage_Temperature_11	263.425 C
Stage_Pressure_12	3.01325 bar	Stage_Temperature_12	266.773 C
Condenser Specification Value		640	
Reboiler Specification Value		-1E-10 mol/s	
Global Stage Efficiency		G6	
Condenser Calculated Value		640	
Reboiler Calculated Value		91.4696 mol/s	
Stream 'Feed' Stage Index		6	
Stream 'Bottom' Stage Index		11	
Stream 'Distillate' Stage Index		0	
Estimated Height		7000 mm	
Estimated Diameter		5.90226E+06 mm	

From the simulation, the column height is obtained 7000mm, the condenser and reboiler duty is obtained 1.82118E+10kW and 1.81351E+10kW, respectively.

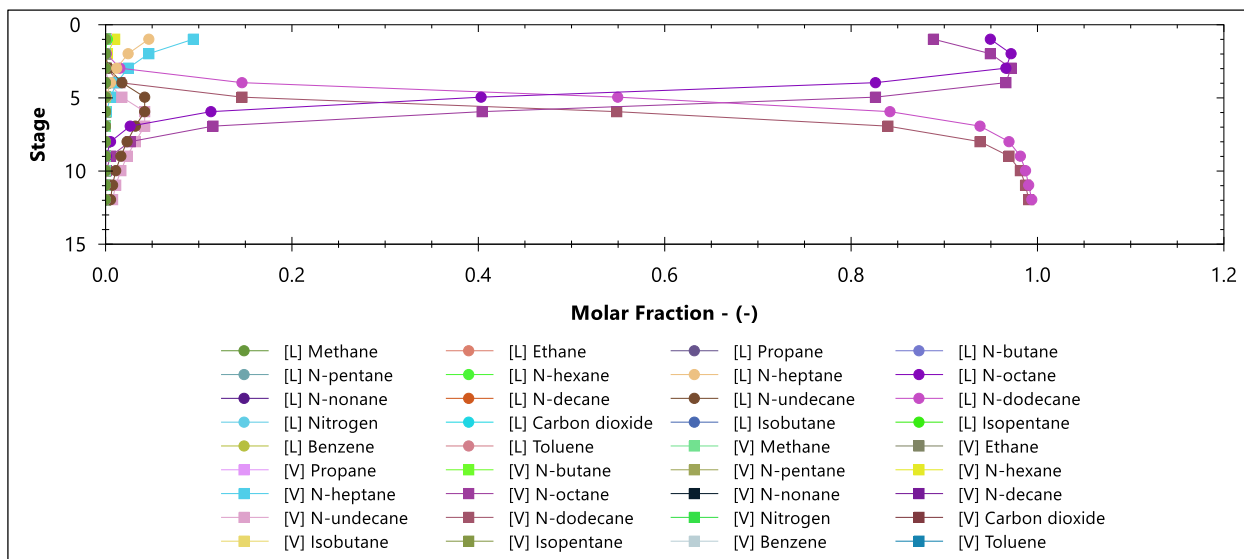


Fig. 6.12: Component flow inside distillation column

Fig. 6.12 represents the distribution of hydrocarbons at various stages of the distillation process which assists in assessing the fractionation of the long carbon chain into its components.

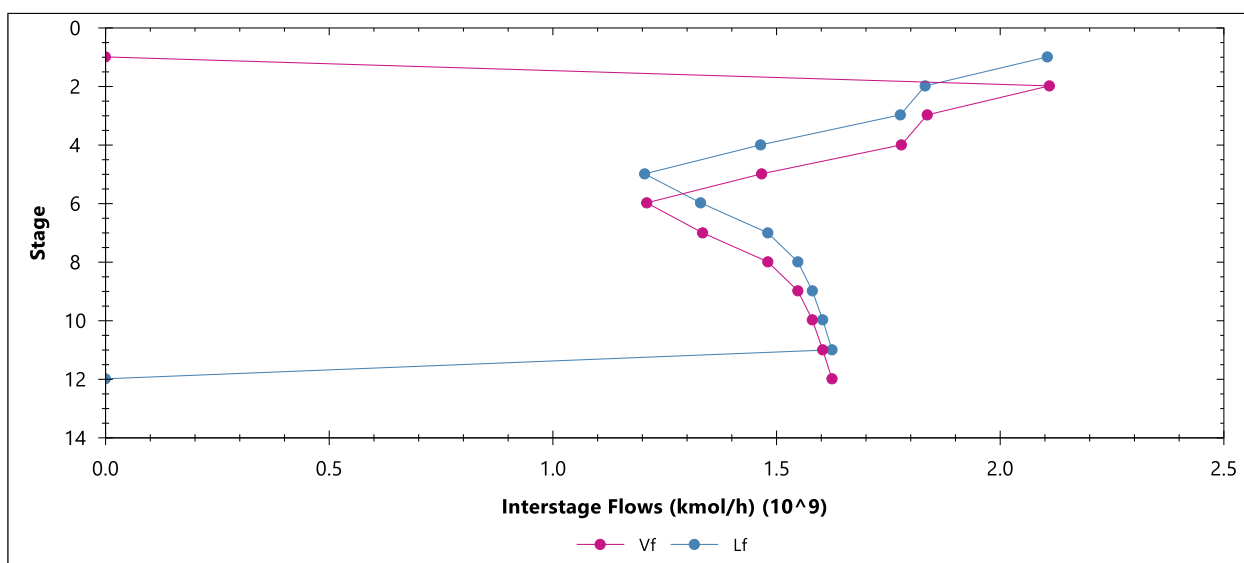


Fig. 6.13: Interstage flow inside distillation column

Fig. 6.13 represents the interstage flow inside distillation column providing a detailed view of how each component distributed across different trays. Thereby helping to optimize operating conditions, reflux ratios, feed rates or temperatures. The flow ranges from 0 to 2×10^9 Kmol/h for vapor and liquid fraction.

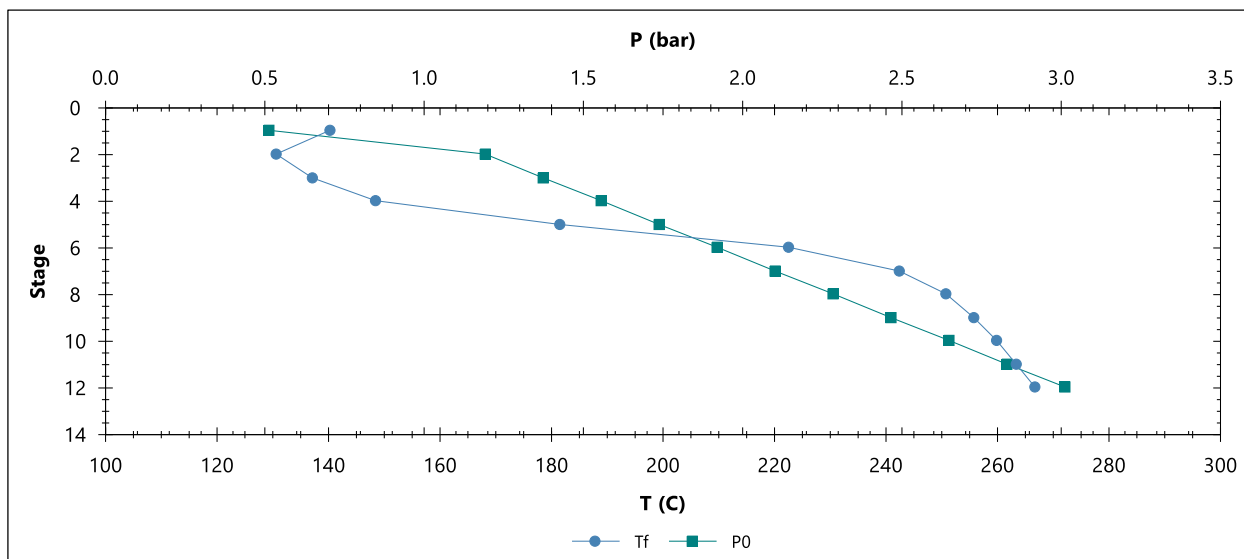


Fig.6.14: Temperature profile inside distillation column

The temperature profile for the distillation column is displayed through Fig. 6.14. The temperature ranges between 120 to 280 °C. This helps to analyze the heat requirements at different stages allowing operators to optimize heat input and minimize energy usage.

Table 6.13 shows the estimated properties for the feed. The compositional weight% data is converted into mole fraction; density is obtained 2.19858×10^6 kg/m³. Mass flow rate is calculated 3.73758×10^8 kg/hour. Input pressure is obtained 51.2391 bar.

Table 6.13: Feed property data from distillation column

Feed	Value	Mixture Molar Fraction	
Temperature, °C	360	Methane	1.42603E-06
Pressure, bar	51.2391	Ethane	1.42093E-06
Mass Flow, kg/h	3.73758E+08	Propane	1.98777E-05
Molar Flow, kmol/h	3.29291E+06	N-butane	2.77566E-05
Volumetric Flow, m ³ /h	170	N-pentane	0.000143448
Density (Mixture), kg/m ³	2.19858E+06	N-hexane	0.00235315
Molecular Weight (Mixture), kg/kmol	113.504	N-heptane	0.0467066
Specific Enthalpy (Mixture), kJ/kg	659.277	N-octane	0.950316
Specific Entropy (Mixture), kJ/[kg.K]	1.27574	N-nonane	0.000104339
Molar Enthalpy (Mixture), kJ/kmol	74830.6	N-decane	2.08388E-05
Molar Entropy (Mixture), kJ/[kmol.K]	144.802	N-undecane	7.46185E-05
Thermal Conductivity (Mixture), W/[m.K]	0.0351278	N-dodecane	0.000102898
		Nitrogen	1.01859E-09
		Carbon dioxide	1.01859E-09
		Isobutane	1.43917E-05
		Isopentane	9.88614E-06
		Benzene	0.000103514
		Toluene	1.06321E-08

The feed after distillation yields two material streams: distillate and bottom. Compositional mole fraction for distillate as well as other properties are shown in Table 6.14. The temperature is estimated to be 140.41 degree Celsius, and pressure is 0.513 bar which satisfies the primary conditions. Density increases to 596.905 kg/m³.

Table 6.14: Distillate property data from distillation column

Distillate	Value	Molar Fraction	
Temperature, °C	140.401	Methane	1.42603E-06
Pressure, bar	0.51325	Ethane	1.42093E-06
Mass Flow, kg/h	3.73758E+08	Propane	1.98777E-05
Molar Flow, kmol/h	3.29291E+06	N-butane	2.77566E-05
Volumetric Flow, m ³ /h	626160	N-pentane	0.000143448
Density (Mixture), kg/m ³	596.905	N-hexane	0.00235315
Molecular Weight (Mixture), kg/kmol	113.504	N-heptane	0.0467066
Specific Enthalpy (Mixture), kJ/kg	-79.1447	N-octane	0.950316
Specific Entropy (Mixture), kJ/[kg.K]	-0.11331	N-nonane	0.000104339
Molar Enthalpy (Mixture), kJ/kmol	-8983.25	N-decane	2.08388E-05
Molar Entropy (Mixture), kJ/[kmol.K]	-12.8611	N-undecane	7.46185E-05
Thermal Conductivity (Mixture), W/[m.K]	0.0935374	N-dodecane	0.000102898
		Nitrogen	1.01859E-09
		Carbon dioxide	1.01859E-09
		Isobutane	1.43917E-05
		Isopentane	9.88614E-06
		Benzene	0.000103514
		Toluene	1.06321E-08

Table 6.15 reflects results for Bottom products where temperature has risen to 266.773 degree Celsius and pressure to 3 bar. The volumetric flow rate is 103.511 m³/ hour and density 541.596 kg/m³.

Table 6.15: Bottom product property and molar fraction

Bottom	Value	Molar Fraction	
Temperature, °C	266.773	Methane	1.15203E-20
Pressure, bar	3.01325	Ethane	3.49627E-19
Mass Flow, kg/h	56061.2	Propane	6.68755E-17
Molar Flow, kmol/h	329.291	N-butane	1.26951E-15
Volumetric Flow, m ³ /h	103.511	N-pentane	7.82656E-14
Density (Mixture), kg/m ³	541.596	N-hexane	1.60926E-11
Molecular Weight (Mixture), kg/kmol	170.248	N-heptane	9.57616E-09
Specific Enthalpy (Mixture), kJ/kg	283.917	N-octane	2.32161E-05
Specific Entropy (Mixture), kJ/[kg.K]	0.766778	N-nonane	3.98192E-07
Molar Enthalpy (Mixture), kJ/kmol	48336.4	N-decane	1.2341E-05
Molar Entropy (Mixture), kJ/[kmol.K]	130.543	N-undecane	0.00603802
Thermal Conductivity (Mixture), W/[m.K]	0.083056	N-dodecane	0.993926
		Nitrogen	7.80287E-25
		Carbon dioxide	5.85993E-23
		Isobutane	3.45943E-16
		Isopentane	3.45006E-15
		Benzene	1.08779E-12
		Toluene	6.55134E-15

The temperature at the top and bottom of the column is kept between 127 and 134 °C and 300 and 302 °C at ERL. The ratio of reflux is 1.8–2. The simulation yielded temperatures of 267 °C and 140 °C for the top and bottom sections. Reflux ratio is kept constant at 1.5. Once more, in actual operation, 33 trays are utilized, and the distillation tower is 85 feet (26 meters) tall overall. The resultant value from the simulation was 12 trays and 7 meters. Thus, there is some deviation from actual field data in the results obtained. The reason for the variations in tray counts and column heights is that while condensate has a shorter carbon chain than crude oil, which is utilized as feed in ERL. So, the reduced column height and tray number can distill the product efficiently.

Next another distillation is performed where the pseudo-cut fractions obtained from the feed are distilled into a shortcut column as seen from Fig. 6.15. Here the condition is maintained at atmospheric temperature. The volumetric flow rate is set at 170 m³/hour and reflux ratio is set at 1.5.

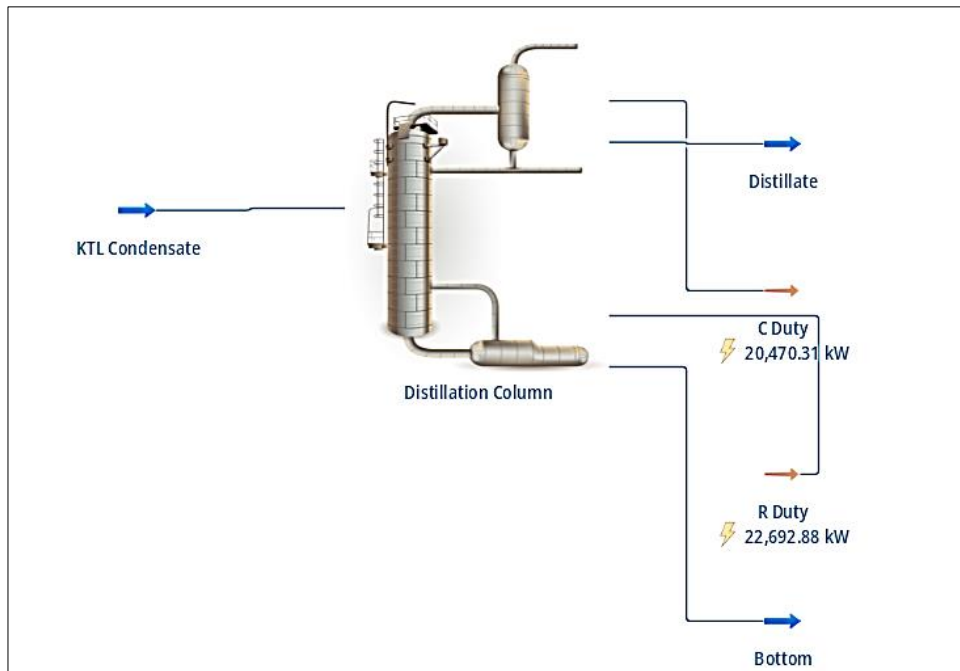


Fig. 6.15: Shortcut distillation for KTL condensate pseudo cuts (separator)

Physical and thermodynamic parameters are calculated using the Peng Robinson thermodynamic model. Table 6.16 shows the molar fraction of the cuts.

Table 6.16: Component molar fraction for pseudo component (Mixture)

Component	Mixture Molar Fraction	Component	Mixture Molar Fraction
C_2061_NBP_44	0.0618342		
C_2061_NBP_91	0.25982	C_2061_NBP_66	0.0740831
C_2061_NBP_129	0.109136	C_2061_NBP_105	0.144185
C_2061_NBP_169	0.0298025	C_2061_NBP_144	0.191993
C_2061_NBP_212	0.0128796	C_2061_NBP_191	0.017712
C_2061_NBP_255	0.00861623	C_2061_NBP_234	0.0102584
C_2061_NBP_297	0.00667358	C_2061_NBP_276	0.00749196
C_2061_NBP_22	0.0594634	C_2061_NBP_319	0.00605029

Table 6-17 illustrates that the estimated minimum reflux ratio is 1.05, the actual stage is 15, the ideal feed stage is 5, and the pressure in the reboiler and condenser is kept at 0.1889 bar.

Table 6.17: Shortcut distillation column properties

Property	Value
Reflux Ratio	1.5
Heavy Key Molar Fraction	0.01
Light Key Molar Fraction	0.01
Condenser Pressure, bar	0.1889
Reboiler Pressure, bar	0.1889
Minimum Reflux Ratio	1.05303
Minimum Stages	7.48651
Optimal Feed Stage	4.69571
Stripping Liquid Molar Flow, kmol/h	7018.61
Rectify Liquid Molar Flow, kmol/h	1551.31
Stripping Vapor Molar Flow, kmol/h	2585.53
Rectify Vapor Molar Flow, kmol/h	2585.52
Condenser Duty, kW	20470.3
Reboiler Duty, kW	22692.9
Actual Stages	14.9318
Temperature, °C	30
Pressure, bar	0.188934
Mass Flow, kg/h	127169
Molar Flow, kmol/h	5467.3
Volumetric Flow, m ³ /h	170

The calculated value for condenser and reboiler duty is 20470.3 and 22693 KW respectively. The Critical properties and NBP obtained for this stream are shown in Table 6.18.

Table 6.18: Critical properties and NBP for pseudo components

Database	DWSIM
Type	Petroleum Fraction (Pseudo-compound)
CAS ID	3043-268
Molecular Weight	8.898912
Critical Temperature, K	440.8609
Critical Pressure, Pa	5346424
Critical Volume, m ³ /kmol	0.192279
Critical Compressibility	0.280468
Acentric Factor	0.131645
Gibbs Energy of Formation (Ideal Gas at 298.15 K), kJ/kg	-4893.5
Enthalpy of Formation (Ideal Gas at 298.15 K), kJ/kg	0.122858
Normal Boiling Point, K	267.5469

Estimated molecular weight is 8.89, critical temperature is 334 °F, critical pressure is 775.62 psia, normal boiling point is 267.54 K and acentric factor is 0.13. Model specific properties are shown in Table 6.19.

Table 6.19: Model specific property for pseudo components

MODEL-SPECIFIC PROPERTIES	
Chao Seader Acentric Factor	0.111449
Chao Seader Solubility Parameter	8.09339
Chao Seader Liquid Molar Volume	72.76769
Rackett Compressibility	0.099885
PR Volume Translation Coefficient	1.061625
SRK Volume Translation Coefficient	1.231557

The specific gravity, Watson characterization factor, K, viscosity, and temperature for pseudo components is represented in Table 6-20.

Table 6.20: Pseudo component properties

PSEUDOCOMPOUND (PETROLEUM FRACTION)-RELATED PROPERTIES	
Specific Gravity	0.711228
Watson K	11.02086
Temperature for Viscosity Data Point 1, K	311
Viscosity @ T1, Pa.s	2.44E-07
Temperature for Viscosity Data Point 2, K	372
Viscosity @ T2, Pa.s	4.53E-07

Data calculated for feed (pseudo-components) are shown in Table 6-21. The molecular weight is 23.26 for the mixture.

Table 6.21: Property table for pseudo component (mixture)

Density (Mixture), kg/m ³	748.056
Molecular Weight (Mixture), kg/kmol	23.26
Specific Enthalpy (Mixture), kJ/kg	-1576.73
Specific Entropy (Mixture), kJ/[kg.K]	-3.31011
Molar Enthalpy (Mixture), kJ/kmol	-36674.8
Molar Entropy (Mixture), kJ/[kmol.K]	-76.9932
Thermal Conductivity (Mixture), W/[m.K]	0.270447
Kinematic Viscosity (Overall Liquid), m ² /s	5.77561E-07
Dynamic Viscosity (Overall Liquid), Pa.s	0.000432048
Heat Capacity (Overall Liquid), kJ/[kg.K]	2.75205
Heat Capacity Ratio (Overall Liquid)	1.40285
Mass Flow (Overall Liquid), kg/h	127169
Molar Flow (Overall Liquid), kmol/h	5467.3
Volumetric Flow (Overall Liquid), m ³ /h	170
Compressibility Factor (Overall Liquid)	0.000238333

Table 6-22 compiled the mole fraction data for vapor and overall liquid fraction of feed.

Table 6.22: Component molar fraction for pseudo component (vapor and overall liquid)

Pseudo cuts	Molar Fraction (Vapor)	Molar Fraction (Overall liquid)
C_2061_NBP_22	0.424799	0.0594634
C_2061_NBP_44	0.213046	0.0618342
C_2061_NBP_66	0.117409	0.0740831
C_2061_NBP_91	0.161402	0.25982
C_2061_NBP_105	0.0530002	0.144185
C_2061_NBP_129	0.0149218	0.109136
C_2061_NBP_144	0.0144169	0.191993
C_2061_NBP_169	0.000769721	0.0298025
C_2061_NBP_191	0.000171341	0.017712
C_2061_NBP_212	4.59963E-05	0.0128796
C_2061_NBP_234	1.31231E-05	0.0102584
C_2061_NBP_255	3.8152E-06	0.00861623
C_2061_NBP_276	1.1071E-06	0.00749196
C_2061_NBP_297	3.16748E-07	0.00667358
C_2061_NBP_319	8.86159E-08	0.00605029

The calculated properties for the top (distillate) and bottom product are shown in Table 6.23. The molecular weight obtained for top and bottom product is 16 and 25, density is 747.54 and 679.116 m³/hour accordingly.

Table 6.23: Property table for pseudo component (mixture)

Property	Value	
	Distillate	Bottom
Temperature, °C	-5.21056 C	58.2147
Pressure, bar	0.1889	0.1889
Mass Flow, kg/h	16545	110624
Molar Flow, kmol/h	1034.21	433.08
Volumetric Flow, m3/h	22.1326	162.895
Density (Mixture), kg/m3	747.54	679.116
Molecular Weight (Mixture), kg/kmol	15.9978	24.9542
Specific Enthalpy (Mixture), kJ/kg	-1803	-1470.56
Specific Entropy (Mixture), kJ/[kg.K]	-5.10505	-3.05816
Molar Enthalpy (Mixture), kJ/kmol	-28844.1	-36696.8
Molar Entropy (Mixture), kJ/[kmol.K]	-81.6695	-76.3141
Thermal Conductivity (Mixture), W/[m.K]	0.258489	0.261469

The number of components remaining in the top and bottom stream after distillation is also calculated and shown in Table 6-24.

Table 6.24: Composition molar fraction in distillate and bottom products

Compound ID	Mixture Molar Fraction	
	Distillate	Bottom
C_2061_NBP_22	0.314347	1.14563E-07
C_2061_NBP_44	0.326761	2.79752E-05
C_2061_NBP_66	0.348769	0.01
C_2061_NBP_91	0.01	0.318102
C_2061_NBP_105	0.000109987	0.177797
C_2061_NBP_129	5.06925E-08	0.134598
C_2061_NBP_144	1.00409E-09	0.236785
C_2061_NBP_169	5.28094E-14	0.0367553
C_2061_NBP_191	2.01297E-17	0.0218441
C_2061_NBP_212	8.42371E-21	0.0158844
C_2061_NBP_234	3.08118E-24	0.0126517
C_2061_NBP_255	9.19378E-28	0.0106264
C_2061_NBP_276	2.16083E-31	0.0092398
C_2061_NBP_297	3.90636E-35	0.00823049
C_2061_NBP_319	5.32638E-39	0.00746179

The atmospheric distillation approach typically considers the entire set of theoretical trays and equilibrium stages in a distillation column; however, shortcut distillation does not consider all step. Furthermore, the shortcut distillation is based on empirical equations and heuristics, frequently used for

preliminary or conceptual studies. In contrast, atmospheric distillation provides a detailed and accurate representation of the separation process. When the two test results are of the study are compared, it may be concluded that the shortcut column uses less energy.

Chapter 7 : ANALYSIS

The phase behaviour analysis of Kailashtila gas field and the differences between experimental and simulated results have been discussed here. The model's acceptability as well as findings of the proposed model is discussed in section 7.2. In section 7.3 the performance of condensate in refinery and the energy efficiency of distillation column have been presented.

7.1 PHASE BEHAVIOUR OF KAILASHTILA GAS FIELD

To evaluate the error, the formation volume factor is taken into considerations. Since some data of middle gas sand layer was not possible to determine, the rock and fluid properties of LGS is considered like that of MGS. The differences between experimental and simulated results are expressed through Table 7.1 to Table 7.9.

Table 7.1: Deviation for different rock and fluid properties

Property	UGS			LGS		
	Actual value	Simulated results	deviation	Actual value	Simulated results	deviation
Z factor	0.851	0.8572	0.0072	0.954	0.8931	-0.064
Viscosity, cP	0.021	0.0194	-0.076	0.02	0.0188	-0.06
Dew point pressure, P_{sat} , psia	2725	2579.92	-5.3(before tuning)	2814	2636.17	-6.3
		3012.91	10.6(after tuning)		2654.52	-5.7
Molecular weight.lb/mol	18.3	18.12	-0.0098	18.3	18.44	-0.0076
LGR bbl/MMscF	11.2	0.008857 (112.9 MMscf/bbl)	-0.999	11.2	10 (0.1 MMscf/bbl)	-0.107

As seen from the Table 7.1, the differences for Z factor, viscosity, molecular weight, LGR ranges between -0.1 to 0.1 for both upper and lower gas field. The simulated value for saturation pressure for fluctuates between -10 to +10 for both cases.

The values for relative volume are ranges between 0.00443 and 0.00463 Rvol/Svol as seen from CCE experiments. The values estimated from simulation ranges 0.9 to 33 V/V_d. The deviation is almost 1.5% and it is because in simulation the Svol is taken as the dew point volume.

Table 7.2: Differences for relative volume (UGS)

Rel Vol V/V _d		Weight	1.00		
Pressure	Exp	Before	%Dev	After	%Dev
psia	value	tuning	before	tuning	after
3345.00	0.9027	0.7962	-11.8	0.9158	1.5
3000.00	0.9891	0.8727	-11.8	1.0038	1.5
2962.49	1.0000	0.8823	-11.8	1.0151	1.5
2725.00	1.0793	0.9507	-11.9	1.0949	1.4
2500.00	1.1710	1.0305	-12.0	1.1872	1.4
2000.00	1.4623	1.2863	-12.0	1.4807	1.3
1500.00	1.9758	1.7380	-12.0	1.9998	1.2
1000.00	3.0454	2.6810	-12.0	3.0843	1.3
500.00	6.3363	5.5848	-11.9	6.4245	1.4
100.00	32.9986	29.0983	-11.8	33.4714	1.4

The % deviation for liquid volume fraction lies in the negative region (Table 7.3).

Table 7.3: Comparison for liquid vol%

Liq Vol		Weight=	1.00		
% of V _d					
Pressure	Exp	Before	%Dev	After	%Dev
psia	value	tuning	before	tuning	after
2962.49	0.00			0.03	
2725.00	0.17		-100.0	0.13	-26.0
2500.00	0.32	0.03	-89.9	0.20	-37.6
2000.00	0.59	0.21	-64.9	0.34	-43.2
1500.00	0.80	0.35	-56.4	0.47	-41.6
1000.00	0.90	0.44	-51.5	0.56	-37.9
500.00	0.84	0.40	-51.8	0.52	-38.4
100.00	0.47	0.18	-60.7	0.26	-43.8

From IPEC/PVT experiment the ranges for Z factor is obtained from 0.86 to 0.98 and the simulated results show a good agreement with that (Table 7.4).

Table 7.4: Z factor value from CCE/CME test

Z Factor		Weight=	1.00		
Gas					
Pressure	Exp	Before	%Dev	After	%Dev
psia	value	tuning	before	tuning	after
2500.00	0.876	0.875	-0.1	0.876	0.0
2000.00	0.876	0.874	-0.2	0.875	-0.2
1500.00	0.889	0.887	-0.3	0.887	-0.2
1000.00	0.915	0.913	-0.2	0.913	-0.2
500.00	0.952	0.951	-0.1	0.951	-0.1
100.00	0.989	0.989	0.0	0.989	0.0

The experimental and estimated results for viscosity exhibit minor difference (Table 7.5).

Table 7.5: Percent deviation for viscosity

Gas Visc		Weight=	1.00		
cP					
Pressure	Exp	Before	%Dev	After	%Dev
psia	value	tuning	before	tuning	after
2500.00	0.0200	0.0183	-8.7	0.0182	-9.0
2000.00	0.0170	0.0165	-2.7	0.0165	-2.8
1500.00	0.0160	0.0151	-5.7	0.0151	-5.7
1000.00	0.0140	0.0139	-0.5	0.0139	-0.5
500.00	0.0140	0.0131	-6.7	0.0131	-6.7
100.00	0.0130	0.0125	-3.6	0.0125	-3.6

Less than 0.1% deviation is seen for relative volume (Table 7.6).

Table 7.6: Differences for rel volume (LGS)

Rel Vol		Weight=	1.00		
V/Vd					
Pressure	Exp	Before	%Dev	After	%Dev
psia	value	tuning	before	tuning	after
4379.00	0.6593	0.6593	0.0	0.6635	0.6
4000.00	0.7040	0.7040	0.0	0.7085	0.6
3500.00	0.7810	0.7810	0.0	0.7860	0.6
2814.00	0.9418	0.9418	0.0	0.9479	0.7
2636.17	1.0000	1.0000	0.0	1.0065	0.7
2500.00	1.0517	1.0517	0.0	1.0587	0.7
2000.00	1.3126	1.3126	0.0	1.3212	0.7
1500.00	1.7692	1.7692	0.0	1.7807	0.7
1000.00	2.7164	2.7164	0.0	2.7340	0.6
500.00	5.6264	5.6264	0.0	5.6629	0.6
100.00	29.1890	29.1890	0.0	29.3780	0.6

The maximum variation at saturation pressure, which is greater than 5%, is indicated by the value derived from simulation (Table 7.7). Other values are within a tolerable range.

Table 7.7: Comparison of liquid vol% (LGS)

Liq Vol		Weight=	1.00		
% of Vd					
Pressure	Exp	Before	%Dev	After	%Dev
psia	value	tuning	before	tuning	after
2814.00	0.00			0.01	
2500.00	0.05	0.05	7.4	0.06	25.2
2000.00	0.28	0.28	1.1	0.29	3.3
1500.00	0.46	0.46	0.2	0.47	1.1
1000.00	0.55	0.55	0.4	0.56	1.2
500.00	0.49	0.49	0.7	0.50	1.5
100.00	0.21	0.21	-0.4	0.21	1.0

There is good agreement between the Z factor values for both scenarios (Table 7.8).

Table 7.8: Z factor value from CCE/CME test

Z Factor		Weight=	1.00		
Pressure	Exp	Before	%Dev	After	%Dev
psia	value	tuning	before	tuning	after
4379.00	0.978	0.9781	0.0	0.9781	0.0
4000.00	0.9540	0.9540	0.0	0.9540	0.0
3500.00	0.9261	0.9261	0.0	0.9261	0.0
2814.00	0.8979	0.8979	0.0	0.8979	0.0
2636.17	0.8931	0.8931	0.0	0.8932	0.0
2500.00	0.891	0.891	0.0	0.891	0.0
2000.00	0.890	0.890	0.0	0.890	0.0
1500.00	0.901	0.901	0.0	0.901	0.0
1000.00	0.923	0.923	0.0	0.923	0.0
500.00	0.956	0.956	0.0	0.956	0.0
100.00	0.990	0.990	0.0	0.990	0.0

The difference in viscosity between the experimental and simulated data is within a reasonable range (Table 7.9).

Table 7.9: Percent deviation for viscosity(LGS)

Gas Viscosity		Weight=	1.00		
cP					
Pressure	Exp	Before	%Dev	After	%Dev
psia	value	tuning	before	tuning	after
2814.00	0.0190	0.0194	2.0	0.0194	2.0
2636.17	0.0190	0.0188	-1.2	0.0188	-1.2
2500.00	0.0180	0.0183	1.7	0.0183	1.7
2000.00	0.0170	0.0167	-1.8	0.0167	-1.8
1500.00	0.0150	0.0153	2.3	0.0153	2.3
1000.00	0.0140	0.0143	1.8	0.0143	1.8
500.00	0.0130	0.0134	3.3	0.0134	3.3
100.00	0.0130	0.0129	-0.7	0.0129	-0.7

Following an analysis of the data, the study has drawn some findings. The KTL field's density and specific gravity indicate that it is a medium-density fluid. The fluid's compressible character is indicated by the Z factor value, which approaches 1 as the pressure decreases and the fluid begins to behave like an incompressible fluid at isothermal conditions. The sample's retrograde behaviour under isothermal conditions is indicated by the creation of two phases in the CVD and CME experiments. Both UGS and LGS's dew point pressures are below the reservoir's starting pressure, meeting the requirement that the dew point pressure be lower than the reservoir's initial pressure.

7.2 MODEL ANALYSIS

The model is developed considering existing conservation of mass law, EOS of being used in petroleum engineering field. The model's validity is evaluated using actual field data. Because it was not feasible to test the model's validity in an actual case, the author was forced to rely on computational outcomes. The model is designed for the area close to the well bore where the phase transitions from single to two. The characteristics of a specific well and reservoir determine how far the wellbore effect expands and where condensate banking occurs. Therefore, the outcomes for the three KTL wells may differ for other gas fields. Again, because the pressure transient test could not be carried out in real time, the study relied on empirical correlation to calculate the effective wellbore radius. Table 5.4 displays the difference between the experimental, q_{MW} , and the estimated, q_M . The pressure took 4.3 feet to stabilize at the well's distance. The idea was to display the reservoir's flow rate at various points. Furthermore, P_{wf} and P_R are computed to see whether they fall inside the real pressure range. For example, well 1 at 15 feet from the well will have a flow of 697.85 MMscfD and a reservoir pressure of 3515 psia (or 3609 from the calculation). The pressure will

appear constant since the flow approaches a steady state. Then, P_{wf} for the second well, assuming it is positioned at 15 feet from well 1, will be 3381.58 psia.

The study attempted to estimate the pressure that could exist in that scenario because the average reservoir pressure is a hypothetical term that assumes the reservoir is infinite and the pressure is not disturbed by an external boundary. So at some point, calculated P_R exceeds the average reservoir pressure. The result analysis for the three well has been summarized in Table 7.10.

Table 7.10: Calculated value for well1, 2 And 3

Property	Well 1	Well 2	Well 3
Gas Layer	Lower	Upper	Middle
Initial Reservoir Pressure, psia	4366	3332	4263
Average Reservoir Pressure, psia	3515	3332	3463
Bottomhole Flowing Pressure, psia	3479.3	3202.2	3112.82
Measured flow rate at bottomhole condition, q_{MW} , MMscfD	13.96	151.84	4.712
Calculated distance from wellbore, ft	20	20	240
AOFP, MMscfD	58.619	75.051	158.984
Relative Deviation between measured and calculated flow rate, MMscfD	0 to 65.67	0 to 65.67	0 to 799
$e D1(r-r_w)$	1	1	1
Radius of investigation, ft	735	600	530
Wellbore radius, ft	0.3	0.3	0.3
Near well bore region, ft	4.3	5	226.5

The near wellbore radius for wells 1 and 2 is estimated to be 4.3 feet and 5 feet, respectively, with a relative error ranging from 0 to 65.67. In the case of well 3,

the close wellbore effect is observed to be predominant at 226.5 feet from the wellbore, with a relative error calculated between 0 and 799. This might occur from the inability to ascertain the fluid and rock properties in this area and the use of assumed data in calculations.

The flow pattern observed from Fig. 5.3. 5.4, 5.5, 5.6 and 5.7 follows the traditional trend of inflow performance and radius Vs pressure curve for the three wells. Additionally, the pressure and flow rate calculations fall within the range found in actual field experiments. Thus, the model and its solution can be regarded as legitimate and additional investigation can be recommended.

7.3 PERFORMANCE EVALUATION OF CONDENSATE AND DISTILLATION PROCESS

In Chapter 6, calculation has been performed for condensate sample. Before that, the fluid's composition is recombined to determine whether it accurately represents the composition of the KTL gas field sample. The fluid was collected from the separator that contained gas and condensate. The C1 percent in UGS and LGS was found to be 0.9403 and 0.9415, respectively, while the simulated value for the recombined sample is 0.93463. This can be observed by comparing the mole fraction from Tables 4-2 and 6-1. The difference is only 0.00567 and 0.00687. So, all three samples represent gas samples. The normal critical temperature and pressure is -81.9 °C and pressure is 667.8 psia [52] and the estimated critical properties of C1 from simulation is -82.55 °C and 667.2 psia and for other fraction the calculated properties are found to have a close match with existing data. Thus, there is good convergence seen in the computed and simulated findings. The critical pressure of the recombined sample is estimated 562.04 psia and 553.67 °F .

Table 7.11: Comparison between lab and simulated properties

Property	UGS	LGS	Recombined	
			UGS	LGS
Pseudo- critical pressure,	5.020	6.583	5.9	7.76
Pseudo-critical Temperature	1.691	1.745	0.27	0.31
Z factor	0.851	0.954	0.893 (at P_{dew})	
Dew point pressure, psia	2725	2814	1333.74	
Gas formation Volume factor	0.00442(initial)	0.00390 (initial)	0.012 (at P_{dew})	
GOR, bbl/MMscf	11.2	11.18	5	

Comparing the results, it has been found that the properties of the recombined fluid is somewhat like that of UGS fluid. For P_{dew} and GOR the error is -0.5 and -0.55.

The ASTM distillation temperature range for KTL is 48 to 259 °C and the TBP temperature range is 11 to 330 °C. The specific gravity 0.778 corresponds to medium dense petroleum product. More products with lighter compositions can be obtained by further distilling the pseudo-products that the simulation produced. The stream has been divided into fifteen sections, or "pseudo-cuts." And calculations have been made for determining the thermophysical and physical properties, such as specific gravity, molecular weight, critical pressure, and temperature. To verify the discrepancies between the estimated values and those displayed in Table 7.12, a quality check is carried out between the simulated and experimented data. For molecular weight, the difference is 0%, while for API gravity, it is -6.83%. Based on modelling, the NBP is 310.36 °C, while the VABP is 263.84 °C based on correlations.

Table 7.12: Quality check for KTL condensate

Petroleum Assay Characterization Quality Check	
Molecular Weight (Specified):	23.26
Molecular Weight (Calculated):	23.26
Molecular Weight Error:	0.00%
API (Specified):	50.3700
API (Calculated):	53.8085
API Error:	-6.83%
Normal Boiling Point (Calculated Average):	310.36 F

After that, the condensate sample is fed into an atmospheric distillation column with a theoretical stage of 12. The simulation is used to observe the distillate and bottom products' quality and thermal condition in redistil the product. 3.01325 is the increased pressure for the bottom product. To determine the product quality (if the distillate is distilled again), the pseudo-cuts are then fed into a shortcut distillation column. The second distillation is known as fractionation or redistillation. The simulation indicates that feed should be introduced at stage 5 after 15 theoretical stages. A comparison has been made in Table 7-13.

Table 7.13: Comparative chart for atmospheric and shortcut distillation

Property		Atmospheric Distillation Column	Shortcut Distillation Column
Temperature , °C	Feed	360	30
	Distillate	140.401	-5.21056
	Bottom	266.773	58.2147
Pressure, bar	Feed	51.2391	0.188934
	Distillate	0.51325	0.1889
	Bottom	3.01325	0.1889
Volumetric Flow, m3/h		170	170
Specific Gravity		0.778	0.711
Density, Kg/m ³	Feed	2.19858E+06	748.056
	Distillate	596.905	747.54
	Bottom	541.596	679.116
Condenser Duty, kW		1.82118E+10	20470.3
Reboiler Duty, kW		-1.81351E+10	22692.9
Estimated Height		7000mm	-
Number of Stages		12	15

The analysis reflects when the temperature drops during the second distillation, less energy is needed. Compared to the earlier distillation products, the resultant product is denser.

Chapter 8 :CONCLUSIONS

This chapter covers the study's results, limitations, and literature gap. In addition, the author suggests improvements and additions to the work's viability.

8.1 GENERAL

The deliverability potentiality of a retrograde reservoir is impacted by condensate formation. Condensate banking in the region of the wellbore has been the subject of years' worth of research, with an emphasis on demonstrating the phenomena's impacts using mathematical and numerical methods. The current study attempts to identify the gaps between the works, even if no single work can accurately capture this occurrence. Additionally, it focuses on analysing a retrograde reservoir's phase behaviour and offers a model that attempts to visualize the flow pattern close to the well. Additionally, the study investigates the efficiency of distillation and the fuelling capability of condensate of the chosen field which may be useful to oil refineries that are considering substituting condensate for crude oil in terms of evaluating feed-stocks, estimating economic value, and developing and simulating the refining process.

8.2 KEY FINDINGS

The main findings of the study are

- Based on the reservoir and fluid parameters (estimated from experiment and simulation), the Kailashtila gas field is a lean gas reservoir that displays some retrograde behaviour under reservoir conditions.

- The field comprises of three sand layers: Upper, middle, and lower gas zone. The gas composition and producing capability is almost same and condensate obtained from the field is medium denser.
- There is relatively little difference between the results provided by the simulation and the experiment. Consequently, reservoir property analysis can be aided by simulation software.
- The scope of the mathematical model's applicability is restricted and contingent upon specific well and reservoir conditions.
- The flow pattern close to the wellbore region is displayed by the analytical solution, which also offers suggestions on how to measure pressure at various locations.
- The KTL condensate has a long temperature range to fully distillate the product. The initial lower temperature suggest that KTL condensate has lower IBP and EP. As a result, this kind of condensate can swiftly create distillate products, but it also runs the risk of losing light products due to their low-temperature vaporization.
- It will need a lot of energy to feed the fluid into an atmospheric column for distillation. It will take less energy to do the distillation operation a second time, but the density will increase. It is advised to again distil the product from the ATM column if specific demands call for a denser product.

8.3 LIMITATION OF THE STUDY

- The little amount of liquid produced by the field meant that the inquiry could not find the critical point in the phase diagram for the KTL field and because the compositions closely matched that of an ideal natural gas composition.

- Some experiments are not physically possible to do, hence the study relies on simulated results to forecast field behaviour. It can lead to a clash with actual field conditions.
- The theoretical assumption and solution form the basis of the model. Even after the sensitivity tests were carried out using real-world field data, it is still unclear if the model could accurately depict real-world field scenarios.
- KTL feed requires a larger temperature range to completely distil the sample, which is a major worry from an economic perspective because the cost and distillation time will be higher for this type of lighter feed. But no such economic analysis has been performed in this study that can agree with the notion.

8.4 IMPLICATION

This work could have numerous applications. First, if an experiment cannot be conducted practically, the suggested method can help assess the behaviour of a petroleum reservoir using a simulated approach. Secondly, the suggested model provides a foundation for scholars to concentrate on the impact of mass flow rate, compressibility, viscosity, and permeability to predict the flow behaviour in situations when condensate banking diminishes gas flow. In conclusion, the third section of the study could be helpful to refineries who are thinking about using condensate instead of crude oil when it comes to constructing and modelling the refining process, assessing feedstocks, and determining economic value.

8.5 RECOMMENDATION FOR FURTHER STUDY

The model is an effort to close the gap between earlier and more recent research on the condensate banking issue. While the work's theoretical acceptance is assured, its practical acceptability remains uncertain. The author

highly advises using a numerical approach and actual field experiments to evaluate the results of the suggested model to resolve any disagreement. The study's final part suggests that, taking the data into account, a refinery can accomplish all its objectives by using a suitable combination of the lighter and heavier samples. In this way, the lighter one will decrease residue at the endpoint and enhance the quality of the final product, while the heavier one will delay the IBP point. The study recommends performing distillation on a mixture of light and heavy weight condensate to detect the response. Though redistillation provides fine-tuned and impurity free compositions, it generally comes with energy costs and therefore benefits must be weighed against the considerations.

Bibliography

- [1].Kool, H., Azari, M., Soliman, M. Y., Proett, M. A., Irani, C. A., & Dybdahl, B. (2001, January). Testing of gas condensate reservoirs-sampling, test design and analysis. In *SPE Asia Pacific Oil and Gas Conference and Exhibition*. Society of Petroleum Engineers.
- [2].Al Ismail, M. I. (2010). *Field Observations of Gas-Condensate Well Testing* (Doctoral dissertation, Stanford university).
- [3].Emmanuel O. Ehirim Lambert, Osuomokpe Kakmuswei, Stewart, Gospel(2019). *Modelling and Simulation of a Gas Condensate Reservoir*. 8, s.l. : American Journal of Engineering Research (AJER), Vol. 8. e-ISSN: 2320-0847 p-ISSN : 2320-0936.
- [4].Fevang, O. (1995). *Gas condensate flow behavior and sampling* (Doctoral dissertation, PhD thesis, Norges).
- [5].www.petrobangla.org.bd. [Online] Petro Bangla. [Cited: 02 28, 2020.]
- [6].Mushfiquir Rahaman. Banglapedia. en.banglapedia.org. [Online] <http://en.banglapedia.org/index.php?title=Condensate>.
- [7].Muskat, M.: *Physical Principles of Oil Production*, McGraw-Hill Book Company, Inc. (1949).
- [8].Eilerts, C.K., Sumner, E.F., and Potts, N.L.: "Integration of Partial Differential Equation for Transient Radial Flow of Gas-Condensate Fluids in Porous Structures," *SPEJ* (1965) 141-152

- [9]. Eilerts, C.K. and Sumner, E.R.: "Integration of Partial Differential Equations for Multicomponent, Two-Phase Transient Radial Flow," *SPEJ* (1967) 125-135
- [10]. Gondouin, M., Iffly, R., and Husson, J.: "An Attempt to Predict the Time Dependence of Well Deliverability in Gas Condensate Fields," *SPEJ* (1967) 112-124; *Trans., AIME*, 240.
- [11]. O'Dell, H.G. and Miller, R.N.: "Successfully Cycling a Low Permeability, High-Yield Gas Condensate Reservoir," *JPT* (1967) 41-47; *Trans., AIME*, 240.
- [12]. Fussell, D.D.: "Single-Well Performance Predictions for Gas Condensate Reservoirs," *JPT* (1973) 258-268, 860-870; *Trans., AIME*, 255.
- [13]. Jones, J.R. and Raghavan, R.: "Interpretation of Flowing Well Response in Gas Condensate Wells," paper SPE 14204 presented at the 1985 SPE Annual Technical Conference and Exhibition, Las Vegas, Sept. 22-25.
- [14]. Jones, J.R., Vo, D.T., and Raghavan, R.: "Interpretation of Pressure Buildup Responses in Gas Condensate Wells," paper SPE 15535 presented at the 1986 SPE Annual Technical Conference and Exhibition, New Orleans, Oct. 5-8.
- [15]. Hassan, A. M., Mahmoud, M. A., Al-Majed, A. A., Al-Shehri, D., Al-Nakhli, A. R., & Bataweel, M. A. (2019). Gas Production from Gas Condensate Reservoirs Using Sustainable Environmentally Friendly Chemicals. *Sustainability*, 11(10), 2838.
- [16]. Afidick D., Kaczorowski N., Bette S.: Production performance of a retrograde gas reservoir: A case study of the Arun Field. SPE-28749-MS. In: SPE Asia Pacific Oil and Gas Conference, Melbourne, Australia, 7–10 November 1994.
- [17]. Hinchman S., Barree R.: Productivity loss in gas condensate reservoirs. SPE 14203. In: SPE Annual Technical Conference and Exhibition, Las Vegas, NV, 1985.
- [18]. Vo D., Jones J., Raghavan R.: Performance prediction for gas condensate reservoirs. *SPE Formation Evaluation*, 1989.

- [19]. Narayanaswamy G., Pope, G., Sharma, M.: *Predicting gas condensate well productivity using capillary number and non-Darcy effects*. SPE-51910-MS. In: SPE Reservoir Simulation Symposium, Houston, Texas, 1999.
- [20]. Narayanaswamy G., Sharma M., Pope G.: *Effect of heterogeneity on the non-Darcy flow coefficient*. SPE Res Eval & Eng., SPE-56881-PA, 1999.
- [21]. Al-Shaidi, S. M. (1997). Modelling of gas-condensate flow in reservoir at near wellbore conditions (Doctoral dissertation, Heriot-Watt University).
- [22]. Ashour, I., Al-Rawahi, N., Fatemi, A., & Vakili-Nezhaad, G. (2011). Applications of equations of state in the oil and gas industry. Thermodynamics-kinetics of dynamic systems, 1, 165-178.
- [23]. Ramdharee, S., Muzenda, E., & Belaid, M. (2013). A review of the equations of state and their applicability in phase equilibrium modeling.
- [24]. Peng, D. Y., & Robinson, D. B. (1976). A new two-constant equation of state. Industrial & Engineering Chemistry Fundamentals, 15(1), 59-64.
- [25]. Merrill, R. C., Hartman, K. J., & Creek, J. L. (1994, September). A comparison of equation of state tuning methods. In SPE Annual Technical Conference and Exhibition? (pp. SPE-28589). SPE.
- [26]. Ashour, I., Al-Rawahi, N., Fatemi, A., & Vakili-Nezhaad, G. (2011). Applications of equations of state in the oil and gas industry. Thermodynamics-kinetics of dynamic systems, 1, 165-178.
- [27]. Ahlers J, Gmehling J. Development of a universal group contribution equation of state. 2.
- [28]. Prediction of vapor-liquid equilibria for asymmetric systems. Industrial & Engineering Chemistry Research. 2002; 41:3489-98.
- [29]. Stryjek R, Vera J. PRSV: An improved Peng—Robinson equation of state for pure compounds and mixtures. The canadian journal of chemical engineering. 1986; 64:323- 3.
- [30]. Le Guennec Y, Privat R, Jaubert J-N. Development of the translated-consistent tc-PR and tc-RK cubic equations of state for a safe and accurate

- prediction of volumetric, energetic and saturation properties of pure compounds in the sub- and super-critical domains. *Fluid Phase Equilibria*. 2016; 429:301-12.
- [31]. Panja, P., Velasco, R., & Deo, M. (2020). Understanding and modeling of gas-condensate flow in porous media. *Advances in Geo-Energy Research*, 4(2), 173-186.
- [32]. Dashtizadeh A, Pazuki GR, Taghikhani V, Ghotbi C. A new two-parameter cubic equation of state for predicting phase behavior of pure compounds and mixtures. *Fluid Phase Equilibria*. 2006; 242:19-28.
- [33]. Mohsen-Nia M, Modarress H, Mansoori GA. A cubic hard-core equation of state. *Fluid Phase Equilibria*. 2003; 206:27-39.
- [34]. Pazuki GR, Mansouri S, Feyzi F. Modified Cubic Equation of State for Prediction VLE Phase Behavior of Fluids: Pure and Mixture. *Separation Science and Technology*. 2007; 42:1883-99.
- [35]. Nasrifar K, Bolland O. Square-well potential and a new α function for the soave-Redlich-Kwong equation of state. *Industrial & engineering chemistry research*. 2004; 43:6901-9.
- [36]. Patel NC, Teja AS. A new cubic equation of state for fluids and fluid mixtures. *Chemical Engineering Science*. 1982;37: 463-73.
- [37]. Hossain, H. M. Z., Sampei, Y., Roser, B. P. (2009a). Characterization of organic matter and depositional environment of Tertiary mudstones from the Sylhet Basin, Bangladesh. *Org. Geochem.*, 40, 743–754.
- [38]. Hossain, N., Hossain, H. M. Z., Kamrul, M., Sarder, I., & Hasan, M. M. (2019). Origin and Accumulation Mechanism of Gas Condensate in Kailashtilla Gas Field, Sylhet Basin, Bangladesh. In *Int.J.Econ.Environ.Geol* (Vol. 10, Issue 3). www.econ-environ-geol.org
- [39]. Petrobangla. (2022). Petrobangla Annual Report 2022.

- [40]. Kailashtilla Gas Field. (n.d.). Kailashtilla Gas Field. Retrieved December 25, 2023, from <https://sgfl.org.bd/site/page/4114d20a-fd5c-4d97-aeb2-ffb9f5971c30/->
- [41]. Intercomp-Kanada Management Limited. (1989). Gas Field Appraisal Project Geological, GeoPhysical and PetroPhysical Report of Kailashtilla Gas Field, Bangladesh.
- [42]. Md. Mizanur Rahman. (2015). Integrated Reservoir Characterization of Kailashtilla Gas Field. Bangladesh University of Engineering And Technology.
- [43]. Tangsriwong, K., Lapchit, P., Kittijungjit, T., Klamrassamee, T., Sukjai, Y., & Laoonual, Y. (2020). Modeling of chemical processes using commercial and open-source software: A comparison between Aspen Plus and DWSIM. IOP Conference Series: Earth and Environmental Science, 463(1), 012057. <https://doi.org/10.1088/1755-1315/463/1/012057>
- [44]. <https://www.slb.com/-/media/files/oilfield-review/1-pvt>, PVT analysis for Oil Reservoir
- [45]. Chang, A. F., Pashikanti, K., & Liu, Y. A. (2013). Refinery engineering: Integrated process modeling and optimization. John Wiley & Sons.
- [46]. Riazi, M. R., & Daubert, T. E. (1987). Characterization parameters for petroleum fractions. Industrial & engineering chemistry research, 26(4), 755-759.
- [47]. Mokhatab, S., & Economides, M. J. (2006). Process selection is critical to onshore LNG economics. World oil, 227(2), 95-99.
- [48]. Riazi, M. R. (2005). Characterization and properties of petroleum fractions (Vol. 50).
- [49]. Al-Assady, Q. M. A. A. (2009). Characterization of petroleum fractions. Iraqi journal of mechanical and material engineering, 9(2), 223-238.
- [50]. <https://www.manualslib.com/manual/1626438/Scion-Instruments-456-Gc.html?page=7#manual>

- [51]. ASTM Committee D-2 on Petroleum Products and Lubricants, Boldt, K., & Hall, B. R. (1977). Significance of tests for petroleum products. American Society for Testing and Materials.
- [52]. Economides, M. J. (2013). Petroleum production systems. Pearson education.


Appendix

Constants for Daubert's distillation curves inter-conversion method

volume %	index number, i	A_i	B_i
0	1	7.4	0.6024
10	2	4.9	0.7164
30	3	3.03	0.8008
50	4	0.87	1.0258
70	5	2.53	0.82
90	6	3.04	0.775
95	7	0.12	1.6606

Similarity Report Summary

Phase Behavior Analysis of a Gas Condensate Reservoir



By
Nadia Mahjabin
17MET012P

Match Overview


16%

1	ece.kuet.ac.bd Internet Source	3%	>
2	Submitted to Internatio... Student Paper	1%	>
3	Debdatta Ratna, "Chara... Publication	1%	>
4	research.tees.ac.uk Internet Source	1%	>
5	www.econ-environ-geol... Internet Source	<1%	>
6	lib.buet.ac.bd:8080 Internet Source	<1%	>

Similarity Report Summary









Phase Behavior Analysis of a Gas Condensate

Reservoir



By

Nadia Mahjabin
17MET012P



Match Overview

16%

1	ece.kuet.ac.bd Internet Source	3%	>
2	Submitted to Internatio... Student Paper	1%	>
3	Debdatta Ratna. "Chara... Publication	1%	>
4	research.tees.ac.uk Internet Source	1%	>
5	www.econ-environ-geol... Internet Source	<1%	>
6	lib.buet.ac.bd.8080 Internet Source	<1%	>

Thesis

ORIGINALITY REPORT

16%

SIMILARITY INDEX

13%

INTERNET SOURCES

7%

PUBLICATIONS

5%

STUDENT PAPERS

PRIMARY SOURCES

1	ece.kuet.ac.bd Internet Source	3%
2	Submitted to International Islamic University Chittagong Student Paper	1%
3	Debdatta Ratna. "Characterization, performance evaluation and lifetime analysis of thermoset resin", Elsevier BV, 2022 Publication	1%
4	research.tees.ac.uk Internet Source	1%
5	www.econ-enviro-geol.org Internet Source	<1%
6	lib.buet.ac.bd:8080 Internet Source	<1%
7	www.coursehero.com Internet Source	<1%
8	hdl.handle.net Internet Source	<1%